NAVAL POSTGRADUATE SCHOOL

MONTEREY, CALIFORNIA

THESIS

HYDRODYNAMIC FORCES ON COMPOSITE STRUCTURES

by

Scott C. Millhouse

June 2014

Thesis Advisor: Young W. Kwon
Second Reader: Maximilian F. Platzer

Approved for public release; distribution is unlimited

THIS PAGE INTENTIONALLY LEFT BLANK

REPORT DOCUMENTATION PAGE

Form Approved OMB No. 0704–0188

1. AGENCY USE ONLY *(Leave blank)*	**2. REPORT DATE** June 2014	**3. REPORT TYPE AND DATES COVERED** Master's Thesis

4. TITLE AND SUBTITLE
HYDRODYNAMIC FORCES ON COMPOSITE STRUCTURES

5. FUNDING NUMBERS

6. AUTHOR(S) Scott C. Millhouse

7. PERFORMING ORGANIZATION NAME(S) AND ADDRESS(ES)
Naval Postgraduate School
Monterey, CA 93943–5000

8. PERFORMING ORGANIZATION REPORT NUMBER

9. SPONSORING /MONITORING AGENCY NAME(S) AND ADDRESS(ES)
N/A

10. SPONSORING/MONITORING AGENCY REPORT NUMBER

11. SUPPLEMENTARY NOTES The views expressed in this thesis are those of the author and do not reflect the official policy or position of the Department of Defense or the U.S. Government. IRB Protocol number ____N/A____.

12a. DISTRIBUTION / AVAILABILITY STATEMENT
Approved for public release; distribution is unlimited

12b. DISTRIBUTION CODE
A

13. ABSTRACT (maximum 200 words)

Using a tow tank environment an experiment was set up to measure for response of composite samples of varying stiffness to a geometrically comparable more rigid aluminum sample which was tested at increasing speeds. Also, a square composite shape was tested in a frame providing clamped boundary conditions. Testing of this sample over varying speeds was also performed at varying position angles and was analyzed for force, strain and flow visualization.

Results show complex behaviors in fluid flow and structural deformation because of the effects of the free surface and fluid-structure interaction. The comparable mass density between composite plates and water results in pronounced fluid structure interaction. Proximity to the free surface highly influences the test data along with the position angle. Negative position angles in combination with high speeds result in an air pocket open to the atmosphere which translates to a sharp decrease in strain on the sample. Positive position angles yields different free surface effects including vortices and the onset of cavitation.

14. SUBJECT TERMS Fluid structure interaction, FSI, finite element, finite volume, ANSYS, E-glass, composite material, coupled interaction, transient acceleration, transient fluid, transient velocity, transient stress, transient force, towing tank.

15. NUMBER OF PAGES
179

16. PRICE CODE

17. SECURITY CLASSIFICATION OF REPORT	**18. SECURITY CLASSIFICATION OF THIS PAGE**	**19. SECURITY CLASSIFICATION OF ABSTRACT**	**20. LIMITATION OF ABSTRACT**
Unclassified	Unclassified	Unclassified	UU

NSN 7540–01–280–5500

Standard Form 298 (Rev. 2–89)
Prescribed by ANSI Std. 239–18

THIS PAGE INTENTIONALLY LEFT BLANK

Approved for public release; distribution is unlimited

HYDRODYNAMIC FORCES ON COMPOSITE STRUCTURES

Scott C. Millhouse
Lieutenant, United States Navy
B.S., Drexel University, 2004
MEM, Old Dominion University, 2012

Submitted in partial fulfillment of the
requirements for the degree of

MASTER OF SCIENCE IN MECHANICAL ENGINEERING

from the

NAVAL POSTGRADUATE SCHOOL
June 2014

Author: Scott C. Millhouse

Approved by: Young W. Kwon
Thesis Advisor

Maximilian Platzer
Second Reader

Knox T. Millsaps
Chair, Department of Mechanical and Aerospace Engineering

THIS PAGE INTENTIONALLY LEFT BLANK

ABSTRACT

Using a tow tank environment, an experiment was set up to measure for response of composite samples of varying stiffness to a geometrically comparable more rigid aluminum sample, which was tested at increasing speeds. Also, a square composite shape was tested in a frame providing clamped boundary conditions. Testing of this sample over varying speeds was also performed at varying position angles and was analyzed for force, strain and flow visualization.

Results show complex behaviors in fluid flow and structural deformation because of the effects of the free surface and fluid-structure interaction. The comparable mass density between composite plates and water results in pronounced fluid structure interaction. Proximity to the free surface highly influences the test data along with the position angle. Negative position angles in combination with high speeds result in an air pocket open to the atmosphere which translates to a sharp decrease in strain on the sample. Positive position angles yields different free surface effects including vortices and the onset of cavitation.

THIS PAGE INTENTIONALLY LEFT BLANK

TABLE OF CONTENTS

LIST OF FIGURES

THIS PAGE INTENTIONALLY LEFT BLANK

LIST OF TABLES

THIS PAGE INTENTIONALLY LEFT BLANK

LIST OF ACRONYMS AND ABBREVIATIONS

A	area (m^2)
a	acceleration (m/s^2)
AEM/S	Advanced Enclosed Mass/Sensor
C_D	coefficient of drag
CFD	computational fluid dynamics
CVN	Nuclear Powered Aircraft Carrier
D	flexural rigidity ($Pa \cdot m^4$)
DDG	Guided Missile Destroyer
E	Young's Modulus (GPa)
ϵ	strain
F	force (N)
FEA	finite element analysis
FSI	fluid-structure interaction
h	thickness (m)
ℓ	length (m)
LPD	Landing Platform Dock
MCM	Mine Countermeasure Ship
NAVSEA	Naval Sea Systems Command
NSWCCD	Naval Surface Warfare Center, Carderock Division
NPS	Naval Postgraduate School
R^2	residual squared
t	time (sec)
U	fluid velocity (m/s)
USS	United States Ship
$V_{(f,m)}$	volume fraction; fiber, matrix (%)
ν	Poisson's Ratio
w	plate deflection (m)

THIS PAGE INTENTIONALLY LEFT BLANK

ACKNOWLEDGMENTS

I would like to thank Dr. Young Kwon for his guidance on this project which pushed me to exhaustively look into composite force responses. Also, Mr. John Mobely, in the NPS machine shop, provided guidance on numerous pieces I designed for this thesis. His timely return of these products and extreme quality never failed to impress. Thanks to Mr. Thomas Christian, who designed the data acquisition system for the tow tank: this program is not only robust but proved to be extremely user friendly.

Finally, the NPS tow tank was inoperable for nine months due to material issues identified for safety and environmental concerns. These issues would have prevented the completion of this project had it not been for the tireless effort of Mr. Doug Seivwright, who contracted an environmental repair company and personally oversaw the repairs for the safety issues. It is efforts like his that allow research like this at NPS to occur.

THIS PAGE INTENTIONALLY LEFT BLANK

I. INTRODUCTION

A. OVERVIEW

Composite materials provide numerous opportunities for the United States Navy. Generally speaking, a composite material is any material made up of two or more distinctly different materials, which provide a very broad range of items that would be classified a composite [1]. For example, concrete is a mixture of cement and stone making it a composite as well as plywood formed by a combination of layers of wood and glue. To be sure, alloys may contain other items than the base metal, but these would not be a composite because all constituents of the material are metallic.

Since wood is considered a natural composite, the U.S. Navy used composites as the primary material for all ships for the first 100 years of its existence. Once iron and steel technology advanced to the point where production and material handling were feasible, the benefits of stronger, tougher materials took hold over wood as naval construction material since the primary engagement technique was a broadside blow into the side of an adversary's ship. As naval warfare has advanced, the need for direct ship-to-ship engagement has diminished, but the need for strong metal superstructures has not decreased, as ships today are larger and contain heavier equipment that weaker composites hulls could not properly support. Even though the traditional large ships of the Navy still use steel and aluminum as the primary construction material, smaller ships have recently employed a much wider use of composites such as the mine countermeasure ship (MCM), built with plywood and fiberglass sheathing as construction materials [2]. Figure 1 shows the dismantling of USS Guardian, a MCM that was grounded on a reef and required disassembly in theater for removal. In the figure, the sheathing is removed and the plywood composite materials can be seen. Also, naval employment of composites for topside applications has advanced rapidly in recent years with widespread uses in LPD-17's Advanced Enclosed Mass/Sensor (AEM/S) system, CVN-77's main mast, and DDG-1000 deck house. All of these examples show how the weight saving, maintenance reducing, ease of production advantages of composites can be exploited. For example, the CVN-77 main mast is 27 long tons, making it 5 long tons

lighter compared to the steel equivalent [3]. For a ship with a 50-year life span, this provides a considerable savings opportunity.

Figure 1 USS Guardian (MCM-5) salvage, from [4]

Once again, technology is advancing, not only is composite material science advancing, but the need to support heavy equipment is decreasing as other technologies are allowing large items like generators to become smaller and lighter. A general trend in composite technology is to make material of lower density, and therefore, less weight, while maintaining or increasing strength. As a construction material, composites provide many advantages that could be leveraged. Using composites over steel not only provides a weight savings that decreases cost of construction and operation but also can reduce cost of maintenance, as steel and aluminum are highly susceptible to corrosion in a marine environment. Furthermore, composite materials can greatly alter the fabrication process available to shipbuilder, providing flexibility and further cost savings. Finally,

successful employment of composites in ship construction can improve performance and other ship handling characteristics, providing a ship to the sailor that is more capable for the nation's defense.

Numerous naval activities are invested in the use of composite materials for hull construction to take advantage of these benefits. Much investigative effort is being performed by the Office of Naval Research and along with other research facilities such as Naval Surface Warfare Center, Carderock Division (NSWCCD) and the Naval Postgraduate School. This effort also involves commercial fabricators, industrial shipbuilders and public and private universities. Even more so, international collaborative efforts with the German and Japanese navies have been performed to investigate the use of composites in the hull of ships [5]. The U.S. Navy is clearly signaling its desire for composite material usage in ships through such a large and expansive research effort.

As these newer composites become tangible replacements to steel and aluminum, engineering investigation of composite materials is required to ensure that the right composite is used in the correct application. The hull of the ship provides a place where use of composite material could be very beneficial. First, this area is in direct contact with corrosive salt water, creating the challenge of immersed access for inspection and making preservation expensive. Second, the skin of the hull is materially a large portion of the ship, and saving a small amount of weight per area of hull would result in an extremely large savings of weight for the ship. Using any new material for the hull presents a unique challenge, however, because at any time the hull of the ship is being dynamically loaded by the surrounding ocean.

B. PREVIOUS RESEARCH

The dynamic loading experienced by the hull from the surrounding marine environment is not the same as a direct impact to the hull. A direct impact from another rigid body will cause dynamic loading but could also cause damage to the composite structure which could include cracking and delamination. Analysis of the dynamic loading of composite materials in the marine environment in this study will only

investigate hydrodynamic forces and will not investigate damage of the composite but only the reaction of the composite material to the loading applied.

The use of composite materials for large naval ships was investigated by Galanis [6] for applications of ships 100 feet in length and a hull made of composite materials. His analysis considered a nominal DDG-51-type destroyer. He mentions numerous ideas that are important for consideration of construction from composite such as in dynamic loading of the composite structures over the short duration and inertial effects on the material. Also, in the transient stage of dynamic loading, higher system stress and displacement will be experienced than is experienced in steady state loading of composites. Although he concedes that dynamic loading in the marine environment has not been well studied, he concludes that composites are a possible material that could be used for large ship hull construction when considering impacts, structural loading from the ship itself, cost, feasibility of manufacturing, and military standards required for construction of a U.S. Navy surface ship. This is an important conclusion, because it means that understanding the interaction of the composite material with the marine environment is an important endeavor due to the fact that composites represent a legitimate alternative to current metallic ship construction materials and provide numerous advantages.

Investigation into the interaction of fluids and composites has recently occurred by a number of individuals. Most of this work has been done through mathematical modeling of fluid structure interaction (FSI). FSI couples computational fluid dynamics (CFD) and computational structural dynamics via finite element analysis (FEA). FSI offers modeling of the interaction between the two systems but it is still a developing field with many key questions surrounding it. FSI is a science in itself with debates on how to best couple each systems solver and how to balance one solver over the other [7].

In the realm of FSI, Kendall began looking at the problem of fluid interaction on composite structures and developing a mathematical model to investigate dynamic loading of composites [8]. This model began to investigate the loading of composites compared to the loading of steel along with response in a wet environment and dry

environment. His results demonstrate that water fluid interaction with the structure clearly influences the behavior of the response.

Ma and Mahfuz expanded on FSI analysis to look at composite ship structures. Their research investigated sandwich construction of composites in an FSI model for areas of high stress gradient and also for failure criteria [9].

Similarly, Knutton has recently investigated FSI to explore peak pressure and stresses in composites in a fluid environment [10]. His model began to look at numerous variables which could be changed along with acceleration applied to the composite. This model is useful for beginning to understand how initial acceleration of the composite interacts with the marine environment, which is where dynamic loading of the composite occurs. A critical variable that he investigated was the velocity profile input and the initial acceleration of the FSI composite model.

C. OBJECTIVE

This study will create and analyze two rectangular composites made of an E-glass matrix and a resin matrix which will be used to compare with an aluminum sample of the same dimensions. The two composite samples will be of different thicknesses, one of 6 layers of E-glass and one of ten layers, to investigate how stiffness of the composite influences the pressure force reaction when hydro-dynamically loaded and provide comparison to the aluminum sample which will act as a rigid body. The NPS tow tank provides an environment for hydrodynamic loading of composite samples and is capable of variable speeds.

Furthermore, another 6 layer sample will be created and clamped in a solid aluminum frame and instrumented with strain gages. The clamping by the aluminum frame will serve as a boundary condition on all four sides of the composite sample. Not only will this sample be tested for pressure force reaction and strain at three locations on the plate but will also be tested and positive and negative angles rotated in the direction of travel around point of attachment to the testing equipment. In addition these samples will be investigated with videography to understand the interaction with the free surface.

Finally, the velocity profile of each sample will be developed by use of recording time and position at each testing speed. Understanding the velocity profile is required for comparative analysis with numerical solutions of fluid structure interactions with composite materials.

II. METHOD OF SOLUTION

A. APPLICABLE THEORY

This study demonstrated the intra-discipline approach that must be taken when considering true mechanical engineering problems. The problem is not a wholly mechanics, fluids, nor materials thesis but combines aspects of each. Therefore, an understanding of each subject is required to develop a solution to the problem.

Composites can be classified into two categories, particulate and fibrous. They can be further classified from there. Figure 2 provides a hierarchy of composite classification.

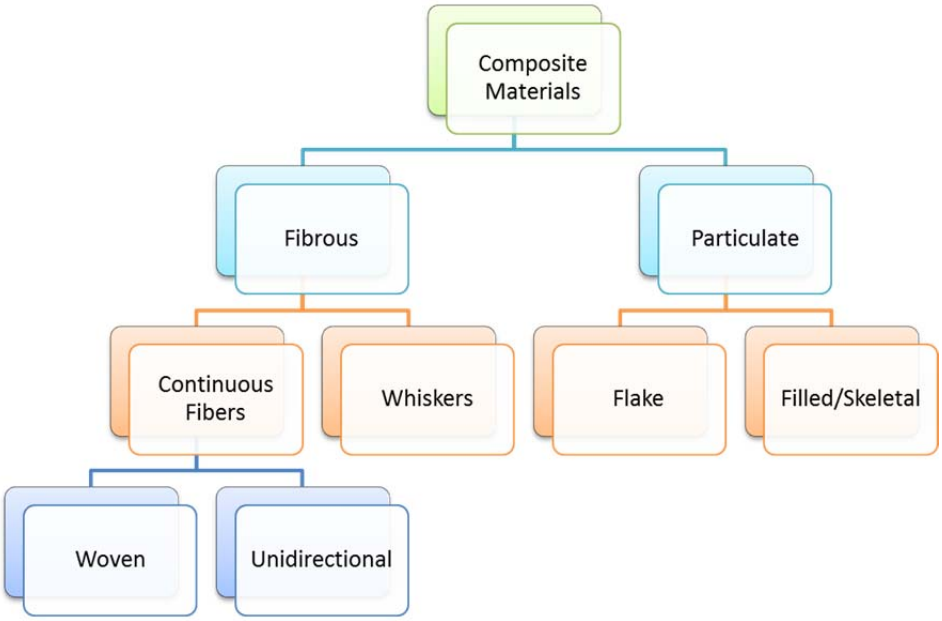

Figure 2 Classification of composites, after [1]

Woven composites in laminate form are of particular interest. Laminate form indicates that the composite is layers of laminar composite. Laminar simply means that the fibers are suspended in a matrix. In the case of this study, the matrix of concern is polymer based while the fibers are glass, commonly known as E-glass. The typical modulus of elasticity for E-Glass ranges on the order of magnitude of 72.5 GPa while the

tensile strength is typically 3,500 MPa [1]. E-Glass is of concern because the basic base materials are relatively inexpensive and easily fabricated compared to other types of composites while its strength to weight ratio is similar to other composites, but its stiffness to weight ratio is superior to other composites, as shown in comparison with other composites in Figure 3.

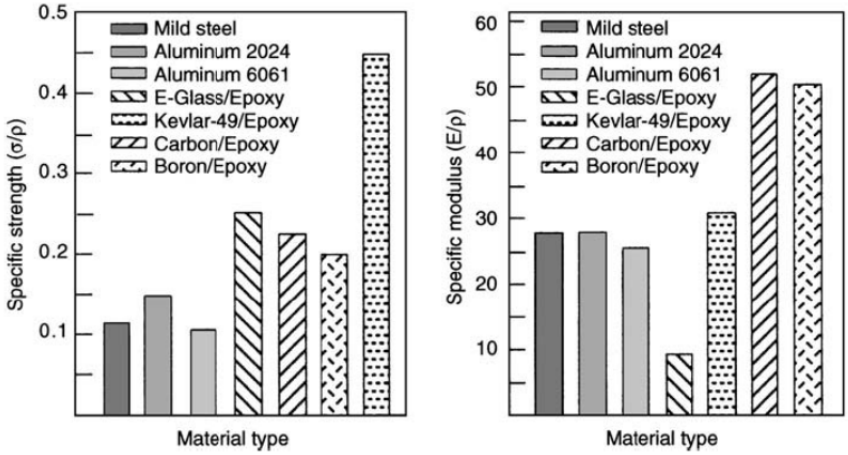

Figure 3 Comparison of composite material properties, from [1]

From a mechanics standpoint, unlike other traditional homogenous materials, composites demonstrate a response to loads that is directionally dependent. When dealing with laminated composites, a nomenclature for direction is one where x-direction is the principal fiber direction, y-direction is the in-plane direction perpendicular to the fibers of interest, and z-direction is out of plane direction perpendicular to the fibers [1]. Because this study used woven fibers and made every attempt to keep the fibers aligned, x- and y-directions can be picked at convenience as both being in-plane while z-direction is out of plane perpendicular to the fibers; this is described in Figure 4. Because the x- and y-direction are the same, it can be assumed that the mechanical properties in these directions are not directionally dependent in this study, whereas the z-direction is.

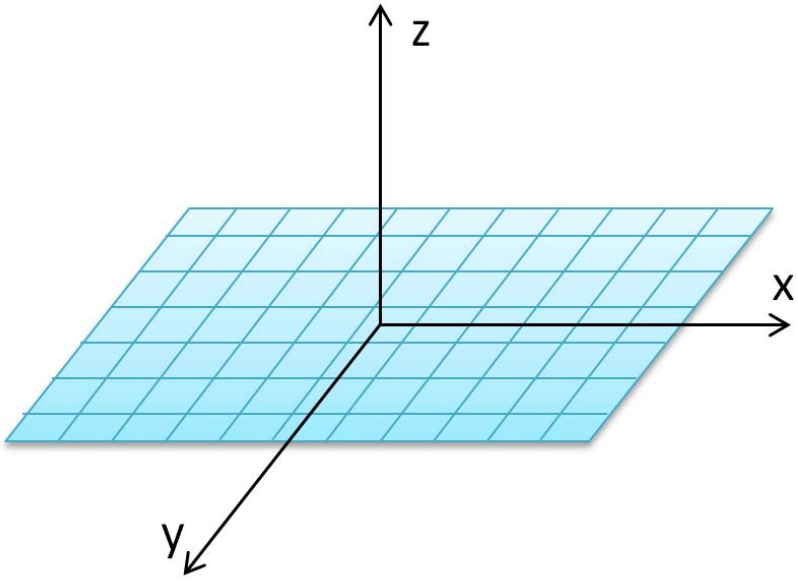

Figure 4 Coordinate scheme for woven fiber composites

Integral to this problem is the marine environment that is causing force and deformation upon the composite piece. The fluid environment a layered composite plate is in can be considered one dimensional for this study, acting only in the z-direction of the already described coordinate system. With water as the operating fluid and since neither appreciable depth nor extreme speeds will be considered, the fluid can be considered incompressible [11]. Fluid flowing over a body imparts two types of force on the body, friction force and pressure force. Determining how much the overall force imparted by the fluid is highly dependent on a number of factors including the speed of the fluid, the material properties of the body and the orientation of the body. The orientation of the body is of special importance, where the same body in different orientation can experience nearly complete friction force or pressure force. Figure 5 shows how a similar thin flat plate, comparable to a plate of composite material, could experience large pressure force and comparatively little friction forces such as in (a) or vice versa in (b).

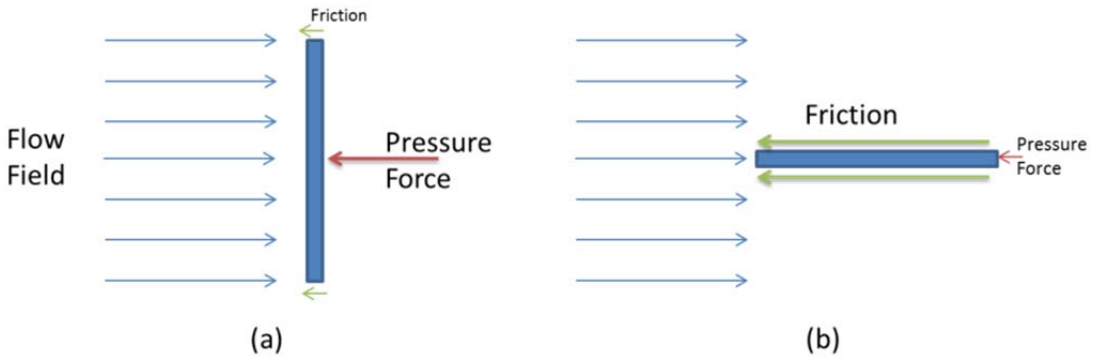

Figure 5 Body orientation influence on imparted fluid force

To account for different geometries and orientations, a coefficient of drag (C_d) has been developed which takes into account the shape of the object flow is going over. The coefficient of drag can be used to determine the force on the body (F_d) by the following equation.

$$F_d = \frac{1}{2} C_d \rho U^2 A \tag{1}$$

where ρ is the density of the fluid, U is the velocity of the fluid and A is the area of the body. The area is something that can fall into three categories based on the type of body. The frontal area is considered if the body has a greater surface area normal to the flow than parallel to the flow similar to Figure 5 (a), the planform area is considered on long slender bodies such as in Figure 5 (b), and the wetted area is considered typically in surface ships and barges. This equation shows that for the same object without changing the orientation, the force is proportional to the square of the velocity [11].

Since of concern for this study is rectangular shaped plates in the flow field, this reduces the need to understand the type of flow for analysis. Using a rectangular body, the sharp corner edges create a separated flow regardless of flow field velocity. However, in this study not only are flows normal to the body of the plate of concern but also flows oblique to the body. Because a composite provides a relatively smooth object, at angles beyond perpendicular to the flow field, only pressure drag will be considered for numerical analysis using the frontal area of the plate. For ease of numerical calculations it will be assumed that the test pieces experience a uniform pressure force

equal to the force of drag. A square composite piece with all four edges held firmly can be modeled as a plate with clamped boundary conditions on all sides. The governing equation for plate deflection is

$$\nabla^4 w = \frac{F}{D} \tag{2}$$

where w is the plate deflection, F is the pressure load on the plate, in this case the drag force, D is the flexural rigidity of the plate. Flexural rigidity is defined by

$$D = \frac{Eh^3}{12\left(1-v^2\right)} \tag{3}$$

where E is the modulus of elasticity or Young's Modulus, h is the plate thickness and v is Poisson's ratio [12]. The clamped boundary conditions on all sides along with a ratio of length to width of 1.0, since square, results in the central deflection as given in Equation (4) for the uniform pressure loading F.

$$w = \frac{0.00126 F \ell^4}{D} \tag{4}$$

For this equation, the deflection is taken from the center location and ℓ is the length of an edge of the plate [13]. For a square composite piece, strain should be equivalent in the x- and y-directions.

Determining Young's Modulus becomes difficult with a non-homogeneous solid such as a composite. Knowing that the composite being used is of a woven composite also adds a degree of difficulty in determining the Young's Modulus. In general for composites, the Young's Modulus is calculated based on the volume fraction of fibers to matrix. For fiber composites, loading is considered as either longitudinal with the fiber or transverse. When dealing with a weave, some fibers will be in longitudinal loading and at the same time other fibers are in transverse loading [14]. Kwon and Altekin have developed a method to determine the mechanical properties of a woven composite by considering the geometry of the weave and constituent fiber and matrix properties [15].

The process they have developed has been formulated into a Matlab program by Kwon which was used to calculate the material properties of the composites used in this study.

To determine the Young's Modulus of the composite, the values for fiber and the matrix need to be known. The values of the fiber are taken from [14] for E-glass and the values for the matrix are taken from manufacturer's data. Because cure process affects the physical properties of the resin matrix and none of the specified cure cycles provided by the manufacturer was exactly used due to material handling limitations, the most conservative value was used. These values are provided in Table 1.

Table 1 Composite constituent Young's Modulus

	Young's Modulus (GPa)
Resin Matrix	2.72
E-glass	75

The final components needed to use Kwon and Altekin's method to determine the material properties of the composite are the dimensions of the weave. The required dimensions are described in Figure 6.

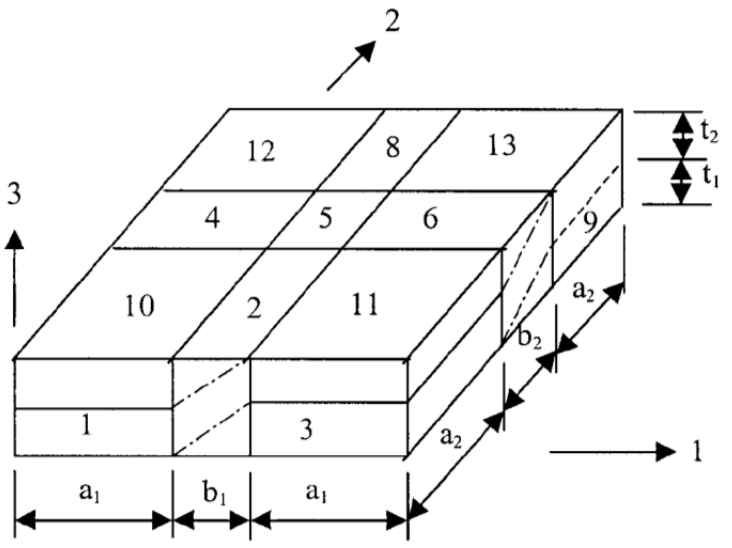

Figure 6 Dimension description for a plain weave composite, from [15]

For the weave used $a_1=a_2$, $b_1=b_2$ and $t_1=t_2$. Thickness in this diagram was denoted as t but h is used in this study for thickness. Manufacturer data for the E-glass cloth used specified the thickness of the cloth as 0.24 mm which matched consistently with a measured thickness of 0.25 mm by the author [16]. The dimension of the weave was measured to be 0.75 mm. Finally, an assumption was made that the volume fraction of fiber was 70%; this value was chosen because it is consistent with values given in [14]. Using this information in the MATLAB program, the material properties of the composite are provided in Table 2.

Table 2 Calculated material properties of sample composite

Young's Modulus (E)	**Poisson's Ratio (*v*)**
20 GPa	0.14

B. EXPERIMENTAL SET UP

1. Test Pieces Used

A number of test pieces were used for experimentation and comparison. All test pieces bolt to a 1x1 inch piece of box tubing test rig for support and testing in the NPS tow tank. An aluminum plate measuring 330x178 mm (13x7 in) was utilized to demonstrate how traditional metals respond to dynamic marine force. This test piece is shown in Figure 7.

Figure 7 330x178 mm Aluminum plate test piece

Two comparative composite plates were used, which are of the same dimensions as the aluminum plate. One composite plate utilized six layers of E-glass while the second composite plate was stiffer at 10 layers of E-glass. Figure 8 shows the six-layer plate, the 10-layer plate is indistinguishable except for thickness; a 1-inch grid has been applied to the plate along with strain gauges applied. Table 3 is also provided for an overview of the three test pieces.

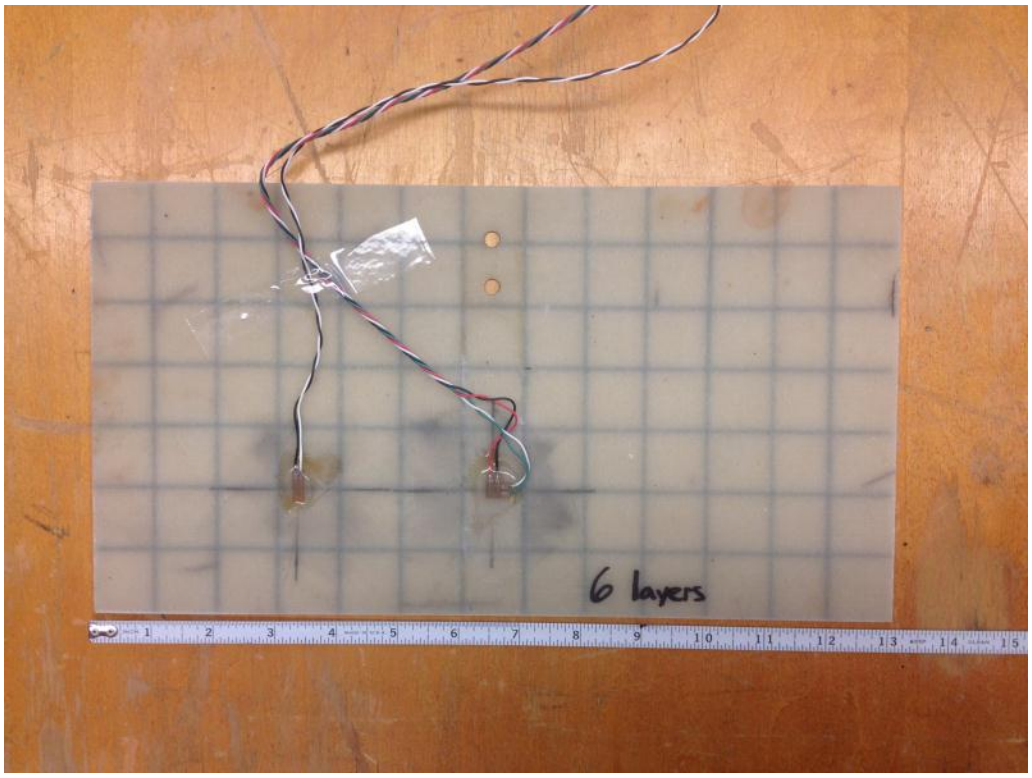

Figure 8 330x178 mm six-layer composite plate test piece

Table 3 Test piece comparison

	Aluminum Plate	10 Layer Plate	6 Layer Plate
Length (m)	0.330	0.330	0.330
Width (m)	0.178	0.178	0.178
Thickness (m)	0.005	0.005	0.005
Weight (kg)	0.736	0.265	0.142
Density (kg/m^3)	2,558.4	1,475.9	1,485.4

Finally, an aluminum frame was designed by the author and fabricated by the NPS machine shop. The frame measures 12x12 inches outside and 10x10 inches inside. A schematic of this design is provided as Appendix A. A composite of any thickness can be placed inside the frame, which provides a rigid boundary condition for the composite. The fame was tested with a six-layer piece of E-glass composite, as shown in Figure 9 and Figure 10.

Figure 9 Front view of frame test piece with six-layer composite

Figure 10 Angle view of frame test piece with six-layer composite

2. Method of Fabrication

All composite materials were fabricated by the author in the Naval Postgraduate School Composite Laboratory. The materials used for the test pieces include woven glass fabric, resin and hardener. Tools required include scale, mixing container, scissors or cutting wheel, tape measure, paint roller and vacuum set up with plate glass. Consumable

products needed to make a composite sample include tape, release ply paper, nylon ply, perforated release film, bleeder cloth, vacuum bag, foam roller pad, and gloves. The resin/hardener combination used was the Toughened Laminating Epoxy M1002 Resin/237 Hardener manufactured by PRO-SET. The ratio used in this study was target ratio of 100:24 by weight as specified by the manufacturer, which was measured and mixed in the lab fume hood as shown in Figure 11.

Figure 11 Resin/Hardener measuring by weight

The woven glass was measured out to sizes larger than desired with the expectation that the composite would be cut to the specified size. Figure 12 shows the woven glass fabric while being measured, a pair of scissors is shown but a cutting wheel can also be used to get a straight cut line of the fabric.

Figure 12 Measuring of woven glass fabric

Release ply-paper is used on a piece of plate glass to easily remove the composite sample once it is cured. On top of the release ply woven glass is layered in-between coats of resin/epoxy mixture in as many layers as desired. The resin/epoxy mixture is spread evenly using a foam roller similar to one used to apply house paint. Once the layers of glass and resin/epoxy mixture are placed, a vacuum system is placed over the sample. The vacuum system involves a nylon peel ply directly over the last layer of resin/epoxy, followed by a perforated release ply, bleeder cloth and the vacuum bag. The vacuum bag is sealed to the plate glass with sealant tape and placed under a vacuum of 10 mmHg overnight. The vacuum set up over the composite sample is shown in Figure 13, the hose in upper left leads to the vacuum pump which only needs to be run until sample is under the required vacuum, at which point the vacuum is kept on the sample by closing the valve at the exit of the sample and the pump is secured electrically.

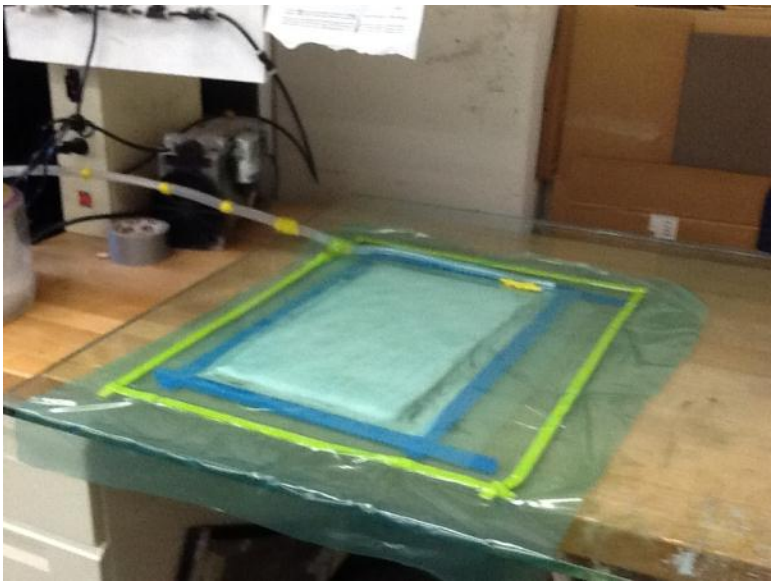

Figure 13 Vacuum set up over composite sample

Once the test pieces are fully cured they can be cut to the desired size, for this the NPS machine shop was utilized; any holes that need to be drilled into the pieces to secure them to testing rigs can also be done after curing also. For the 6- and 10-layer samples only two holes are required to affix the pieces to the test rig. For the frame sample, oversized holes are required evenly spaced out as specified in Appendix A such that sufficient clamping is provided by the frame without cracking the composite sample.

3. Application of Strain Gauges

Strain gauges can be applied to the samples to provide strain information during testing from fluid forces. Strain gages were placed in the x- and y-axis in the center of each sample. Utilizing the symmetry of the sample, a strain gauge could be placed at a quarter location (half-way the distance to the center strain gauges). The procedure to apply strain gages is summarized here as provided by Russell [17]. The orientation scheme of the strain gages on the framed test piece is provided in Figure 14.

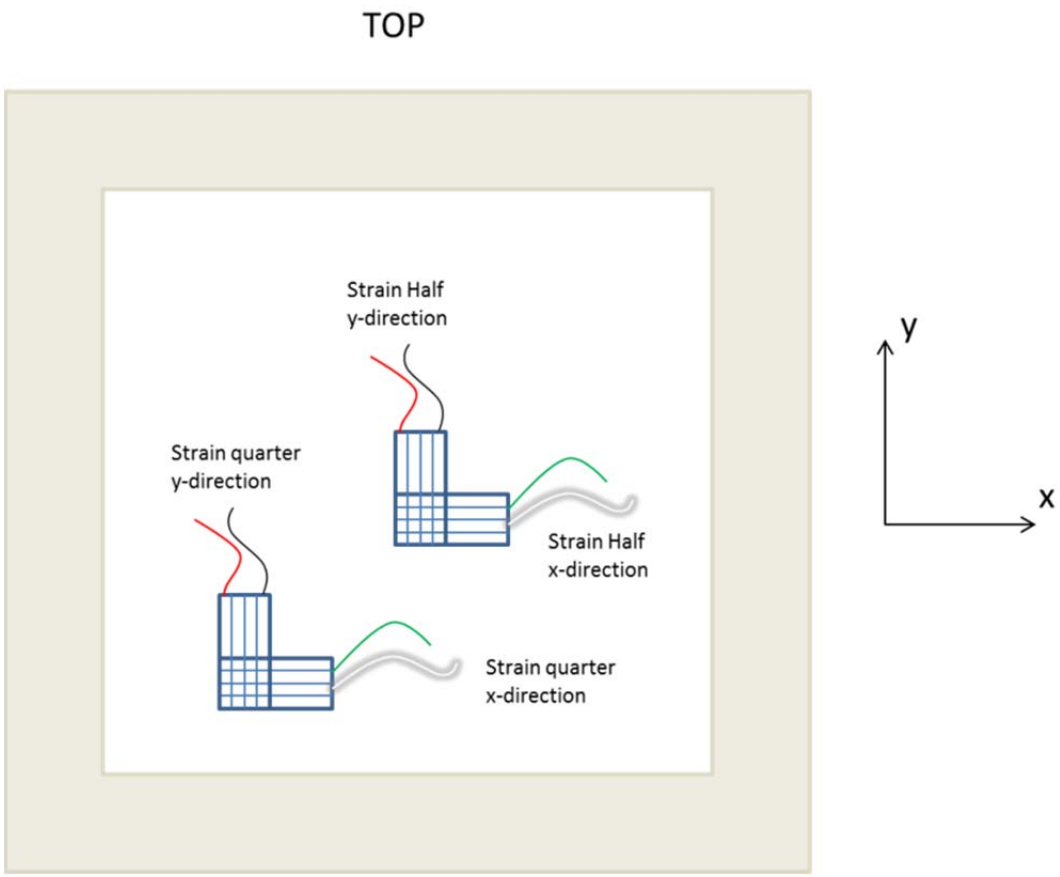

Figure 14 Strain gauge orientation

4. Strain Gauge Procedure

(1) Prepare the plate by placing pencil marking on the x- and y-axis. Sand this area only in the place where the strain gauge is applied, this removes pencil markings but they will remain in unsanded areas for alignment of the gauge. Use acetone and lint free paper to clean any dust from the area where the strain gauge will be placed.

(2) Place the strain gauges on the sample in the orientation aligned with the pencil markings, use a piece of scotch tape to tape the strain gauge in place, then peel this back such that the strain gauge is rolled back facing up off the plate in a loop of tape, the end of the tape remains on the plate acting as a hinge and will allow the gage to be placed back on the plate at the desired orientation.

(3) The bonding agent used is M-Bond AE-10, which comes in a kit by Micro-Measurements. A two-part epoxy it allows only 15 minutes of working time, it is crucial that the strain gages be ready to be applied at the time of mixing the bonding agent. No excess agent should be used, because the loop of tape will be removed after bonding leaving the strain gage in place, so no excess bonding agent should squeeze out from under the strain gauge once placed onto the sticky side of the scotch tape. The cure time once the bonding agent is placed is 48 hours. A small weight is placed on top of the strain gages during the 48 hours to provide clamping pressure for the bonding. Once 48 hours have passed, the scotch tape is removed and the strain gage remains bonded to the sample.

(4) Once the tape is removed, a length of thin gage wire is soldered to the contacts. It is crucial that the correct rosin flux for electronics is used in this step as the heat from the soldering iron is too much for the thin gauge wire and solder and will burn instead of melt. Rosin flux and solder can be purchased from an electronics store and is typically not carried in hardware stores, which only have flux for soldering copper pipe and will not work for this application.

(5) Finally, two coats of waterproofing are applied. The first is M-Coat A, which has a cure time of 48 hours. Enough of this should be applied to sufficiently cover the strain gages and a portion of the wire leads up the protective plastic jacket. After this is cured, a generous amount of RTV coating (MIL-A-46146) is applied, which also should cover the entire strain gage and a portion of the wire's protective jacket. The final cure time for the RTV coating was also 48 hours. Once the coating is cured the sample is ready for testing.

5. Experimental Environment: Towing Tank

To provide a marine environment for the application of transient force to the test pieces, the Naval Postgraduate School's towing tank in the Hydrodynamics Laboratory was used. The tank is 38 feet in length and has a carriage assembly that runs the length of the tank on bearings which provide minimal friction between the carriage and the rails on the tank. Figure 15 shows the overall dimensions of the tow tank. The carriage assembly is multi-use and can be used to mount a variety of test rigs and equipment; for this

experiment the composite pieces were affixed to the carriage via the box tub test rig and a wireless data acquisition system was contained on the carriage

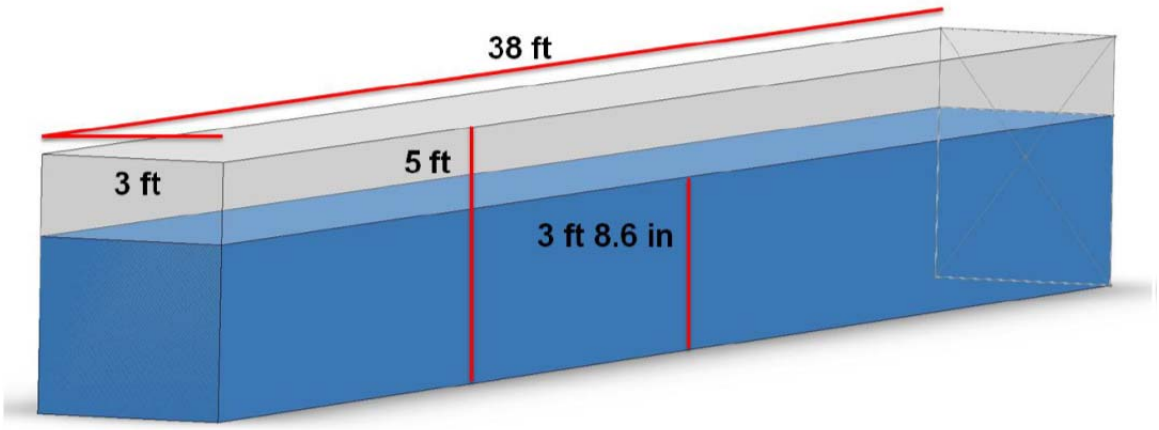

Figure 15 Tow tank dimensions, from [18]

A Baldor Super-E motor capable of 5 horse-power at 230 V, 60 Hz AC power and a maximum speed of 1750 RPM provides motive force for test pieces in the tow tank. The motor is connected to the carriage assembly by a series of pulleys. The motor is controlled by the Baldor VS1SP AC inverter utilizing Voltage/Hz control methods. The controller has numerous modes for operational control which can be set. The controller was only used in Profile Setting which allows a pre-defined speed setting to be entered in the form of RPM/Hz. In Profile Setting, the speed of the motor is changed by changing the frequency supplied to the motor allowing the motor to reach a steady state speed based on that frequency. The minimum speed setting available is 3 Hz while the maximum available is 30 Hz. The maximum speed utilized in this study was 9 Hz as the short length of the tow tank limits how safely the equipment can be used at high speeds. The setting in Hz was compared to the speed of the motor in RPM to verify the linear relation. Figure 16 shows how the increase in motor speed setting in hertz provides a directly linear increase of motor RPM.

Figure 16 Comparison of motor speed setting in hertz to motor RPM

Originally, the carriage only provided the test rig to be mounted perpendicularly to the carriage resulting in the test pieces only able to be tested with the z-axis of the sample parallel to the direction of motion. It was desirable that the z-axis of the test piece be able to be tested at both positive and negative angles to the direction of motion, similar to what a ship's hull would be like against the ocean. The Naval Postgraduate School's machine shop assisted the author in the design and fabrication of an angle selector mount which was added to the carriage as an improvement to the tow tank's testing capabilities. The angle selector allows a range of +/-80° to be tested. The angle selector is shown with the box tube test rig and mounted in close-up in Figure 17 and as an assembly in Figure 18 while Figure 19 shows the angle selector in use in the tank. The schematic for the design is provided as Appendix B.

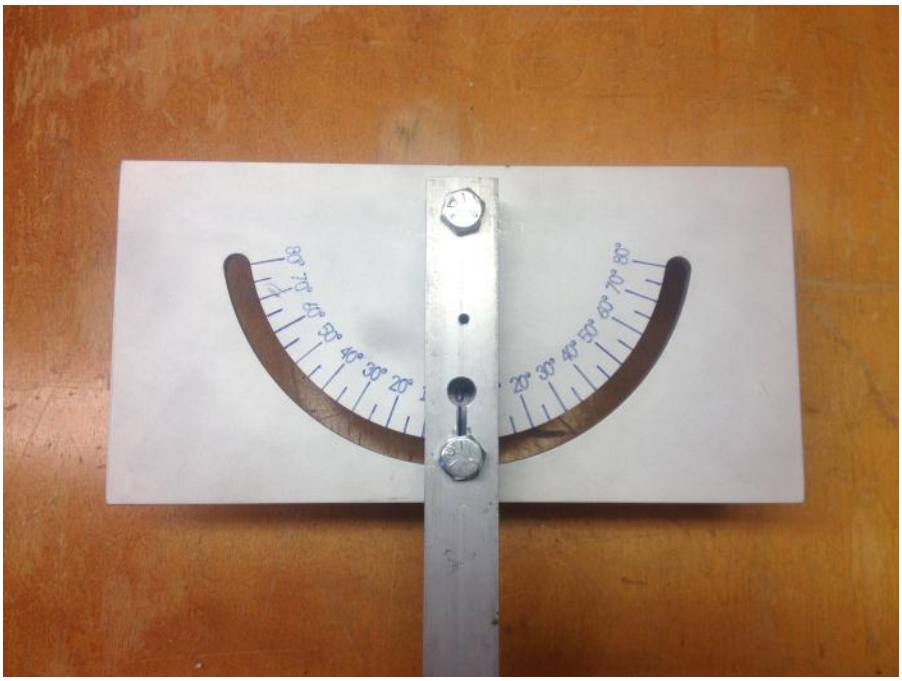

Figure 17 Angle selector close up with box tube test rig cut out to show angle selected

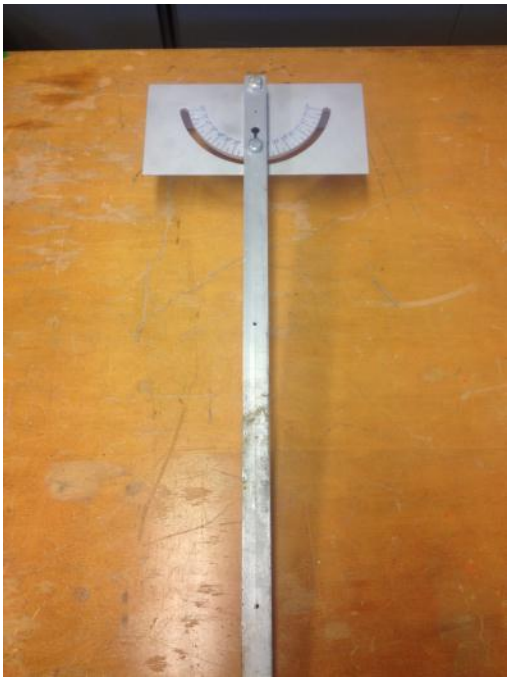

Figure 18 Angle selector with box tube test rig

Figure 19 Angle selector mounted to carriage with frame attached to test rig at -45° in dry tow tank

The tow tank is operated in accordance with the standard operating procedure provided as Appendix C.

6. Data Acquisition System

An electronics data acquisition set up was created by the Naval Postgraduate School's Electronics Technician. Hardware which was used included a Honeywell Model 41 load cell, National Instruments WLS/ENET-9163 wireless data acquisition interface, and National Instruments 9945 quarter inch bridge adapter. The hardware is powered by an external battery which allows wireless transmission to a laptop computer for data storage. The entire electronics set up on top of the carriage is shown in Figure 20.

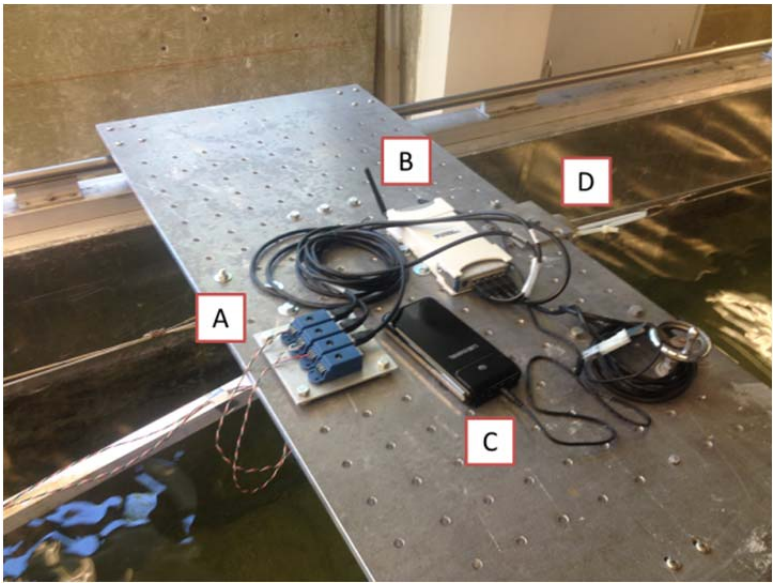

Figure 20 Instrumentation set up with (a) NI 9945 quarter inch adapter harness, (b) NI WLS/ENET-9163, (c) battery pack and (d) Honeywell load cell

A Labview program was written by the Electronics Technician specifically for the tow tank data acquisition system, this system would gather data from the load cell and three strain gage channels. Figure 21 shows a screen shot of this program. To best utilize this program, the option "Save to File" should be selected, which will save all data to a tab delineated text file which can be imported to Microsoft Excel for data analysis. The values recorded are displaced in real time on a graphical strip chart; however this only allows the user to see what is currently being recorded on one channel and does not provide any ability to further analyze data from all channels. The program has been set up by the technician with the appropriate gauge factors such that the output of the time is in seconds, the force is in newtons and the strain gauge channels read out in strain. At any time data can be cleared from the buffer by right clicking on the graphical strip chart output and selecting "Clear Data."

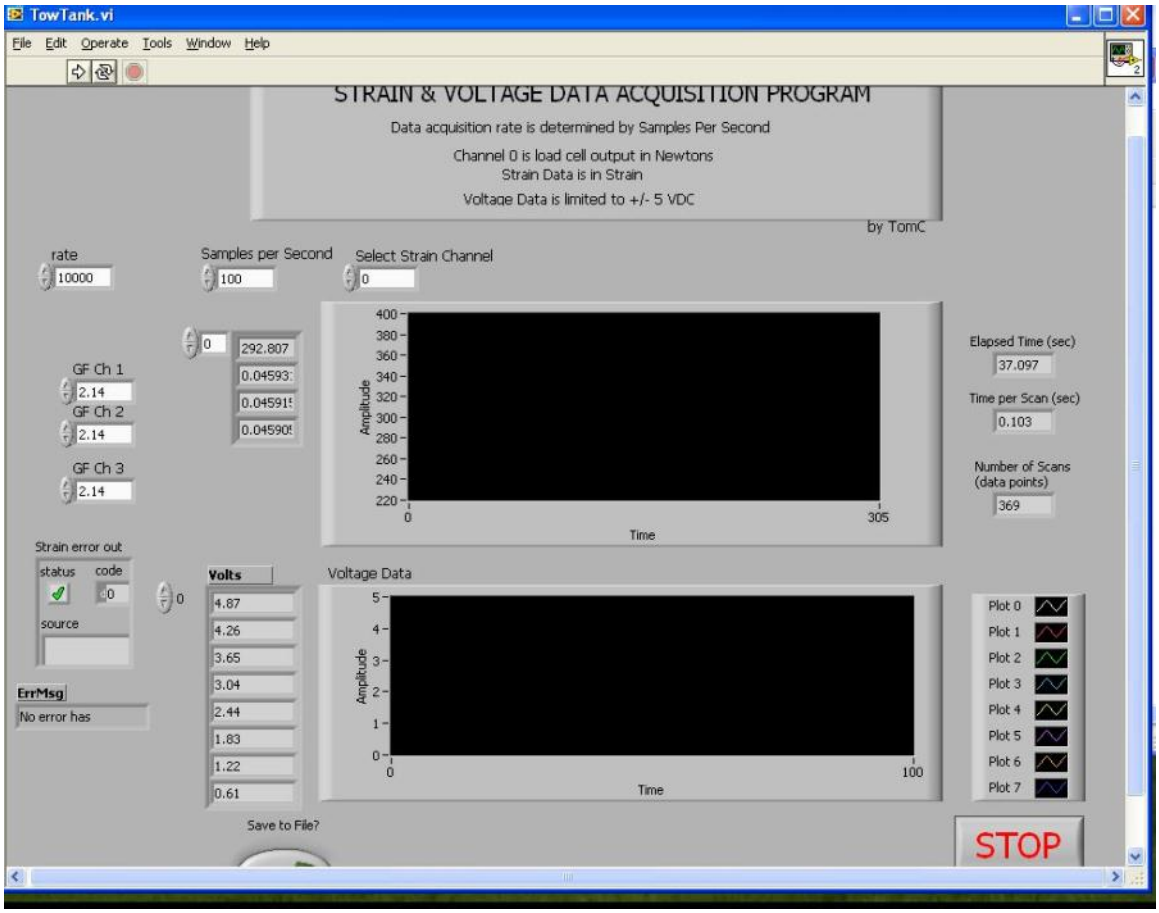

Figure 21 Labview program screenshot for tow tank data acquisition system, from [19]

The load cell is bolted to the carriage and pulled by the drive pulley from the tow tank motor. In conjunction with this experiment, Bryan worked on ensuring calibration of the load cell in [18] which was maintained in calibration for this experiment.

A high-speed camera manufactured by Olympus was utilized to record test runs in the tow tank along with the ability to get time/position data of the test piece during the experiment. The Olympus i-Speed 3 camera was set up to record with centimeter marks ruled on the tank, where playback would allow position to be recorded versus the timestamp of the recording which was to the millisecond. This information can be used to calculate velocity and acceleration. Also, recordings of each test run were saved for future analysis.

C. EXPERIMENTAL PROCEDURE

For each test piece, a test would be run at each speed setting from 3 Hz to 9 Hz. A test would be required to be run in air, which would provide a baseline value that would show the resistance provided by the carriage weight. After this, a test would be required to be run in water. Resolving this data by removing the force required to move the carriage and test piece in air from the force required to move the test piece in water, the force the water imparts on the test piece can be determined as a normalized amount.

Concurrent with each test, the camera would record position and time from the starting position until the test piece was out of the visible range of the camera's view, this information would be collected immediately after the end of the test for velocity and acceleration calculations. Immediately after a test was run, the data would be exported to Microsoft Excel such that position and time data that were manually recorded could be associated with the time, force and strain data for that test run.

It was important to ensure that the water within the tank was set to the same mark as to not introduce a variable depth to the testing depth. This mark was drawn on the tank as being 0.68 meters of water depth. This depth is the deepest the tank can be filled without other equipment mounted on the carriage interfering with water in the tank. At a depth of 0.68 meters, the tank provides 0.27 meters of submergence using the box tube test rig which is also 0.68 meters long. For testing over one day long, this mark must be monitored for evaporation and refilled to the mark.

The testing environment must be controlled such that after every test and the data is recorded, the carriage be brought back to the starting position and sufficient time must pass for any waves from the previous test to die down. With a short tow tank, considerable wave reflection is possible and residual wave action can interfere with readings in subsequent tests. During this time, review of the data and video is possible to ensure the previous run provided worthwhile test information.

Due to the number of test pieces created, and options for testing, Table 4 summarizes the test plan. All test runs were performed at all speed selections between 3 and 9 Hz unless denoted with a *, in which cases the testing speeds were 3, 6 and 9 Hz.

For the rectangular places, the option of having the securing bolts at the top of the plate or the bottom is available when no strain gages are involved. The difference in this orientation is described by Figure 22.

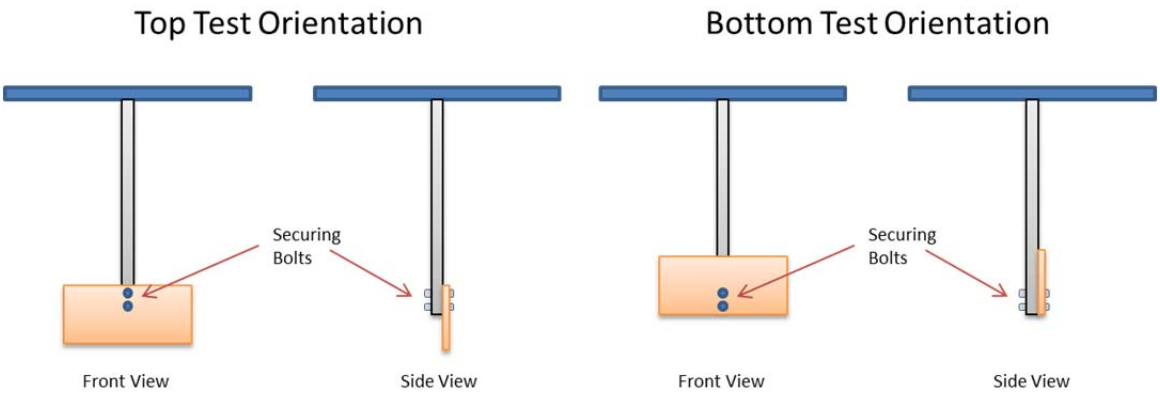

Figure 22 Rectangular test piece orientation

Table 4 Experimental Test Plan

Test Piece	Test Medium	Test Angle	Data Obtained
Aluminum Plate - Top	Air	0°	Force Time vs Position
Aluminum Plate - Top	Water	0°	Force
6 Layer Plate - Top	Air	0°	Force
6 Layer Plate – Top	Water	0°	Force
6 Layer Plate – Bottom	Air	0°	Force
6 Layer Plate – Bottom	Water	0°	Force
10 Layer Plate - Top	Air	0°	Force
10 Layer Plate – Top	Water	0°	Force
10 Layer Plate – Bottom	Air	0°	Force

Test Piece	Test Medium	Test Angle	Data Obtained
10 Layer Plate – Bottom	Water	0°	Force
Frame with 6 Layer Plate	Air	0°	Force Time vs Position Strain
Frame with 6 Layer Plate	Air	+/-70°	Force Strain
Frame with 6 Layer Plate	Water	0°	Force Time vs Position Strain
Frame with 6 Layer Plate	Water	+/-45°	Force Strain
Frame with 6 Layer Plate*	Water	+/-40°	Force Strain
Frame with 6 Layer Plate*	Water	+/-35°	Force Strain
Frame with 6 Layer Plate	Water	+/-30°	Force Strain
Frame with 6 Layer Plate*	Water	+/-25°	Force Strain
Frame with 6 Layer Plate*	Water	+/-20°	Force Strain
Frame with 6 Layer Plate	Water	+/-15°	Force

Test Piece	Test Medium	Test Angle	Data Obtained
			Strain
Frame with 6 Layer Plate*	Water	+/-10°	Force
			Strain
Frame with 6 Layer Plate*	Water	+/-5°	Force
			Strain

D. NOMENCLATURE

A convention is needed to associate specific terms and meanings to eliminate confusion. Part of the experiment investigates the acceleration and velocity of each data set at a speed setting. "Speed Setting" refers to the motor speed specified in Hz. It should be understood that each case may have a different linear speed based on Figure 16. Due to the limitations on optics of the camera versus the length of tank, when investigating the acceleration and velocity response, multiple runs will be taken with measurements in different sections of the tank to get a complete understanding of the velocity profile. A generic velocity profile is shown in Figure 23 where acceleration and steady state velocity regions are along with the two measuring stations called "Starting Position" and "Developed Region."

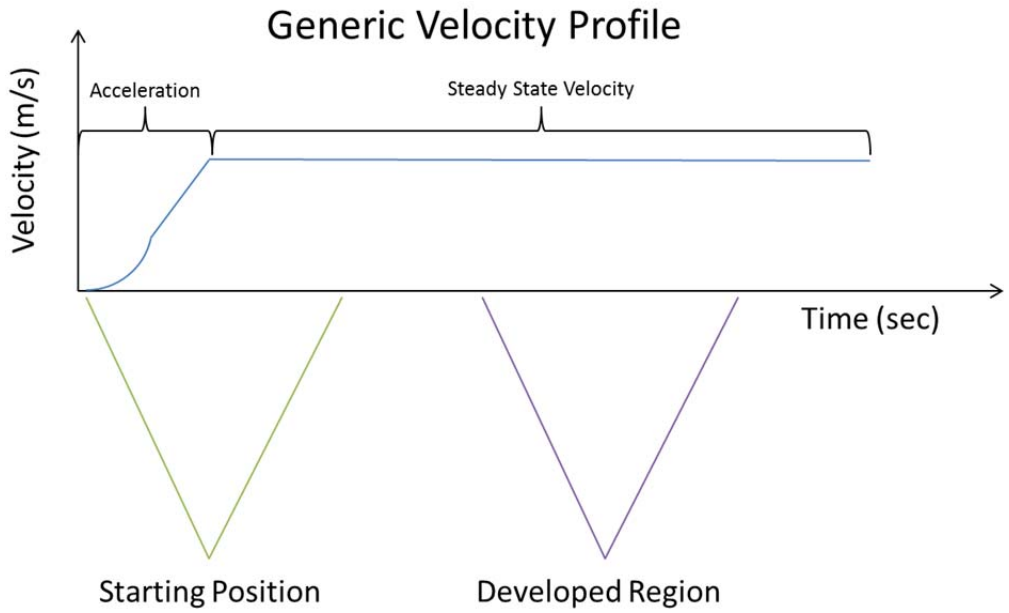

Figure 23 Nomenclature associated with velocity testing

The raw data gathered from the data acquisition system cannot start instantaneously with motion as the operator is manipulating the tow tank motor controller, high speed camera and data acquisition system in order to perform a test. An example of the raw test data is provided in Figure 24 with labeling of the terminology associated with specific events. It is assumed that the transient zone in this data corresponds to the acceleration of the velocity profile.

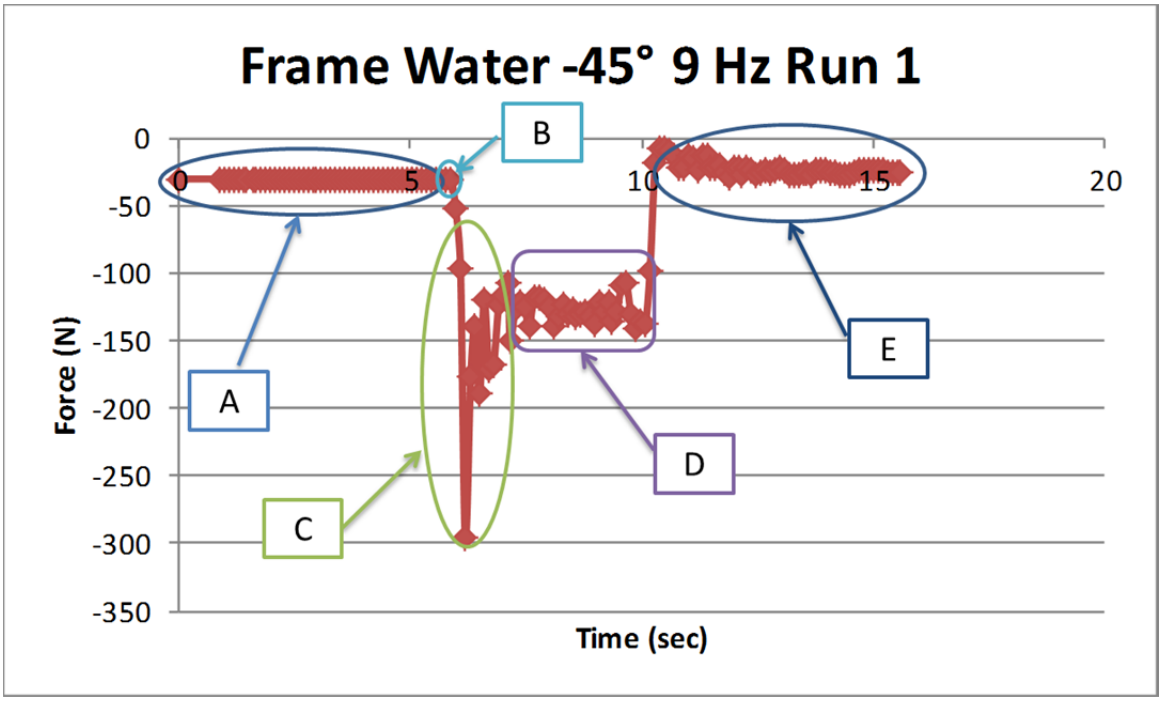

Figure 24 Nomenclature associated with data acquisition system (A) static force, (B) starting point where t=0 and F=0 once normalized, (C) transient zone, (D) steady state zone, and (E) post run static force

For the purposes of this experiment, positive degrees point the test rig forward while negative degrees point the test rig in the reverse direction. A degree reading of 0° is the box tube test rig perpendicular to the carriage. The diagram in Figure 25 is provided to describe the angle selection scheme at the extreme angles available of +/- 80º. The diagram Figure 26 further shows the angle scheme along with the relative locations of testing equipment. An angle of 0º is considered the neutral position while positive angles are positive position of the framed composite test piece and negative angles correspond to a negative position of the test piece

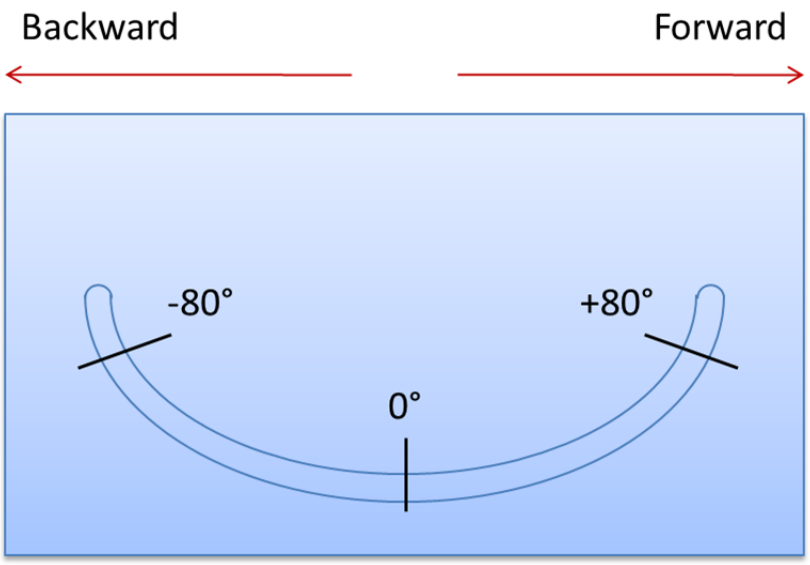

Figure 25 Angle selector orientation scheme

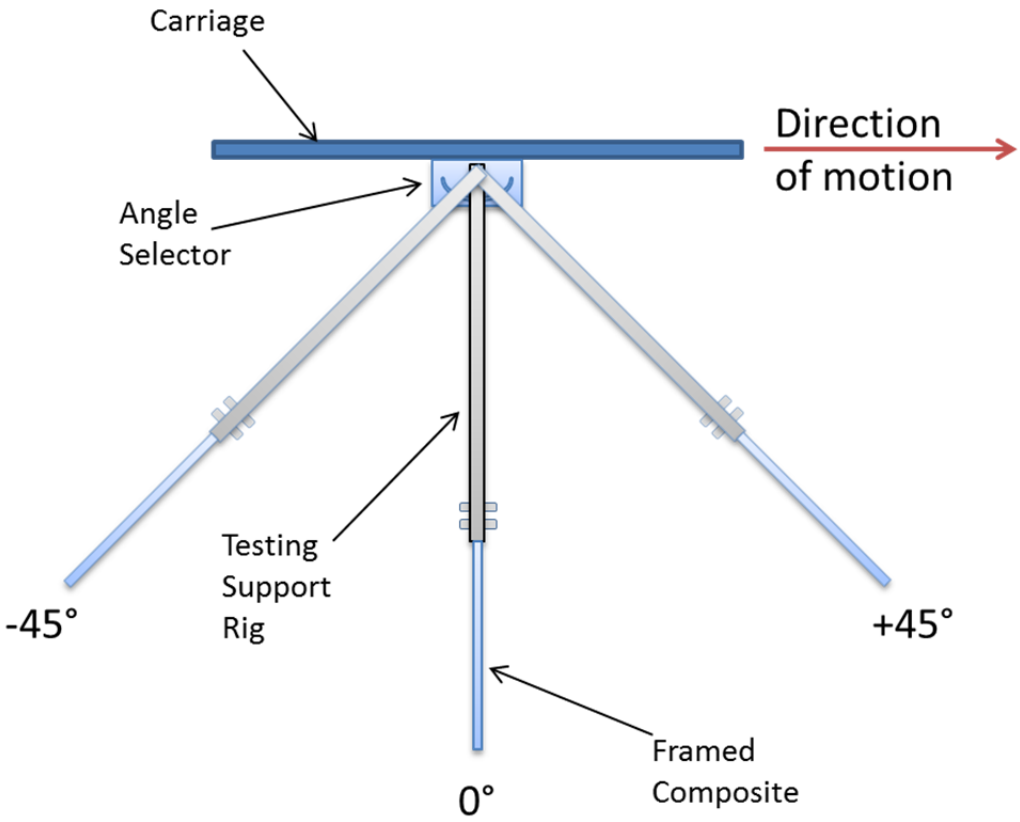

Figure 26 Angle positions and components

III. DATA COLLECTED AND ANALYSIS

A. VELOCITY COMPARISONS

With the test plan showing numerous cases to run with different objects at different speeds and considering Figure 16 demonstrating a slowdown of the Baldor motor with resistance applied, it was important to gather data on each case of speed. Furthermore, as investigated by Knutton in [10] the nature of the velocity profile is an important consideration for FSI models.

1. Position versus Time

Position versus time data was obtained using the methodology described in Chapter II. In the starting region, a second order polynomial line was fit to the accelerating period into the initial states of the steady state velocity region by manually setting the initial position and time as 0. A third order polynomial line was also fit to this data to give a better estimate of acceleration by taking two derivatives of the equation for position as a function of time; the second order polynomial only provides average acceleration in the transient region whereas the third order polynomial provides acceleration as a function of time. The derivation through to acceleration is provided as a table as well as a degree of fit (R^2 of 1 is best fit possible).

The steady state region was investigated to get steady state velocity. In this region velocity is a constant value and acceleration is zero so a linear fit was used. Also, some cases observed position versus time in the developed region to further verify steady state velocity.

2. Velocity versus Time

Velocity data is obtained from the position data by applying a backwards differencing scheme. Once this data was observed, three situations were possible for the transient region. In one situation, the velocity could be linearly increasing at a constant rate, in another situation velocity could be increasing quadratically, and finally the

increase in velocity could be a combination of both linear and quadratic increase. Therefore both linear and polynomial equations are fit to the transient region.

For the linear equation, the equation for final (steady state) velocity should be in the form of $u_f = u_i + at$ where time (t) is graphed on the x-axis, so this should be the form of the trend-line used in the transient region. Since it is known that velocity initial is 0 m/s, the trend-line was forced to have an intercept of 0. For the polynomial equation, the equation for polynomial acceleration is set to a second order polynomial with an initial velocity intercept set to 0.

The Transient to Steady State transition was initially set by visual observation then refined by investigating the acceleration term of the trend-line equation (smaller acceleration is more steady state). Because the transition is not perfectly known, the transition point is included in both the transient and steady state regions. This part of the investigation required a re-visitation of the position versus time data to refine the transition to steady state velocity

Finally, initial data sets had a central differencing scheme applied to investigate if this provided further insight into the velocity profile. Although the addition of the central differencing method provides slightly different data points, it does not change the overall outcome of the analysis and therefore the backwards difference analysis was used on subsequent data sets.

3. Aluminum in Air

Using the weight of carriage with the aluminum sample attached, the starting position was recorded to obtain position vs time and then calculate velocity vs time. For the 3 Hz speed setting this data is provided in Figure 27 and Figure 28. The Remainder of the speed settings are provided in Appendix D. The results of all cases steady state velocity are summarized in Table 5 and provided graphically in Figure 29.

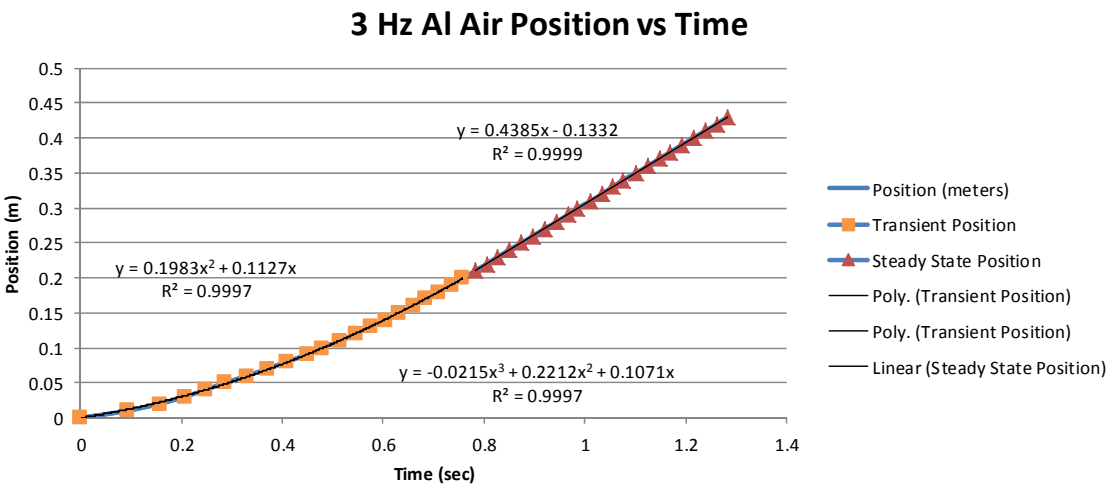

Figure 27 Aluminum sample position vs time at 3 Hz speed setting

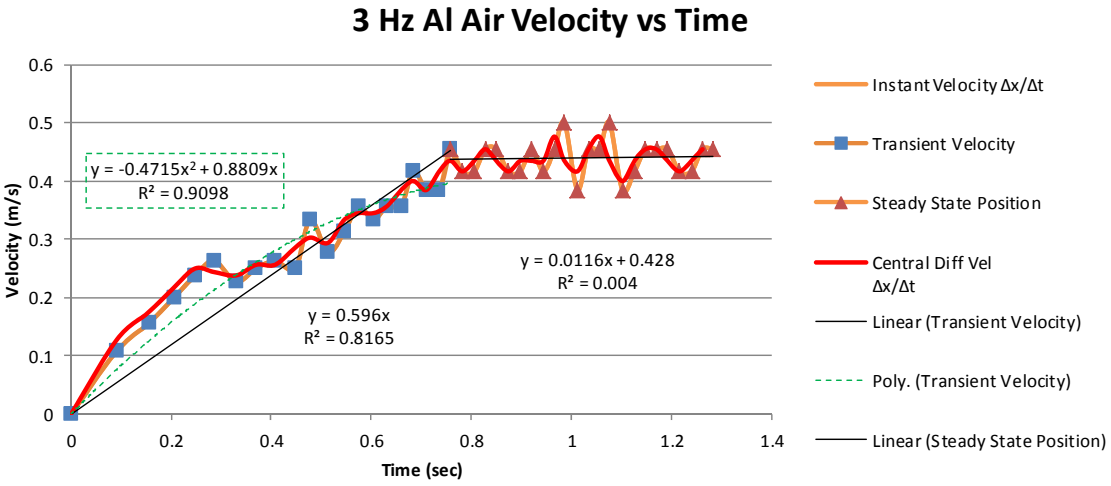

Figure 28 Aluminum sample velocity vs time at 3 Hz speed setting

Table 5 Aluminum steady state starting velocity in air

Speed Setting Hz	Min Reading (m/s)	Average Speed (m/s)	Max Reading (m/s)
3	0.38	0.44	0.50
4	0.50	0.58	0.71
5	0.63	0.76	0.83
6	0.83	0.92	1.00
7	0.83	1.10	1.25
8	1.00	1.30	1.67
9	1.25	1.48	1.67

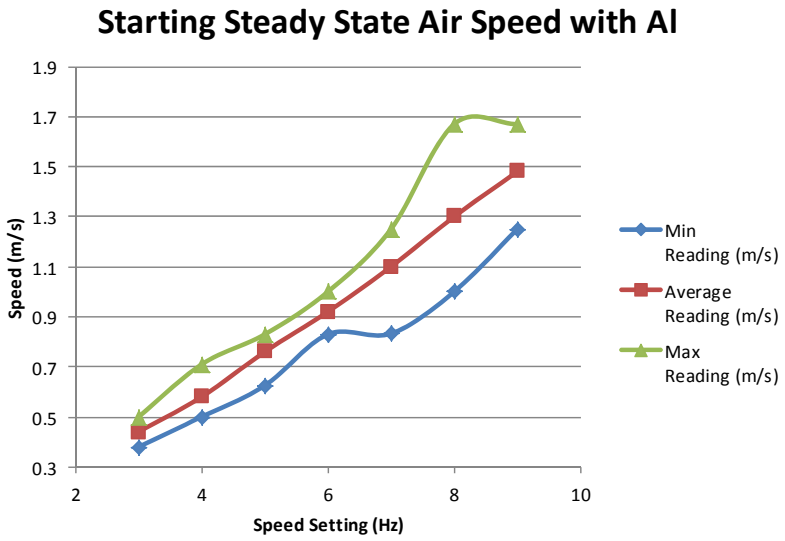

Figure 29 Aluminum sample starting steady state velocity

The aluminum in air starting velocity shows a velocity profile that may start quadratic but transitions to a linear increase until steady state velocity is reached. This phenomenon is hard to understand because it appears that at low speeds it is negatively quadratic while at higher speeds it is positively quadratic. This information can be considered compared to the computer FSI modeling analysis performed by Knutton in [10]. He considered separate cases of step increases in acceleration along with monotonically increasing, linearly increasing and monotonically decreasing acceleration. In practice, there is a combination of these profiles and no one case can be used to describe the nature of the velocity profile. The average starting steady state velocity for the aluminum sample in air shows a strong linear relationship between speed in m/s and the speed setting in Hz which correlates to the control setting for the motor.

4. Six-Layer Composite with Frame in Air

Similar to the aluminum in air test, the same test was done with the frame attached. For the 3 Hz speed setting this data is provided in Figure 30 and Figure 31. The remainder of the speed settings are provided in Appendix D. The results of all cases steady state velocity are summarized in Table 6 and presented graphically in Figure 32.

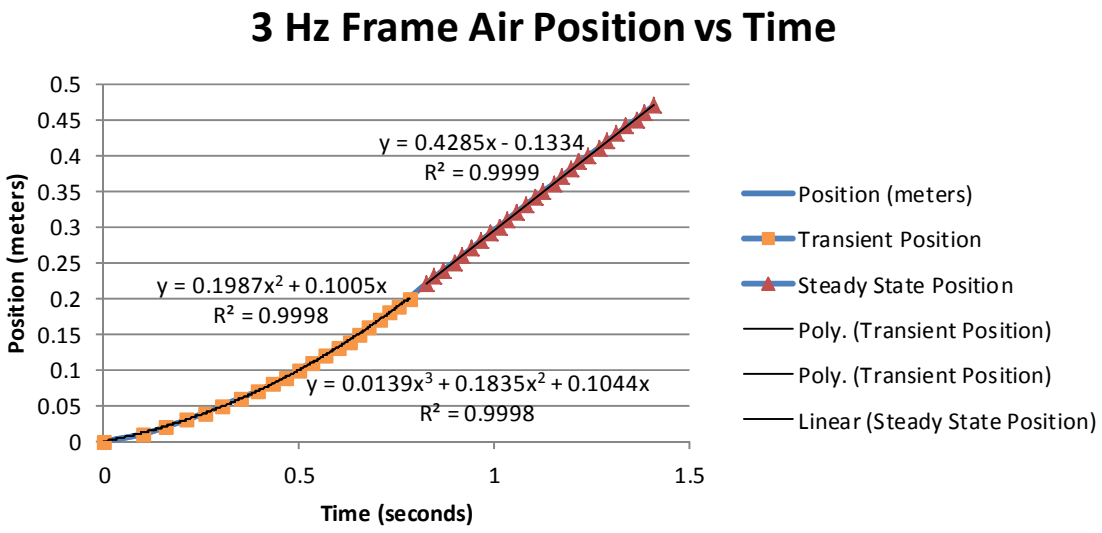

Figure 30 Frame position vs time at 3 Hz speed setting

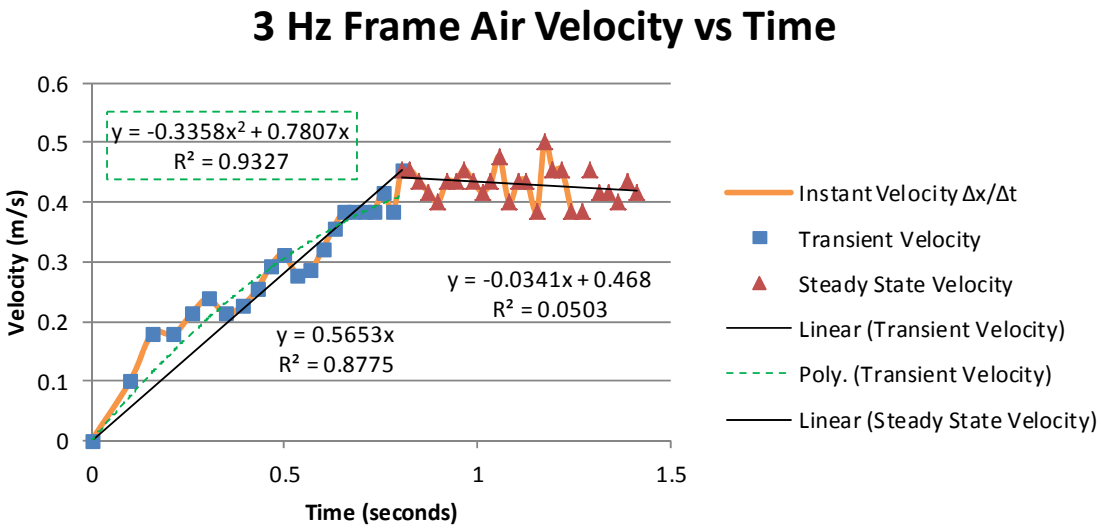

Figure 31 Frame velocity vs time at 3 Hz speed setting

Table 6 Frame with six-layer composite steady state starting velocity in air

Speed Setting Hz	Min Reading (m/s)	Average Speed (m/s)	Max Reading (m/s)
3	0.38	0.43	0.50
4	0.45	0.59	0.67
5	0.63	0.73	0.83

Speed Setting Hz	Min Reading (m/s)	Average Speed (m/s)	Max Reading (m/s)
6	0.83	0.92	1.00
7	0.83	1.05	1.25
8	1.00	1.18	1.67
9	1.25	1.50	1.67

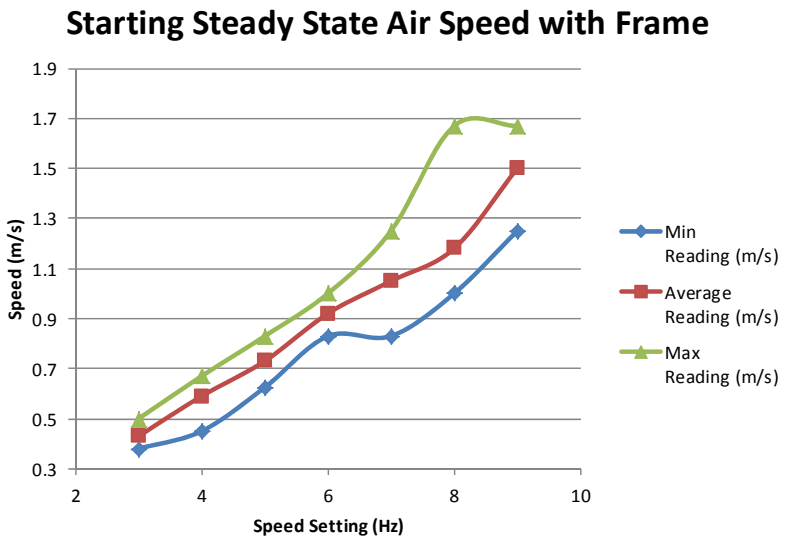

Figure 32 Frame starting steady state velocity in air

Frame velocity profiles look very similar to the aluminum profiles. The same quadratic to linear increase is observed while velocity is increased and once again it appears that at low speeds the quadratic increase is negative while at speed settings above 5 Hz the quadratic increase changes to positive quadratic. This further reinforces the application of the velocity profile that must be considered if a computer modeled FSI will be performed of these scenarios. Again the steady state speed in the starting region is linearly increasing however speed settings around 7 and 8 Hz start to show divergence from the linear increase.

5. Developed Speed of Six-Layer Composite with Frame in Air

The developed region was investigated to further understand steady state speed. The frame sample was tested in this region in air. The results of this test are presented in Table 7 and graphically in Figure 33.

Table 7 Frame with six-layer composite steady state developed velocity in air

Speed Setting Hz	Min Reading (m/s)	Average Speed (m/s)	Max Reading (m/s)
3	0.43	0.44	0.45
4	0.59	0.60	0.62
5	0.74	0.77	0.77
6	0.84	0.93	1.04
7	1.05	1.07	1.09
8	1.20	1.22	1.25
9	1.33	1.37	1.43

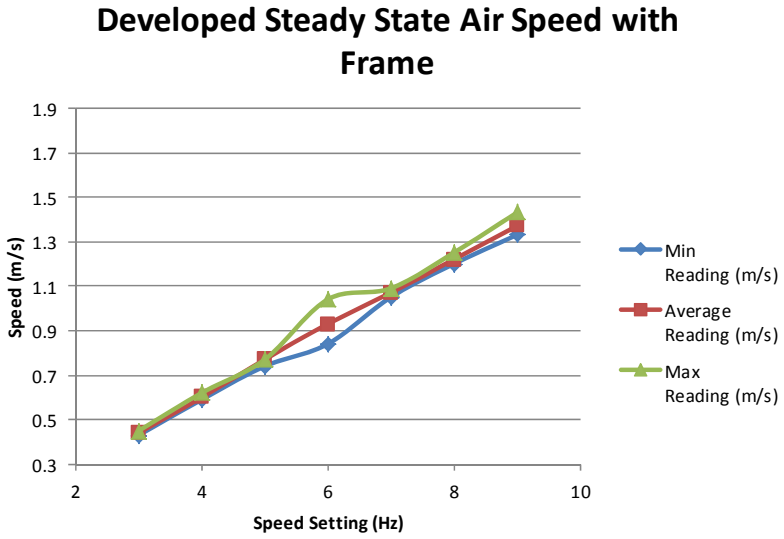

Figure 33 Frame developed steady state velocity in air

Developed speeds show a very linear increase with little variation between the measured maximum and minimum instantaneous speeds from the average speeds. This is unlike the starting region which does not show as much of a linear correlation between the increase in speed for each speed setting and shows great variation between the minimum and maximum instantaneous speeds from the average velocity. This could be because it is up to interpretation when exactly steady state speed is reached in the starting region and steady state speed may not be truly reached in this region even though it is

very close to being realized. Also, vibration of the test rig could introduce changes to the maximum and minimum instantaneous speed of the test piece even though the motor and carriage system is pulling at a constant velocity. Once the test rig has less vibration, for example later in the tank in the developed region, variation of the instantaneous velocity might disappear.

6. Six-Layer Composite in Frame in Water

For the frame, the same test done in air was performed in water. The starting position graphs for the 3 Hz case are provided in Figure 34 and Figure 35 while the remainder of the cases are provided in Appendix D. A summary of the steady state velocity at the starting position is provided in Table 8 and graphically in Figure 36.

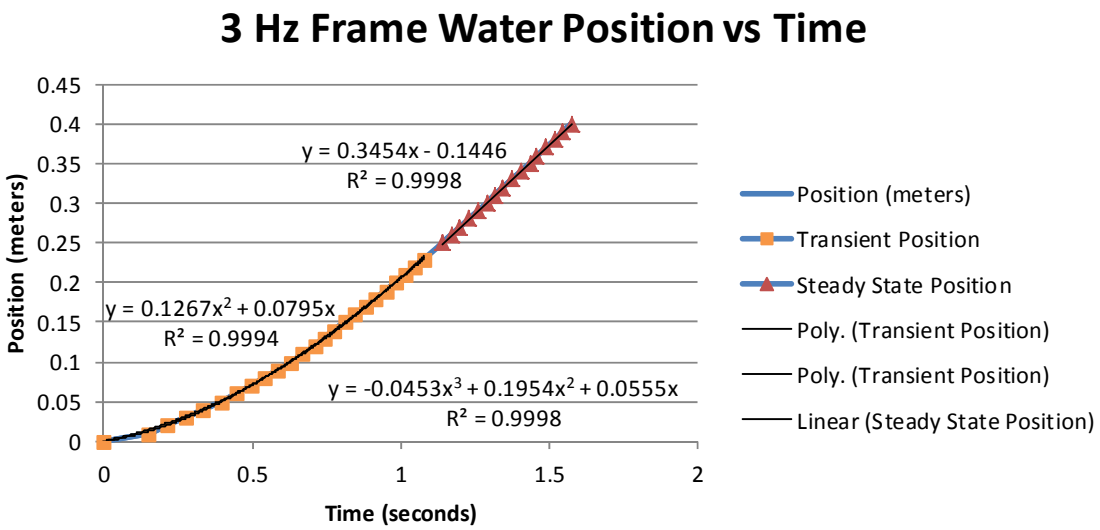

Figure 34 Frame position vs time at 3 Hz speed setting

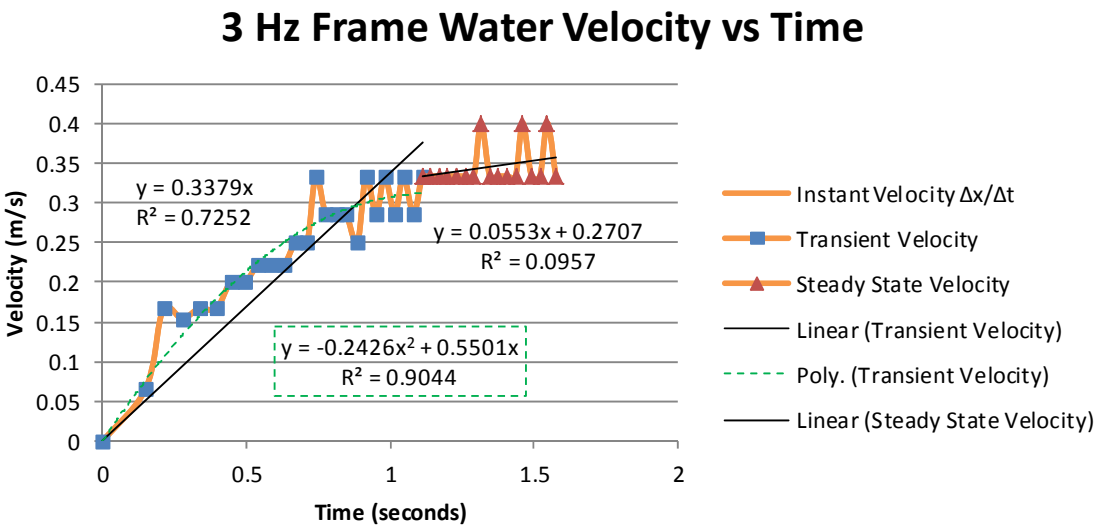

Figure 35 Frame velocity vs time at 3 Hz speed setting

Table 8 Frame with six-layer composite steady state starting velocity in water

Speed Setting Hz	Min Reading (m/s)	Average Speed (m/s)	Max Reading (m/s)
3	0.33	0.35	0.40
4	0.40	0.52	0.67
5	0.50	0.63	0.67
6	0.67	0.78	1.00
7	0.67	0.83	1.00
8	0.71	0.90	1.00
9	0.80	0.92	1.00

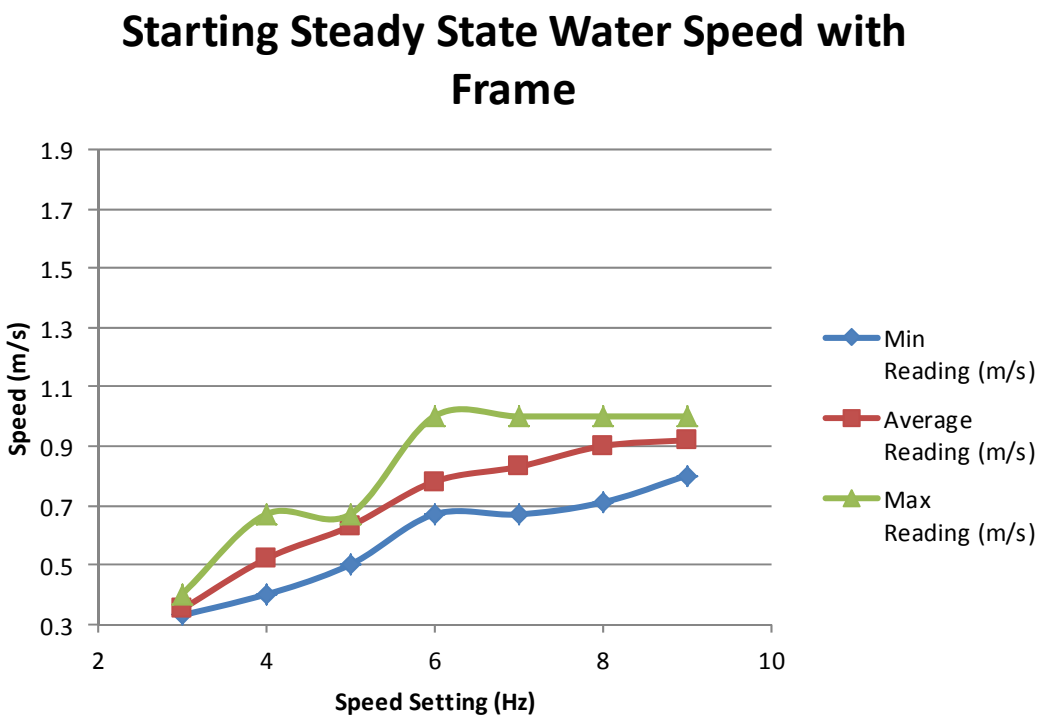

Figure 36 Frame starting steady state velocity in water

The introduction of water provides a great deal of change to the velocity data. The velocity increase still demonstrates the quadratic to linear increase seen in air however this period is much longer with water, specifically the linear portion shows increase in duration. The quadratic increase appears to be positive in all cases and much more pronounced at higher speeds. The steady state speed no longer shows the linear increase but rather a plateau of speed specifically between 8 and 9 Hz speed setting. From the individual velocity profiles it can be seen that since the acceleration portion is longer, the steady state portion available for analysis is much smaller than previously available in the air testing.

7. Developed Speed of Six-Layer Composite with Frame in Water

The final position and time data was for the framed composite in water. The results of this test are presented in Table 9 and graphically summarized in Figure 37.

Table 9 Frame with six-layer composite steady state developed velocity in water

Speed Setting Hz	Min Reading (m/s)	Average Speed (m/s)	Max Reading (m/s)
3	0.40	0.40	0.41
4	0.55	0.56	0.56
5	0.69	0.71	0.71
6	0.85	0.86	0.86
7	0.94	0.96	0.98
8	1.09	1.08	1.14
9	0.96	1.11	1.16

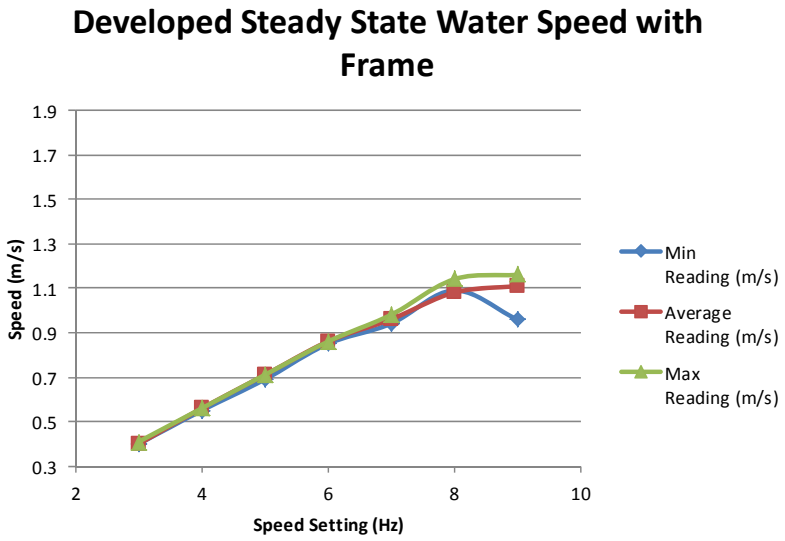

Figure 37 Frame developed steady state velocity in water

The developed speed in water shows a very tight data pattern and linear increase except at higher speeds. It was noticed in the starting data that 8 and 9 Hz there was a plateau in speed which is also pronounced in the developed region. At these speeds the data also shows greater variation which may mean at these high speeds vibration effects continue far down the tank or possibly that the motor has difficulty maintaining speed. This last possibility is unlike because Figure 16 shows that motor speed RPM in water maintains a linear increase even at speeds 8 and 9 Hz.

8. Comparison of Velocity Results

To determine how one case varied from the others, a comparison was performed. Overall the average velocities for framed composite can be graphed together in Figure 38

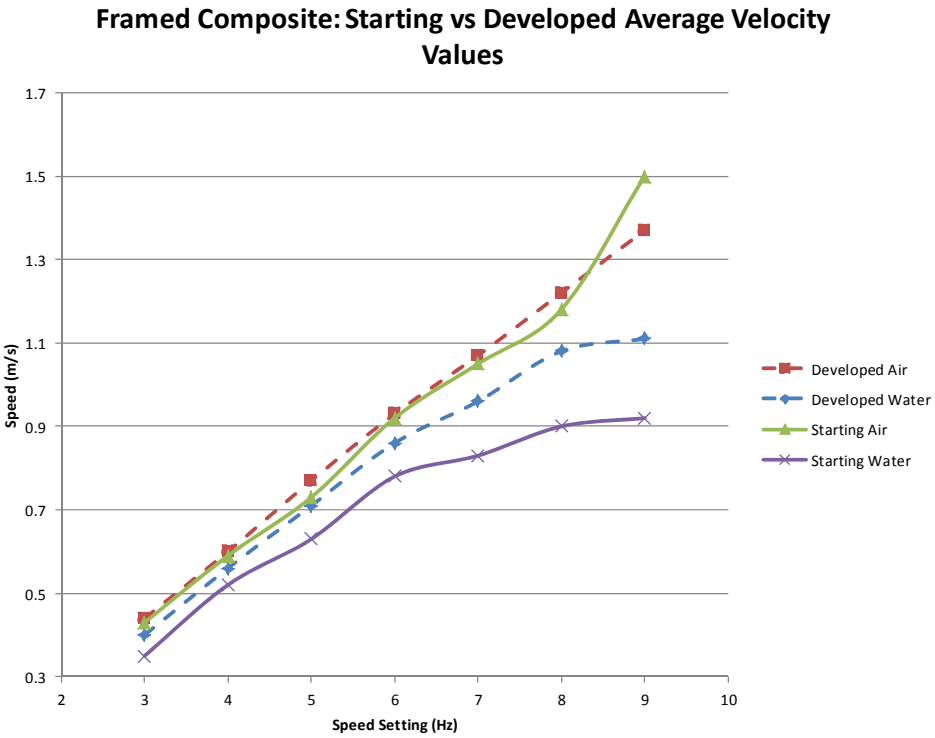

Figure 38 Framed composite summary of average velocities

A difference between the starting velocities of the aluminum sample and the frame in air was examined. The difference between these two cases is provided in Table 10 and graphically in Figure 39.

Table 10 Difference between aluminum sample and framed composite in air starting steady state velocities

Speed Setting Hz	Min Difference (m/s)	Average Difference (m/s)	Max Difference (m/s)	% Avg Difference
3	0	0.01	0	2.3%
4	0.05	-0.01	0.04	1.7%
5	0	0.03	0	4.0%

Speed Setting Hz	Min Difference (m/s)	Average Difference (m/s)	Max Difference (m/s)	% Avg Difference
6	0	0	0	0%
7	0.003	0.05	0	4.7%
8	0	0.12	0	9.7%
9	0	-0.02	0	1.3%

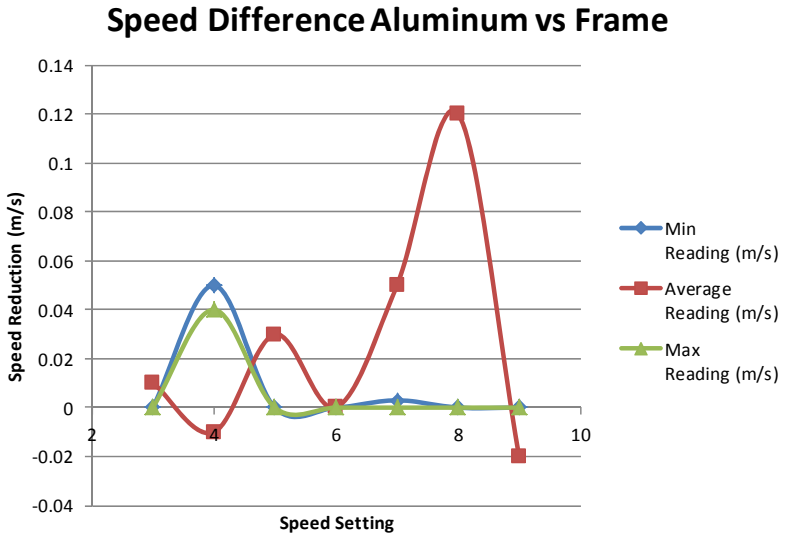

Figure 39 Starting velocity difference in air

Although there is some variation between the aluminum plate and framed composite, the percentage of change at each speed setting is quite low. The main resistance with air is the weight of carriage and test equipment. There is no appreciable weight change between the aluminum plate and frame with composite (which is made of aluminum). Most variation between these cases can be due to the variation of the starting data and that there may be vibrations and the test piece may be close but not at the steady state speed.

It was observed that once the testing medium is changed to water that the speed of the test piece decreases as more force is required to move the test piece. To determine what kind of slowdown was being experienced, a comparison of the starting speed of the framed composite in air was compared to the developed speed. This is provided in Table

11 and graphically in Figure 40. Likewise, the developed data can be compared in a similar manner. This summarized in Table 12 and graphically in Figure 41.

Table 11 Slowdown from air to water using framed composite with starting velocity

Speed Setting Hz	Min Difference (m/s)	Average Difference (m/s)	Max Difference (m/s)	% Avg Slowdown
3	0.05	0.08	0.1	20.5%
4	0.05	0.07	0	12.6%
5	0.125	0.1	0.16	14.7%
6	0.16	0.14	0	16.5%
7	0.16	0.22	0.25	23.4%
8	0.29	0.28	0.67	26.9%
9	0.45	0.58	0.67	47.9%

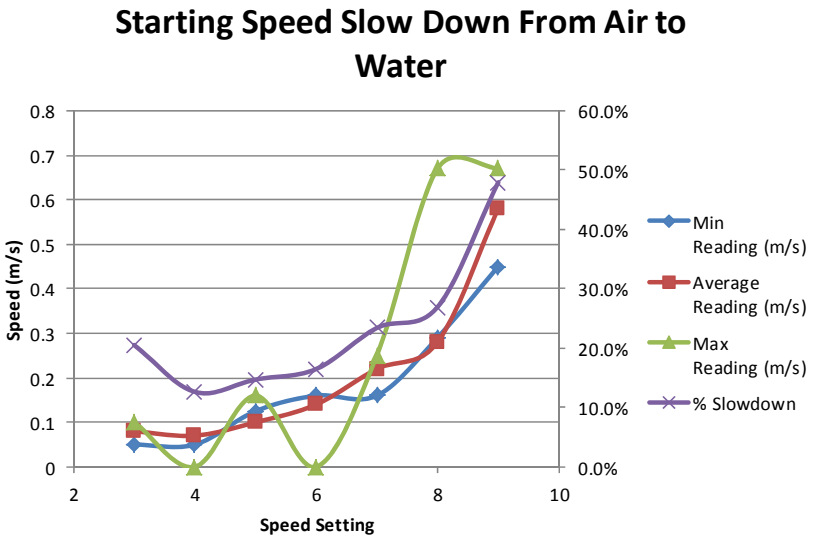

Figure 40 Slowdown from air to water with starting velocity

Table 12 Slowdown from air to water using framed composite with developed velocity

Speed Setting Hz	Min Difference (m/s)	Average Difference (m/s)	Max Difference (m/s)	% Avg Slowdown
3	0.03	0.04	0.04	9.5%

Speed Setting Hz	Min Difference (m/s)	Average Difference (m/s)	Max Difference (m/s)	% Avg Slowdown
4	0.04	0.04	0.06	6.9%
5	0.05	0.06	0.06	8.1%
6	-0.01	0.07	0.18	7.8%
7	0.11	0.11	0.11	10.8%
8	0.11	0.14	0.11	12.2%
9	0.37	0.26	0.27	21.0%

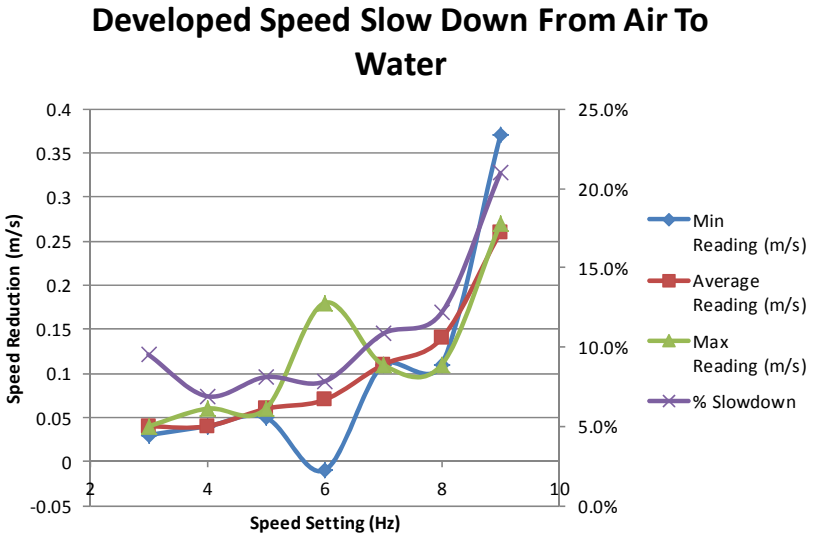

Figure 41 Slowdown from air to water with developed velocity

Most interesting about the slowdown from air to water is a "bathtub effect" for both starting and developed speeds for the percentage of slowdown. In both cases the slowdown at 3 Hz is more pronounced than the following three speeds until the slowdown becomes more pronounced at subsequent speeds of 7, 8 and 9 Hz. This is completely contrary to the results from Figure 16 which show a motor slowdown from air to water but at 3 Hz there is nearly no slowdown and each subsequent speed setting the slowdown grows proportionally.

The final comparison looks at the difference between the starting velocity and developed velocity for the framed composite. This can help provide insight into how well the starting velocity information provides a complete velocity profile in one data set.

If the starting steady state velocity closely matches the developed speed, then the entire speed profile is captured. Table 13 and Table 14 provide a summary of the difference between the starting steady state velocities in water using the framed composite compared to the developed steady state velocity for the same test piece; Figure 42 and Figure 43 provide a graphical summary.

Table 13 Change from starting velocity to developed velocity in air

Speed Setting Hz	Min Difference (m/s)	Average Difference (m/s)	Max Difference (m/s)	% Avg Slowdown
3	0.05	0.01	0.05	2.3%
4	0.14	0.01	0.05	1.7%
5	0.12	0.04	0.06	5.3%
6	0.01	0.01	0.04	1.1%
7	0.22	0.02	0.16	1.9%
8	0.20	0.04	0.42	3.3%
9	0.08	0.13	0.24	9.1%

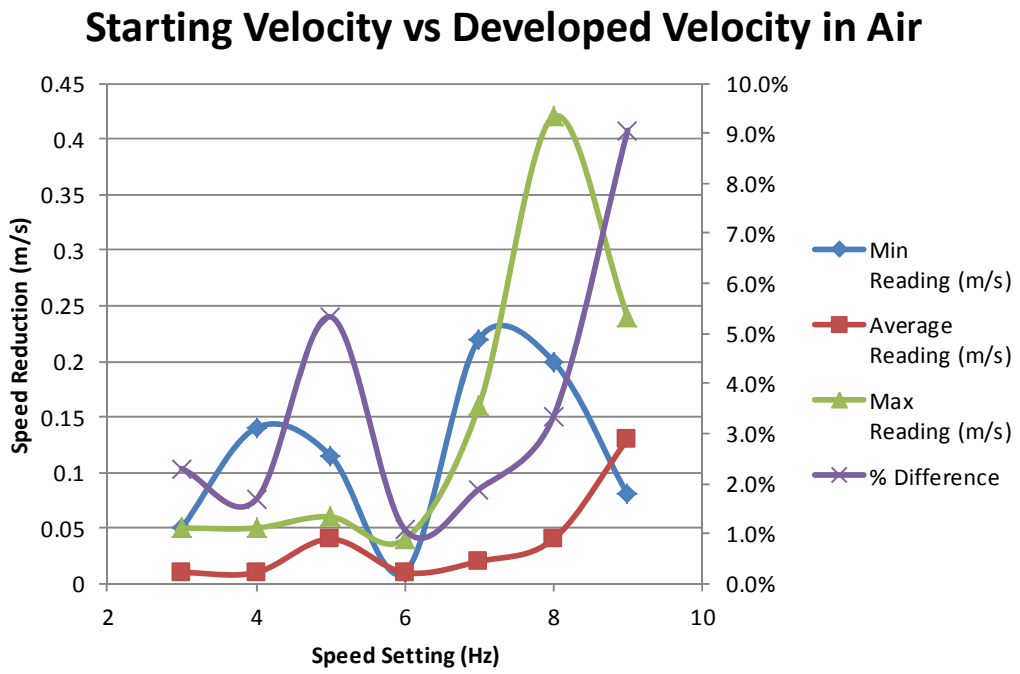

Figure 42 Change in speed from starting velocity to developed velocity in air

Table 14 Change in speed from starting velocity to developed velocity in water

Speed Setting Hz	Min Difference (m/s)	Average Difference (m/s)	Max Difference (m/s)	% Avg Slowdown
3	0.07	0.05	0.01	11.9%
4	0.15	0.04	0.11	6.9%
5	0.19	0.08	0.04	10.8
6	0.18	0.08	0.14	8.9%
7	0.27	0.13	0.02	12.8%
8	0.38	0.18	0.14	15.7%
9	0.16	0.19	0.16	15.3%

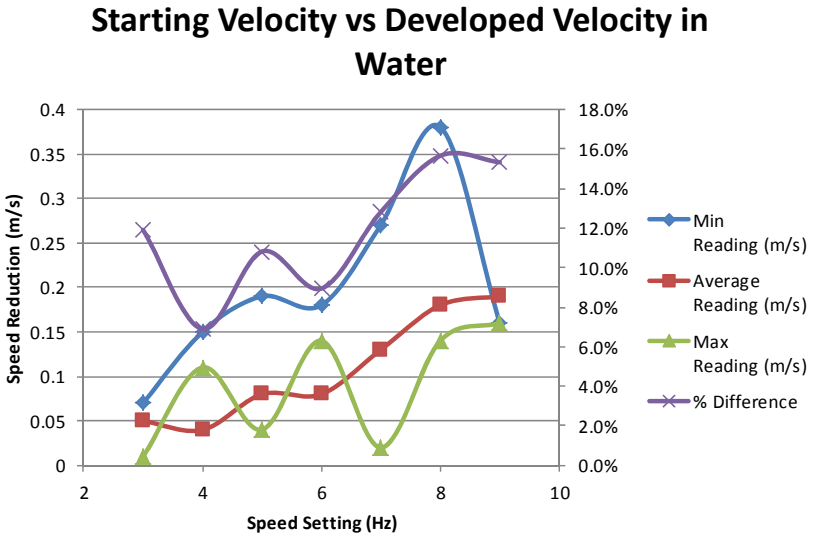

Figure 43 Change in speed from starting velocity to developed velocity in water

There appears to be a slowdown from the starting steady state velocity to the developed velocity but for the air testing this change is very small. It becomes greater when the testing medium is water. However, it was already noticed that the starting velocity in water results in very few test points for steady state velocity. It is difficult to conclude that there is appreciable slowdown in the developed region. When looking at the test data for this scenario in air, at low speeds there is very little difference between starting and developed. This may mean that only at higher speeds could the velocity

profile be perfectly developed right beyond the starting region. This may also be the case for the water scenario where the amount of time needed to reach steady state velocity may be right beyond the measureable edge of the starting region.

9. Acceleration

A prime motivation for investigating the starting region is to determine acceleration. If the starting region is completely outside the starting region's measurable range, knowing acceleration becomes impossible. By taking the steady state velocity and dividing it by the time it takes to reach steady state velocity, the average acceleration can be determined. This was done for the aluminum sample in air, the frame with composite in air and the frame with composite in water and is presented in Figure 44.

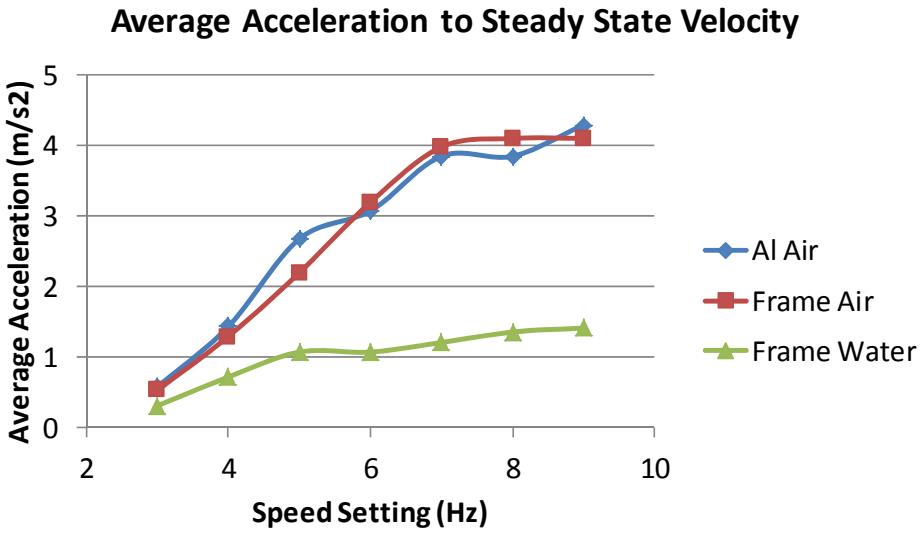

Figure 44 Average acceleration of test pieces

The aluminum and frame comparison in air show very similar acceleration profiles. This also seems to carry over from velocity data that the acceleration begins to plateau at 8 and 9 Hz speed setting. Before this, there is a linear increase in acceleration with speed setting until 7 Hz. In water this is not the same case, a much lower acceleration in general and must slower increase from 5 Hz speed setting on.

B. NUMERICAL CALCULATION DATA

As mentioned previously, equation (1) relates force to the square of velocity for the same object in the same medium at the same orientation. Now that velocity has been determined, equation (1) can be used to provide what the theoretical drag force would be on the samples. By using the density of fresh water as the testing medium, density is 998 kg/m^3 [11]. Dimensions for the area of the rectangular test pieces and the frame have already been provided in Chapter II. The coefficient of drag for a flat plate in three dimensional flows with a normal flow stream can be determined from Table 7.3 in [11] as 1.184 for the rectangular test pieces and 1.180 for the frame test piece. The computed force as a function of the actual velocity of the test pieces in the tow tank is provided in Table 15, Figure 45 and Figure 46, it should be noted that as mentioned in analysis of Figure 37, velocity in water is not directly proportional to speed setting.

Table 15 Theoretical drag force for rectangle and framed samples in water

Speed Setting (Hz)	Velocity (m/s)	Rectangle Sample (N)	Framed Composite Sample (N)
3	0.40	5.55	8.75
4	0.56	10.89	17.15
5	0.71	17.50	27.58
6	0.86	25.67	40.46
7	0.96	31.99	50.41
8	1.08	40.49	63.81
9	1.11	42.77	67.40

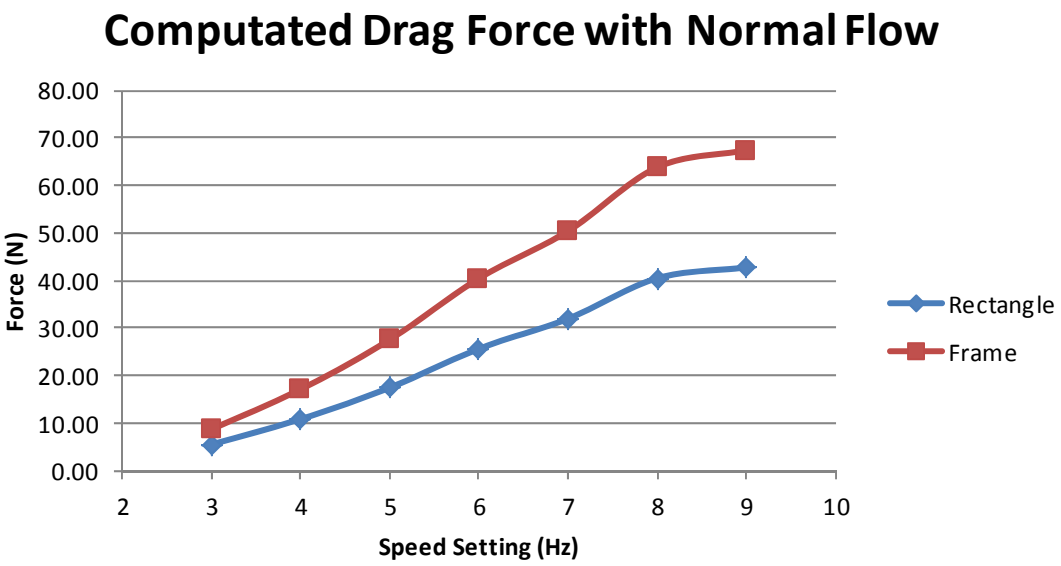

Figure 45 Computed drag force for rectangle and framed composite samples as function of speed setting

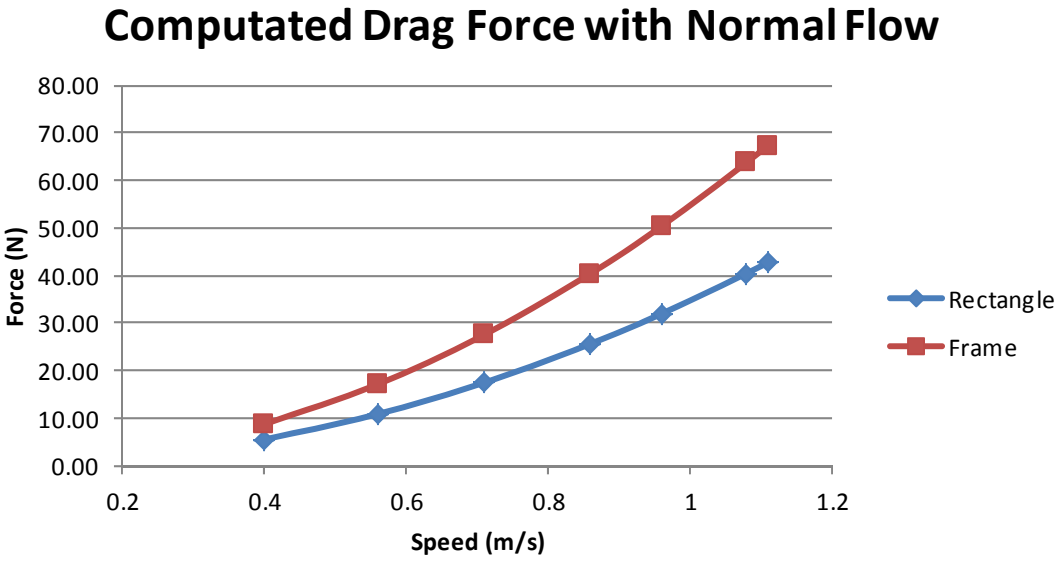

Figure 46 Computed drag force for rectangle and framed composite samples as function of sample speed

Figure 46 shows the quadratic increase in force as velocity increases however Figure 45 shows that when compared to speed setting, the increase is more linear. This is an important observation moving forward with force data which will be compared on a

speed setting comparison because area affects velocity and it was impossible to measure actual velocity of all cases but RPM of the motor was expected to be the same in all cases in the same test medium due to the control setting of the motor. One thing not addressed by the rectangular test pieces is any reduction in apparent area by the composite structures. It is assumed that the aluminum test piece shows no reduction in area under fluid force, however the composite pieces are assumed to reduce apparent area, although slightly, as they deform under load. Also not captured in theoretical computations is any near surface effects that may be experienced as theoretical calculations assume an infinite volume of water. The difference is that in testing, being near walls, reflected waves, and proximity to the surface may change the results. Finally, because changes in relative mass can produce varied responses, the difference in density between a rigid body such as an aluminum plate and water is very large and therefore the response will be easier to quantify. When comparing water and composites though, the densities are much more comparable and therefore understanding the response becomes more difficult.

The test plan calls for testing the framed composite sample at angle which changes the frontal apparent area of the plate. Using the convention for angle described in Figure 25, Table 16 and Figure 47 shows the apparent area along with drag force for this angle. This computation demonstrates that in theory, force response should be equal regardless of positive or negative angle, but this requires an infinite body of water for this assumption to be realized. In a finite body of water such as the NPS tow tank environment it will be difficult to recreate these results but they do provide an overall idea of how the drag response should behave with response to position angle changes.

Table 16 Theoretical forces of framed composite at testing angles

Angle Setting		**-45º**	**-30º**	**-15º**	**0**	**+15º**	**+30º**	**+45º**
Apparent Area (m^2)		**0.066**	**0.080**	**0.090**	**0.093**	**0.090**	**0.080**	**0.066**
Speed Setting (Hz)	**Velocity (m/s)**	**Drag Force (N)**						
3	0.40	6.21	7.61	8.48	8.78	8.48	7.61	6.21
4	0.56	12.17	14.91	16.63	17.22	16.63	14.91	12.17
5	0.71	19.57	23.97	26.73	27.68	26.73	23.97	19.57

Angle Setting		-45°	-30°	-15°	0	+15°	+30°	+45°
Apparent Area (m^2)		0.066	0.080	0.090	0.093	0.090	0.080	0.066
Speed Setting (Hz)	Velocity (m/s)	Drag Force (N)						
6	0.86	28.71	35.16	39.22	40.60	39.22	35.16	28.71
7	0.96	35.78	43.82	48.87	50.60	48.87	43.82	35.78
8	1.08	45.28	55.46	61.85	64.04	61.85	55.46	45.28
9	1.11	47.83	58.58	65.34	67.64	65.34	58.58	47.83

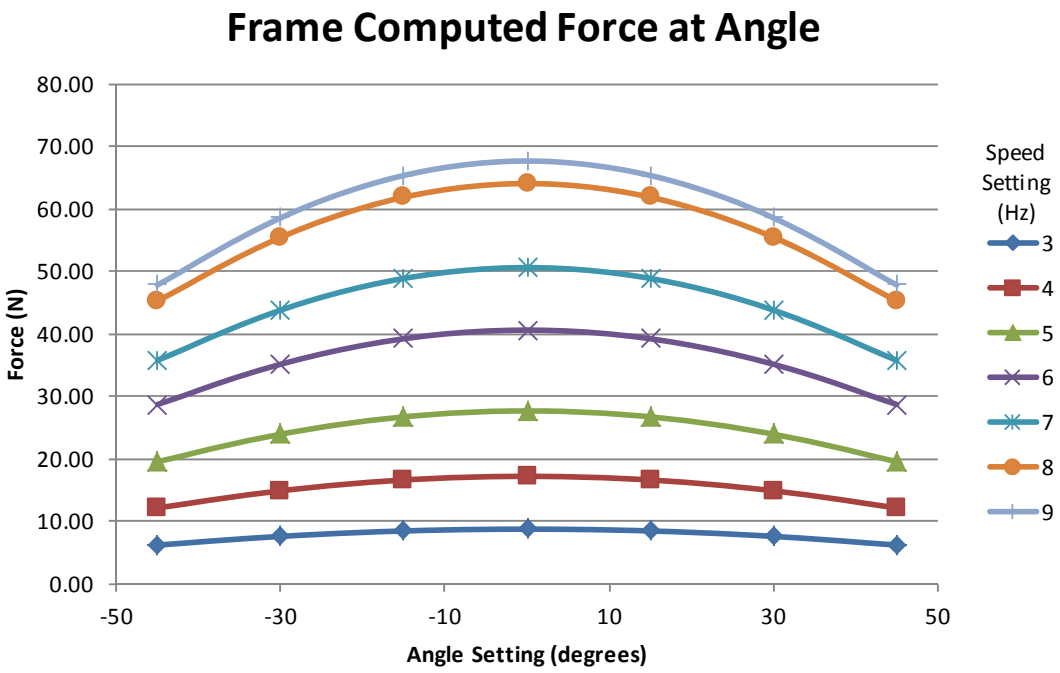

Figure 47 Theoretical framed composite drag force at testing angles

C. RECONFIGURATION OF TANK

During testing the tow tank required repairs for safety and environmental issues. This required complete disassembly of all equipment associated with the tank. Testing needed to be re-performed to assure that the tank was reassembled correctly and that data values provided after repair work was the same as data before repair work. Because the majority of testing performed before tow tank repairs was testing in air, a comparison between air testing with the framed composite before and after tow tank repairs was

performed. A total of three runs before repairs and two comparison runs after repairs were compared on an individual speed basis. During comparison it was determined that the peak magnitude of force was the most comparable across all speeds. Table 17 and Figure 48 provide the comparison of this investigation.

Table 17 Comparison of peak forces before and after tow tank repairs

Speed Setting (Hz)	Run 1	Run 2	Run 3	Comp 1	Comp 2	Percent Change (%)
	Peak Force (N)					
3	72.5	70.0	75.1	73.3	75.5	2.5%
4	113.4	121.8	123.8	119.2	125.7	2.3%
5	152.3	165.5	140.5	149.5	148.5	2.5%
6	171.4	206.8	195.2	213.4	215.7	11.7%
7	232.9	240.6	239.2	231.9	212.9	6.6%
8	193.4	193.1	209.2	217.1	179	0.3%
9	264.1	198.9	243.8	210.6	272.5	2.5%

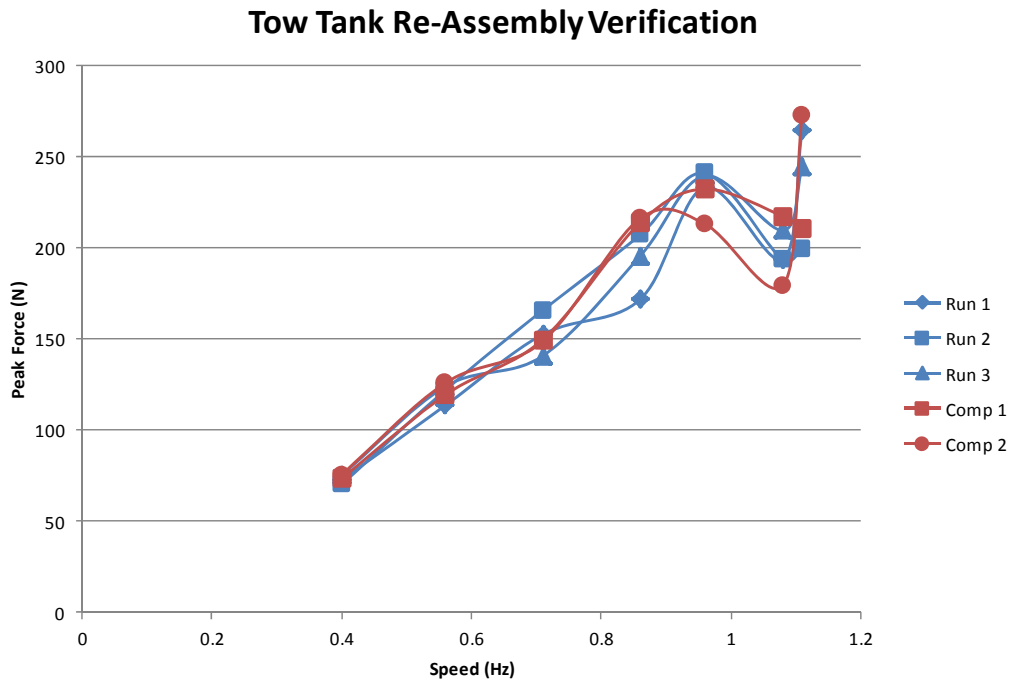

Figure 48 Comparison of peak forces before and after tow tank repairs

By this comparison the tow tank was reassembled correctly and the data runs provide enough overlap that any testing performed before tow tank repairs is able to be compared to testing performed after tow tank repairs.

D. RECTANGULAR SAMPLE TESTING

1. Aluminum Plate Sample

The aluminum plate provides the stiffest resistance of the rectangular test pieces. Each speed was measured in air and measured in water. Also, each test had the static force removed from the data such that at time equal zero, the force was zero. On a speed by speed basis it was determined at which point there was a transition from transient force in the acceleration zone to a steady state force which allows analysis of the transient period and analysis of the steady state period. Due to material limitations of the NPS tow tank during the conduct of this study, forces on the aluminum plate in water were unable to be obtained by the author but data for the aluminum plate was able to be obtained from source data of [18] by Grant Bryan. For demonstration, the 6 Hz speed setting sample is shown in Figure 49 for air and Figure 50 for water. Speed setting of 6 Hz corresponds to a linear velocity of the plate in water of 0.86 m/s.

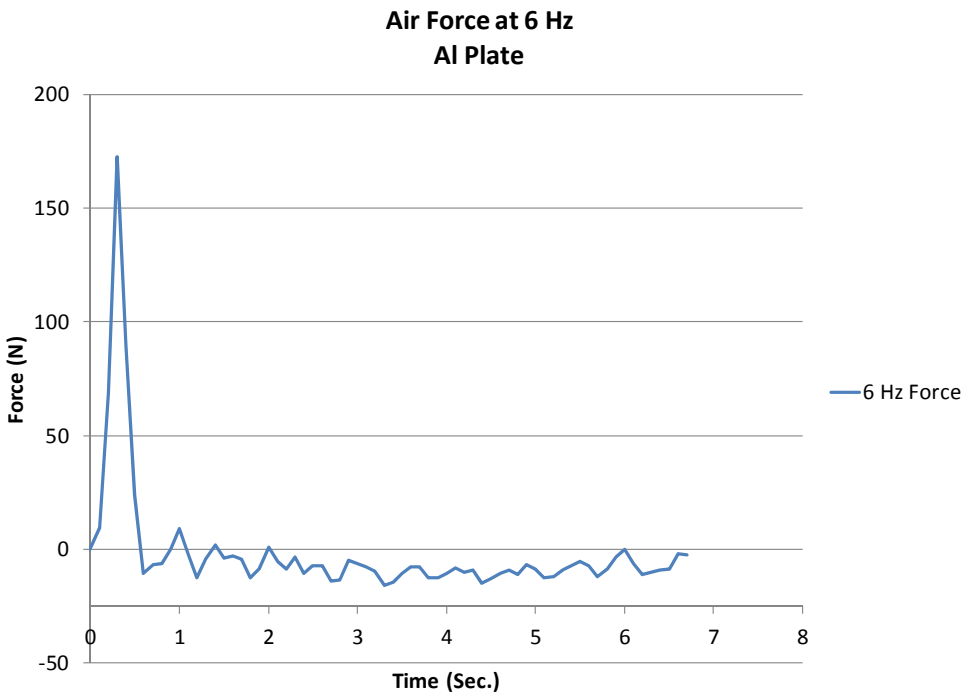

Figure 49 Force on aluminum plate sample in air at 0.86 m/s

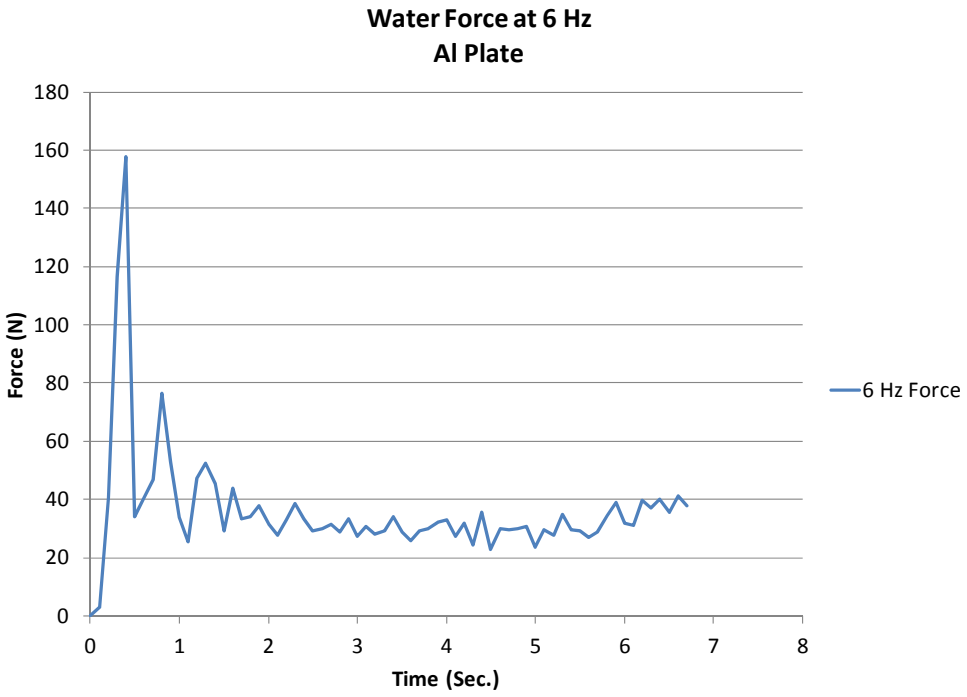

Figure 50 Force on aluminum plate sample in water at 0.86 m/s, after [18]

From the response in air, the initial peak is the force needed to overcome the inertia of the carriage at rest, after this initial impulse of energy into the carriage, no other force is imparted on the carriage as it moves down the tank with minimal air resistance and low friction on the tow tank rails due to lubrication and bearings. Therefore, the peak force can easily be determined from this test along with determining which timeframe is the steady state portion and getting the average force value. When water is added for opposing force, the resulting force diagram becomes noticeably different. No longer is there one peak force and the transient region is now longer, at 1.4 seconds up from the 0.6 seconds required in water. In water there are three distinct peaks of force, each decreasing in magnitude successively. Not only is the carriage at rest whose inertia needs to be overcome, but all fluid in the tank is at rest and will have be accelerated by the test piece, from basic physics this acceleration multiplied by the mass of the water that is moved results in the opposing force.

For each speed such analysis is performed and compiled for comparison across the test scenario. Figure 51 shows the peak transient forces and Figure 52 shows the average steady state forces for all speeds of the aluminum plate test piece.

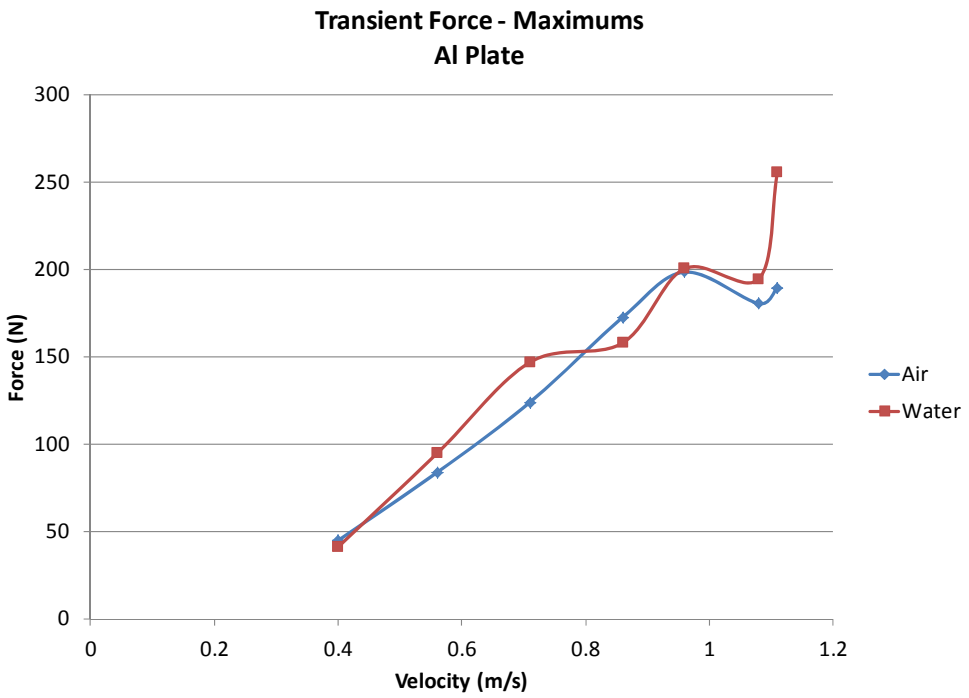

Figure 51 Maximum peak transient force for all speeds of aluminum plate sample, after [18]

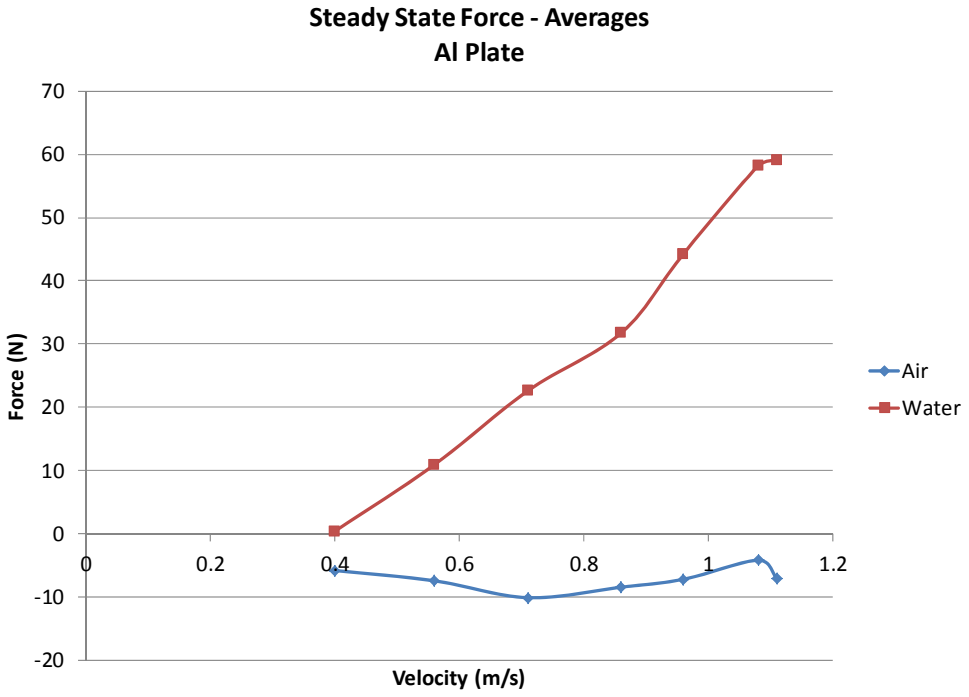

Figure 52 Average steady state force for all speeds of aluminum plate sample, after [18]

2. Ten-Layer Composite Sample with Bottom Test Orientation

The same data sorting for the aluminum plate was performed for all subsequent testing. Putting a composite sample in the bottom orientation adds stiffness to the sample that is not there in the top orientation. Figure 53 shows the peak transient forces and Figure 54 shows the average steady state forces.

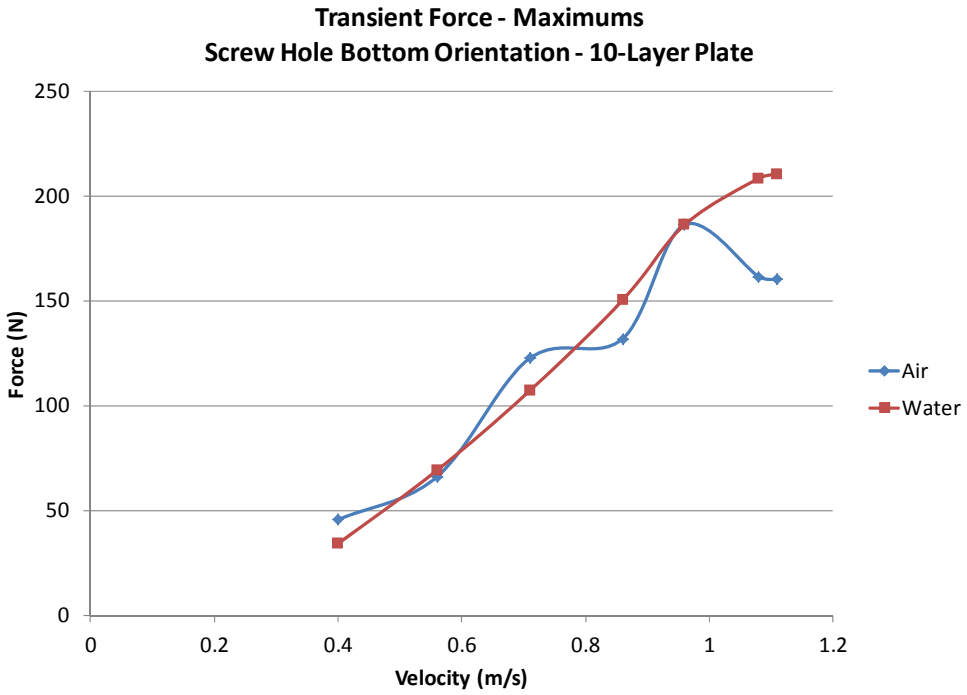

Figure 53 Maximum peak transient force for all speeds of 10-layer composite sample in bottom orientation

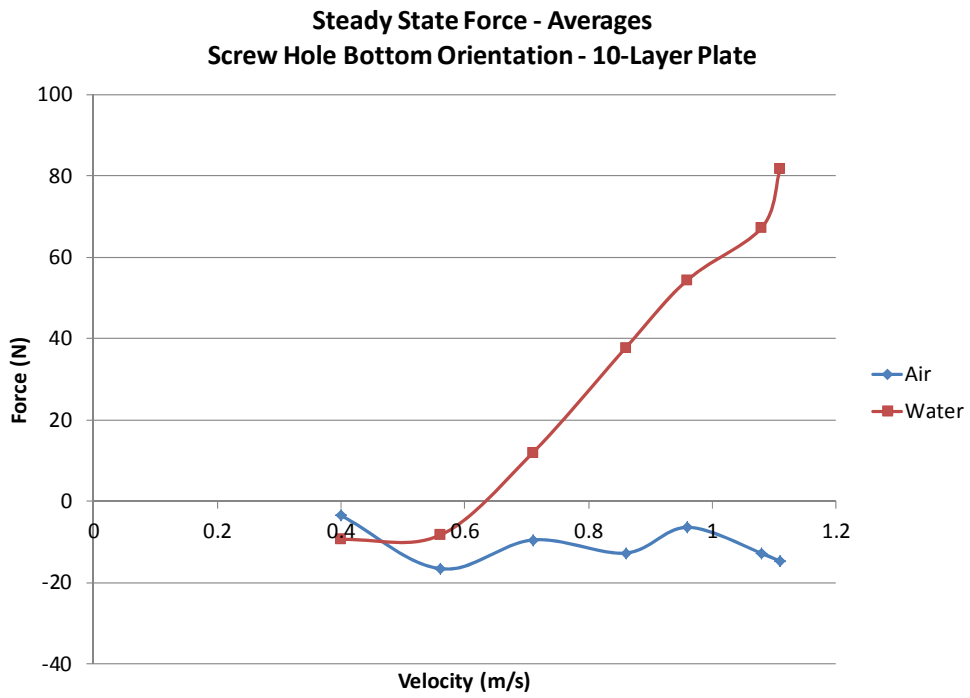

Figure 54 Average steady state force for all speeds of 10-layer composite sample in bottom orientation

3. Ten-Layer Composite Sample with Top Test Orientation

Figure 55 shows the peak transient forces and Figure 56 shows the average steady state forces for the 10-layer composite sample in the top test orientation across all speeds.

Figure 55 Maximum peak transient force for all speeds of 10-layer composite sample in top orientation

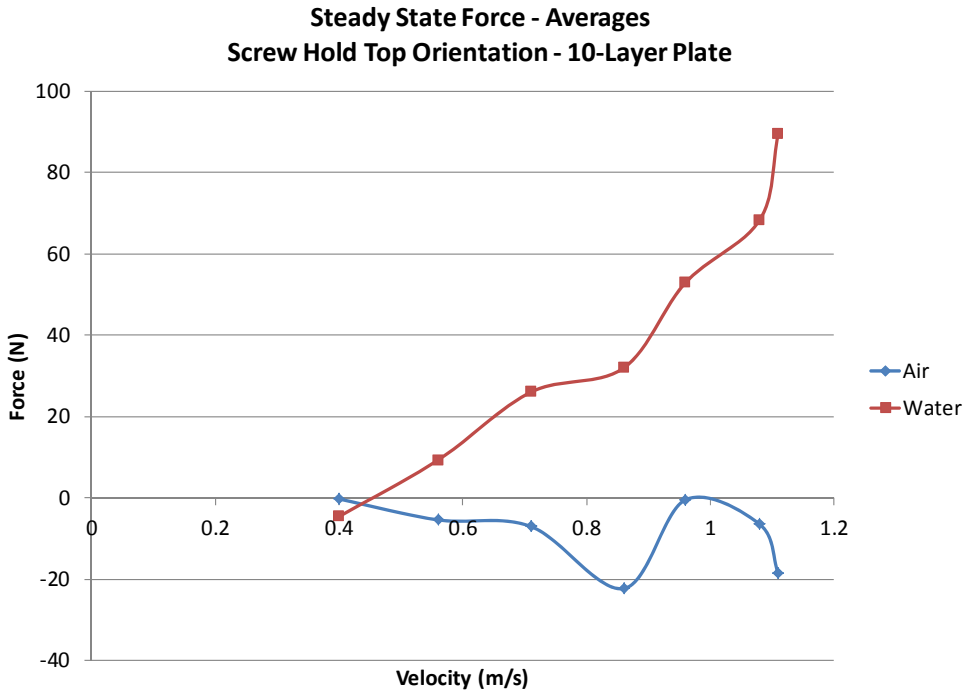

Figure 56 Average steady state force for all speeds of 10-layer composite sample in top orientation

4. Six-Layer Composite Sample with Bottom Test Orientation

Figure 57 shows the peak transient forces and Figure 58 shows the steady state forces for the six-layer composite plate in the bottom test orientation across all speeds.

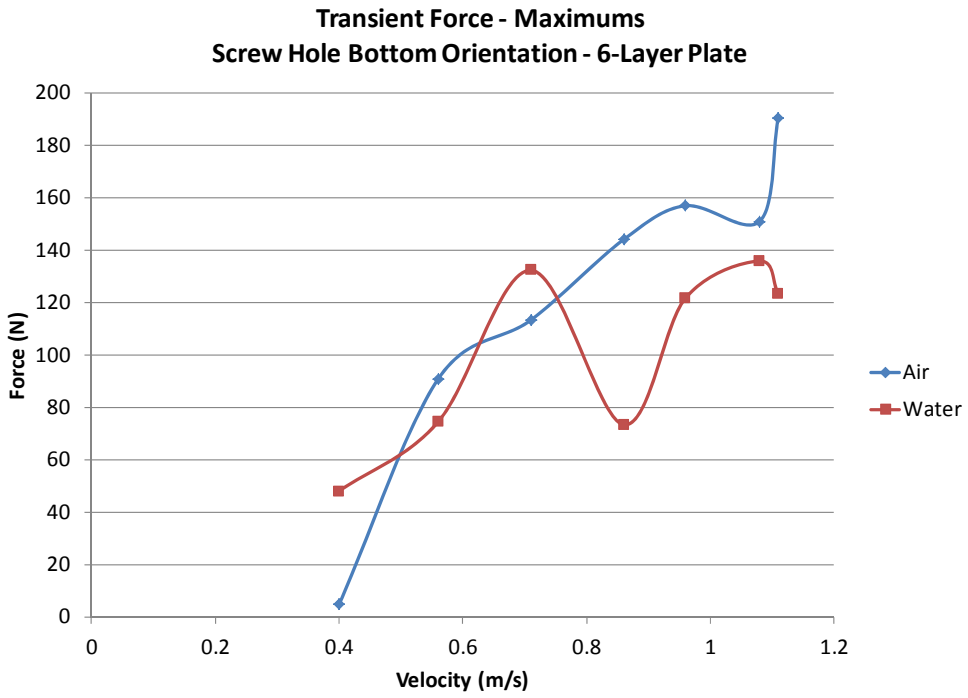

Figure 57 Maximum transient force for all speeds of the six-layer composite sample in the bottom orientation

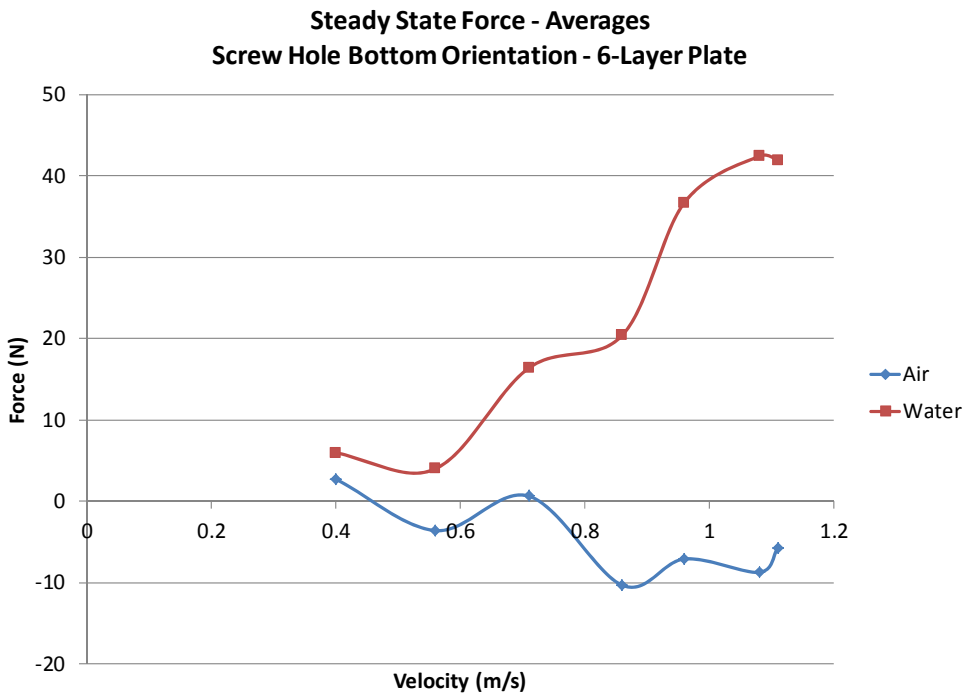

Figure 58 Average steady state force for all speeds of six-layer composite sample in bottom orientation

5. Six-Layer Composite Sample with Top Test Orientation

Figure 59 shows the peak transient forces and Figure 60 shows the steady state forces for the six-layer composite plate in the top test orientation across all speeds.

Figure 59 Maximum transient force for all speeds of six-layer composite sample in top orientation

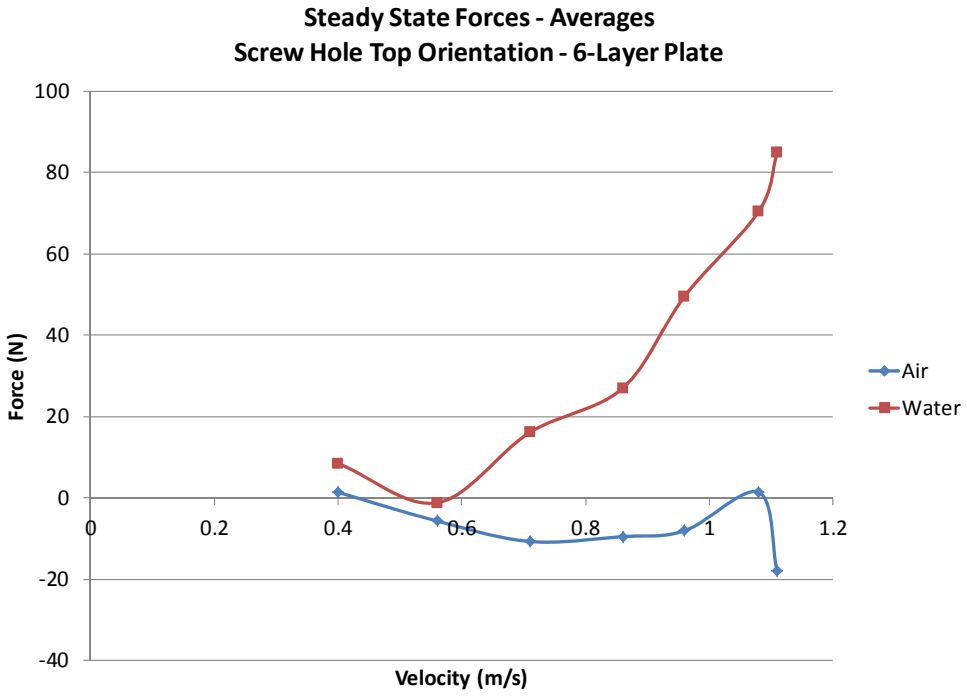

Figure 60 Average steady state forces for all speeds of six-layer composite sample in top orientation

6. Comparison of Cases for Rectangular Test Pieces

To get an across the board comparison between test pieces for the rectangular sample shapes four separate cases were investigated. Comparison of the maximum transient force required to pull each piece in air and the steady state average force in air were looked at. This was to verify that the amount of inertial load by the equipment with no water resistance did increase with speed for the maximum air data and that once at steady state speed, nearly no force was needed to continue to move the carriage, which would indicate that friction from the tow tank equipment was minimal. This is provided in Figure 61 and Figure 62.

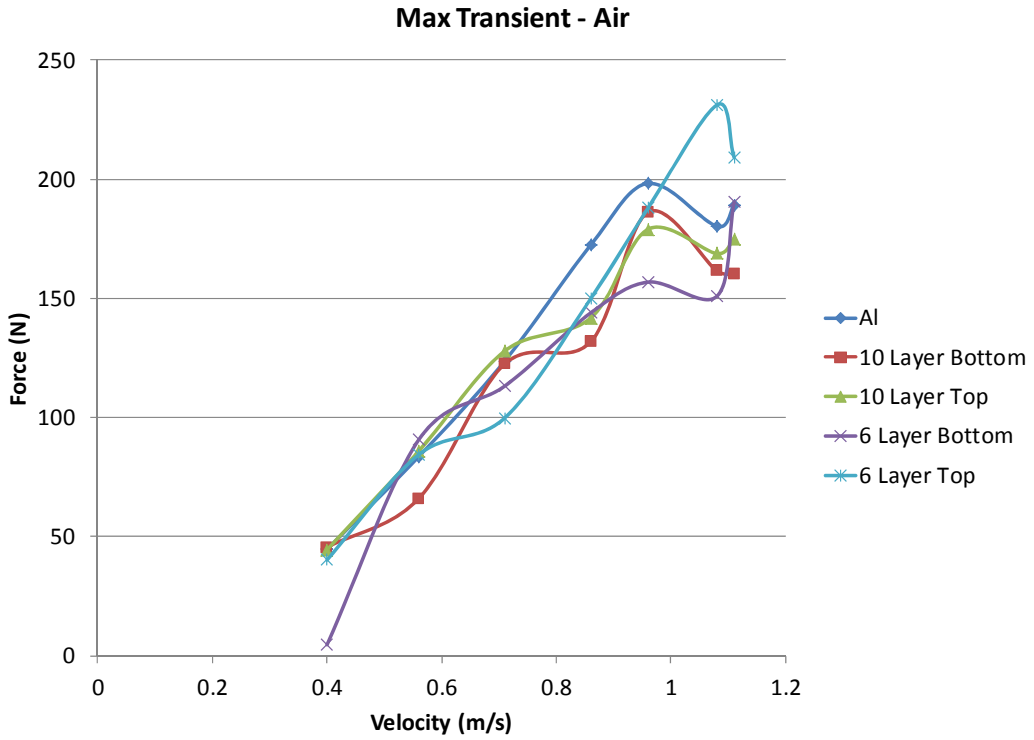

Figure 61 Maximum transient force for air testing with rectangular test pieces

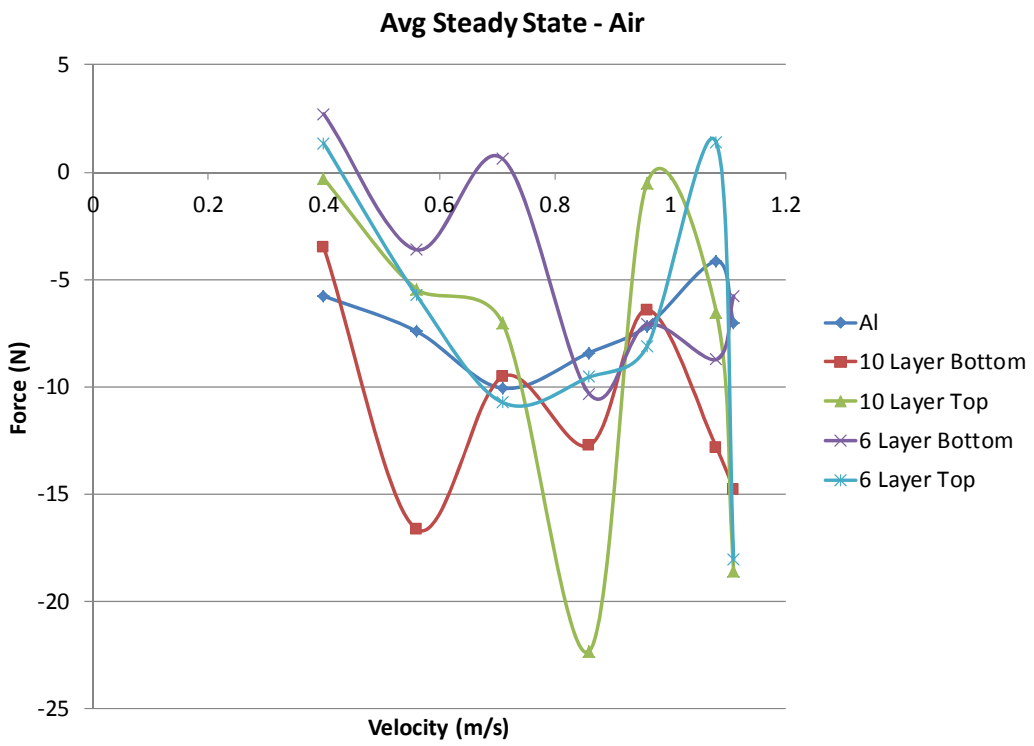

Figure 62 Average steady state force for air testing with rectangular pieces

The maximum transient force in air shows a linear increase until higher speeds are reached associated with 8 and 9 Hz speed setting. The maximum transient force should be completely dictated by the weight of carriage and test equipment in air as the resistance of air provides much less resistance than the inertia force needed to overcome the equipment weight. Since force is mass times acceleration and mass is not changing, this graph should follow the acceleration profile in air provided in Figure 44. Looking at Figure 44 acceleration increases until the 7 Hz speed setting and then plateaus which in general is the way peak force responds. The six-layer plate provides an outlier to this but overall the other cases show force responds like acceleration. The average steady state force shows in general negative force that is not consistent with speed. This is mainly due to the fact that the energy imparted by the motor to overcome the inertia of the carriage and test equipment at rest provides enough force that very little, if any force is again needed to propel the carriage. The bearings and lubrication of the rail system the

carriage rides upon provides very little resistance and the distance traveled is so short no other force is needed beyond the initial starting force for nearly all speeds.

The results of the same analysis but with water will provide the insight needed on how stiffness relates to force. Figure 63 provides the maximum transient force for water and Figure 64 provides the average steady state forces.

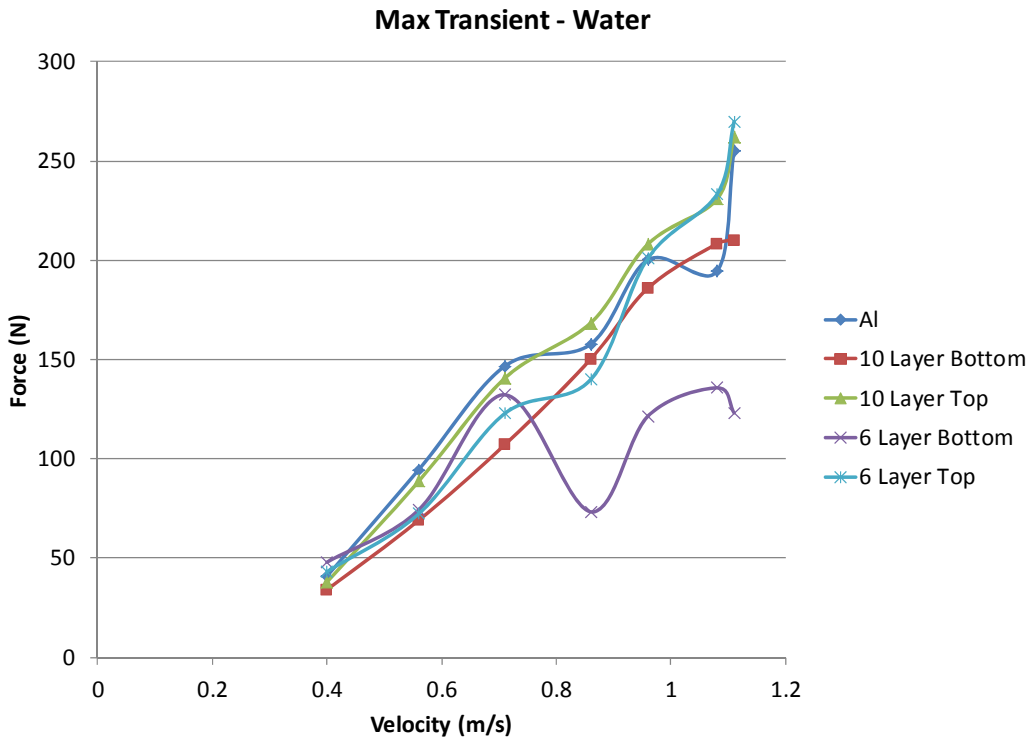

Figure 63 Maximum transient force for water testing with rectangular pieces

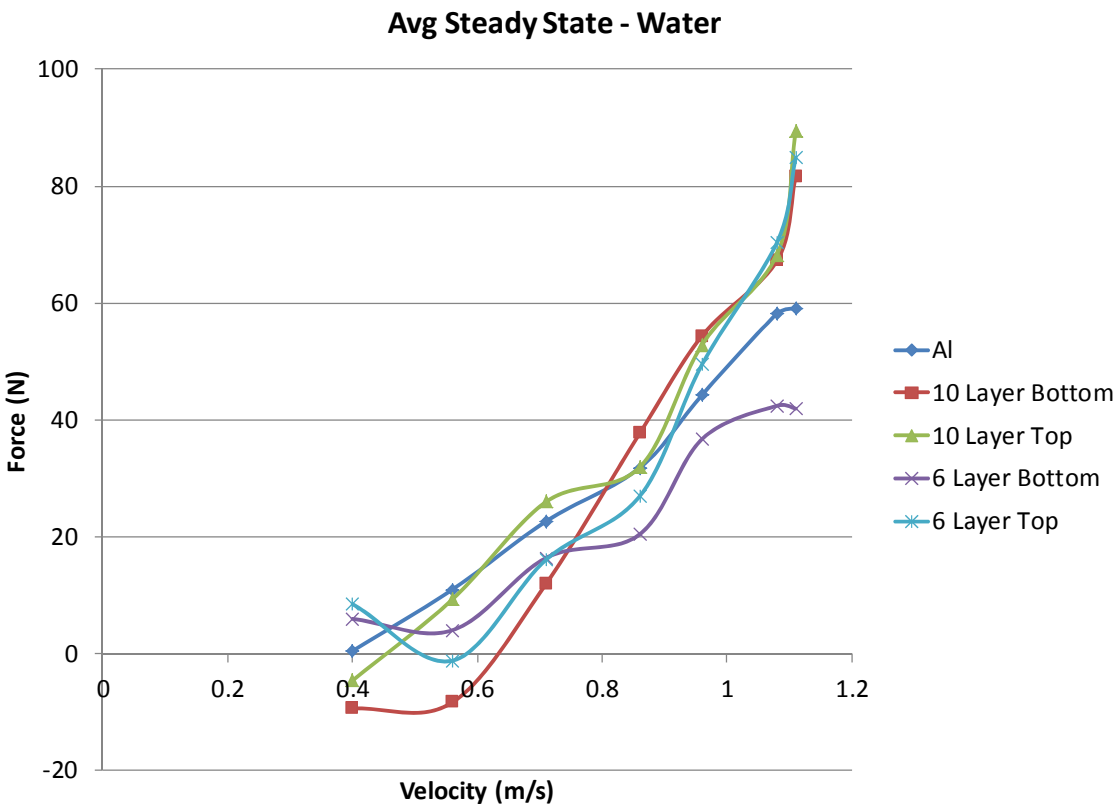

Figure 64 Average steady state force for water testing with rectangular pieces

With some exception the maximum transient force follows a linear increase with velocity increase. The six- and 10- layer composite bottom orientations appear to be outliers. It does not seem that the force response for the transient maximum closely follows the acceleration profile from Figure 44 which would correlate to a plateau of force readings from the 5 Hz speed setting and higher, but these values in general seem to show a fairly linear increase. This is unlike the air response data which appeared to have force and acceleration strongly correlated. The difference here could be a change in mass. Although the testing equipment has not changed in mass, there could be a relative change in mass as speed increases for the amount of water the plate is trying to move. From the velocity profiles in Appendix D, as speed setting increases it takes longer to reach steady state velocity and during this time more mass of water is moved by the test specimen. This increases the amount of force needed and may start to dominate the force response at higher and higher speeds. The relative mass between test pieces also explains

the variation in this data; it appears the aluminum piece follows an expected increase compared to the numerical calculations until the highest speed setting. However, the composite pieces follow no specific pattern with inconsistent changes with force as velocity increases. This comparison is driven by the relative difference in density between the aluminum plate and water and the difference between the composite used and density.

There does not seem to be a correlation between the stiffness of the test piece and force response. Steady state data should be the most reliable data and from this analysis shows an increase in force with speed but it is not apparent if there is any correlation between the materials and the force response. It appears there is almost something akin to an inflection around speed setting 5 Hz which corresponds to a velocity of 0.71 m/s. Prior this velocity, a test piece that took less force, such as the 10-layer bottom case compared to the other pieces, begins to take more force at subsequent speeds 0.71 m/s. Finally, and most troubling, at low speeds many cases take negative force, this should not be possible. Such a situation can be explained in air but in water there is far too much resistance from water to explain this. Ultimately, this may be the limitation of the system to provide accurate data for testing. Due to this, comparison to Figure 45 is difficult. However the general shape of the theoretical data and aluminum does follow closely. This is of specific note because the theoretical calculations only considered a rigid body knowing that it is much harder to numerically calculate the response force for the composite pieces. It is clear that the composite material introduces factors that alter the results but it is difficult to determine how these factors correlate as the experimental data thus far provides no clues.

E. FRAME TESTING

1. Force and Strain Analysis versus Angle

Only one material was tested inside the frame, a six-layer composite plate. However this sample was affixed with strain gauges to take advantage of the clamped boundary condition the frame provides and was tested at various position angles. Furthermore, use of the clamped frame provides no reduction in the apparent area due to

deformation meaning such testing should be easily comparable to theoretical values. The data collection and processing occurred in the same manner as for the rectangular test pieces but with strain added this for this case. Figure 65 and Figure 66 are provided for comparison to how data was collected for the aluminum plate sample discussed previously. Figure 67 shows strain gage data while Figure 68 shows strain gage data with the force of water superimposed on the same graph to show how the peaks in strain line up with the peaks of force.

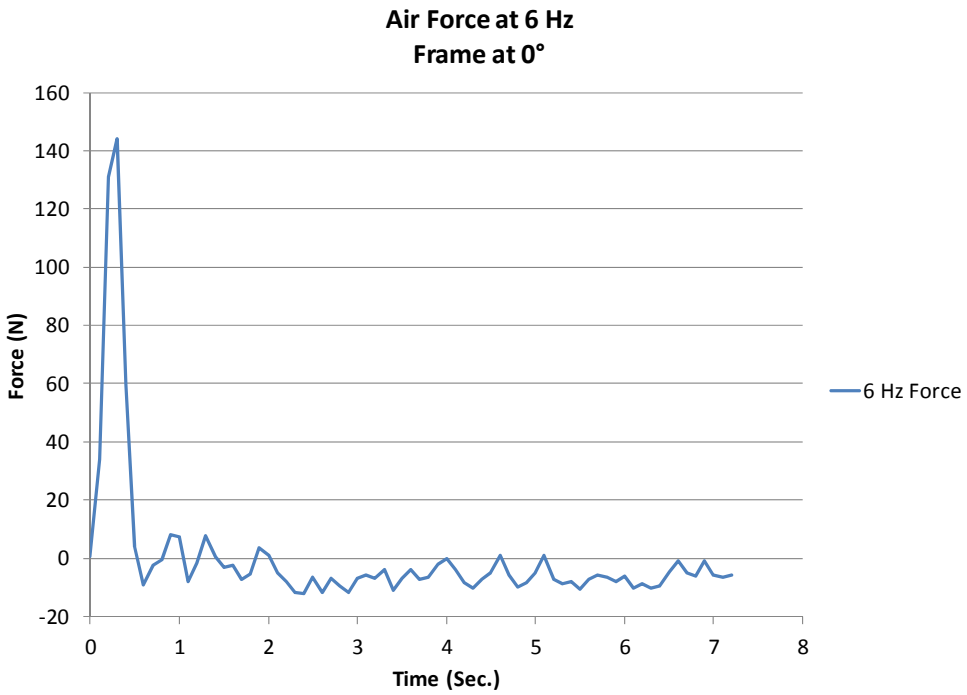

Figure 65 Force on framed composite sample at 0.86 m/s in air

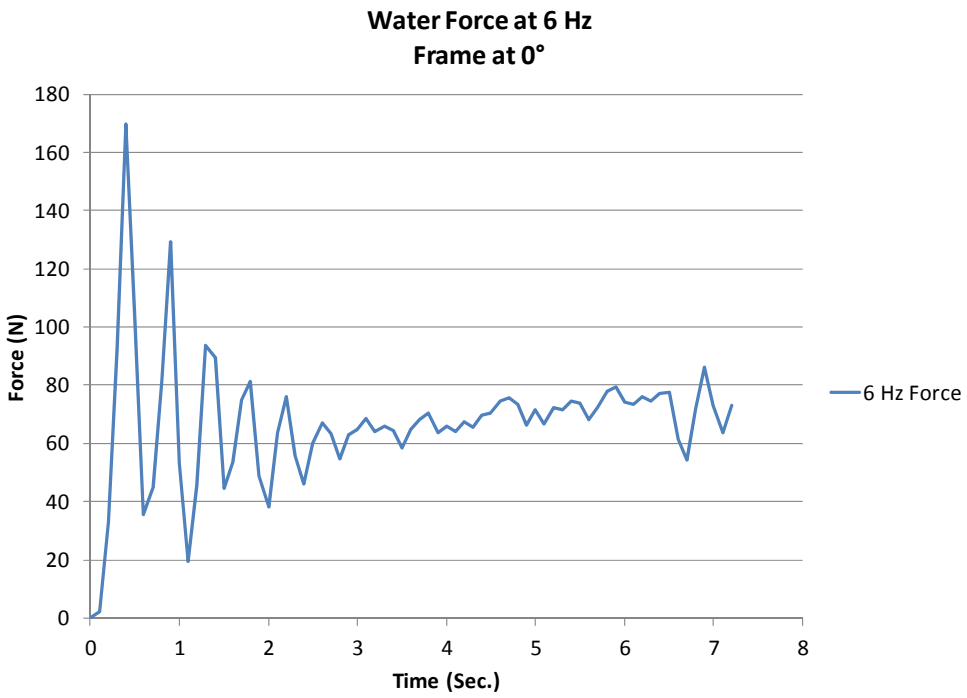

Figure 66 Force on framed composite sample at 0.86 m/s in water

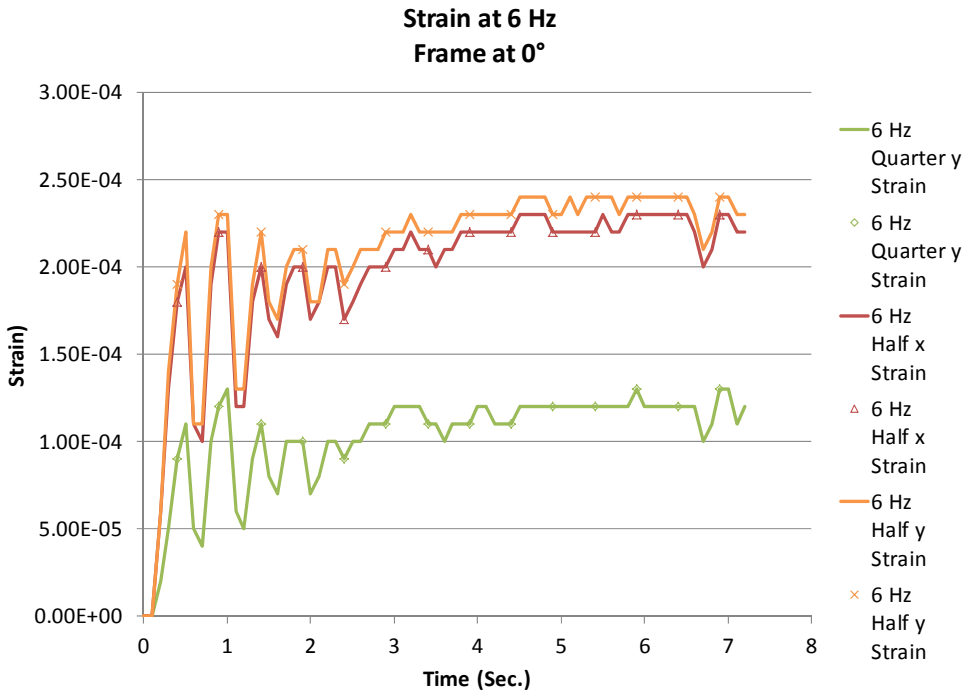

Figure 67 Strain on framed composite sample at 0.86 m/s in water

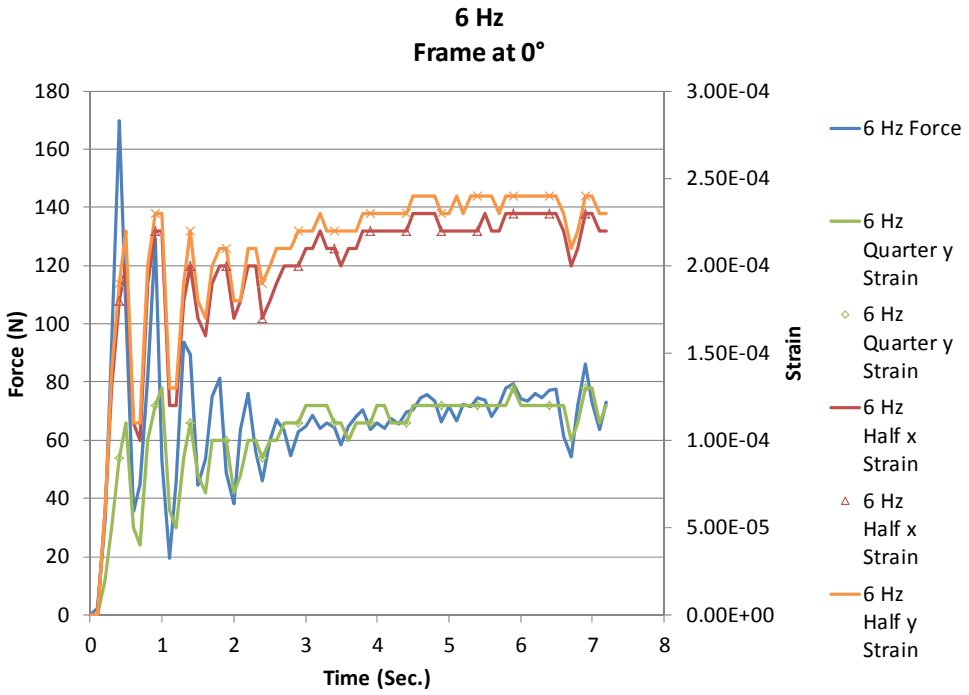

Figure 68 Framed composite force and strain at 0.86 m/s

The force of the framed composite is very similar to the aluminum case, air provides very little resistance against the area of the plate and the mass of the frame is comparable to the mass of the aluminum plate. When water is added however, there transient period becomes even more pronounced, mainly due to the increased area size of the framed composite over the smaller rectangular samples. Now there are five peaks in the transient period and this period lasts about 2.5 seconds whereas the transient period in air remains 0.6 seconds. The strain response corresponds to the force imparted in water however strain does not show a peak value far above the steady state strain values. It is thought that the small peak at the end of the steady state region could be a reflected wave off of the end of the tank meeting up with the test piece before the test piece reaches the end of the tank.

All angles tested and analyzed are presented in Appendix E. Maximum transient force and strain is provided in Figure 69, Figure 70, Figure 71 and Figure 72.

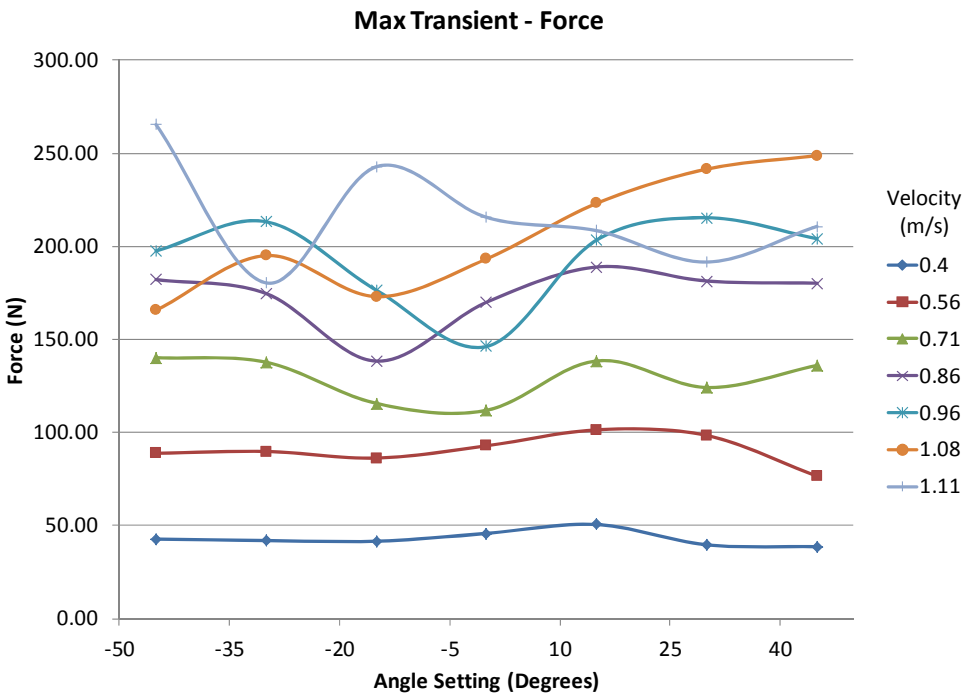

Figure 69 Framed composite maximum transient forces

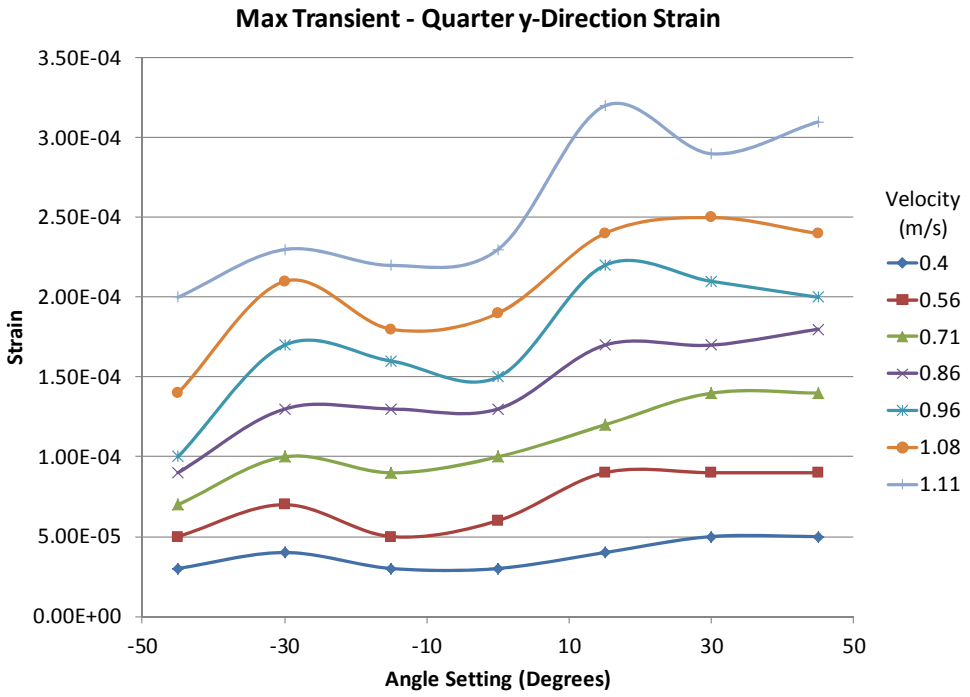

Figure 70 Framed composite maximum strain at quarter location in y-direction

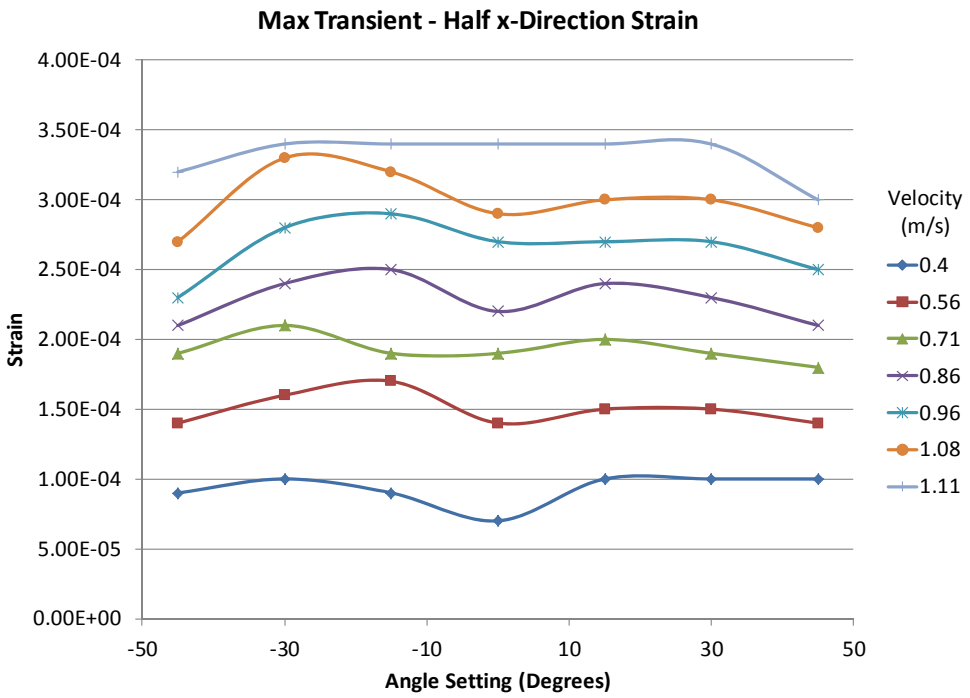

Figure 71 Framed composite maximum strain at half location in x-direction

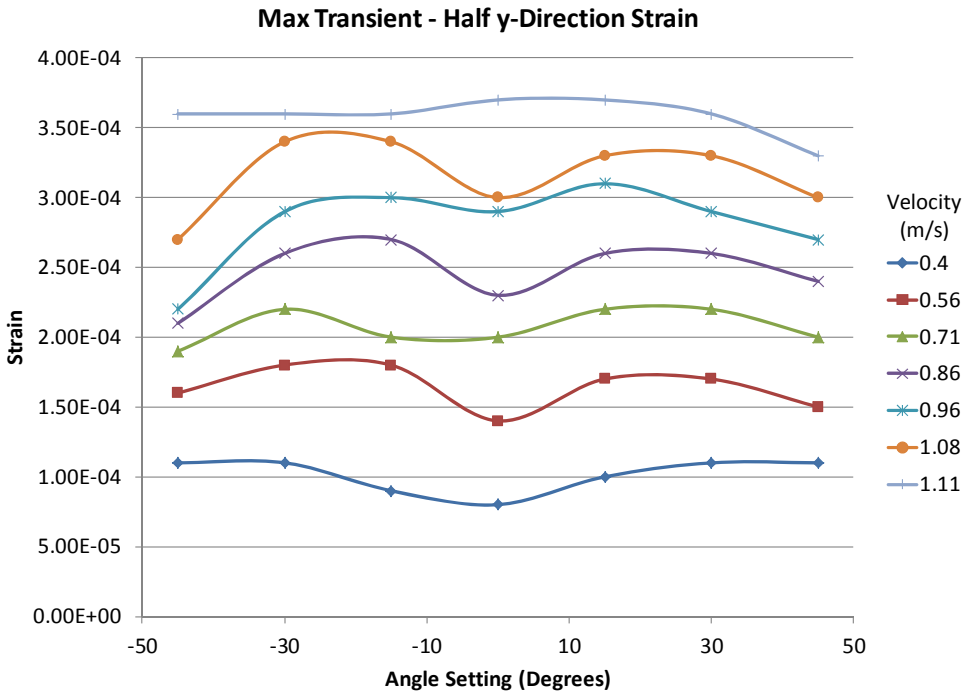

Figure 72 Framed composite maximum strain at half location in y-direction

Analysis of the peak forces shows no overall correlation with angle tested. At low speeds, position angle shows little influence on the force response. At high speed peak force is very sporadic. With the exception of the highest speed, 1.11 m/s, all speeds show some sort of peak force increase from 0º towards positive angles. This may be explained by the fact that towards the surface, water is being pushed forward and lifted up. This trend does not always follow through to the highest angle of 45º however. Strain in the quarter location should demonstrate the least response as it is closest to the clamped boundary. However there is clearly an overall increase in strain at the quarter location in the positive angle direction at all speeds. At lower speeds this levels off between 30º and 45º. However at higher speeds it no longer shows a leveling off. Much like the force, with the exception of the 1.11 m/s velocity there is a decrease in strain at the highest angle. The half location should provide the greatest strain response and due to the symmetrical arrangement of the test piece, should be identical. In general they are similar but not identical. A greater response is shown in the y-direction with more pronounced variation at each speed in the strain response. The most striking trend in both directions at most speeds is the relatively lower amount of strain at 0º compared to angles on either side. In the y-direction for velocities 0.56, 0.86 and 1.08 m/s which corresponds to speed settings of 4, 6 and 8 Hz there is a very symmetrical strain pattern. There may be some fluid phenomena going on in the transient area which is difficult to understand, for example vertical interaction with the inside edge of the clamping frame may provide varied responses which could affect strain at varied locations on the face of the composite. Overall it may be difficult to compare these values to the theoretical response as the theoretical response is for steady state flow. Therefore, steady state flow was examined at all angles and provided in Figure 73, Figure 74, Figure 75 and Figure 76.

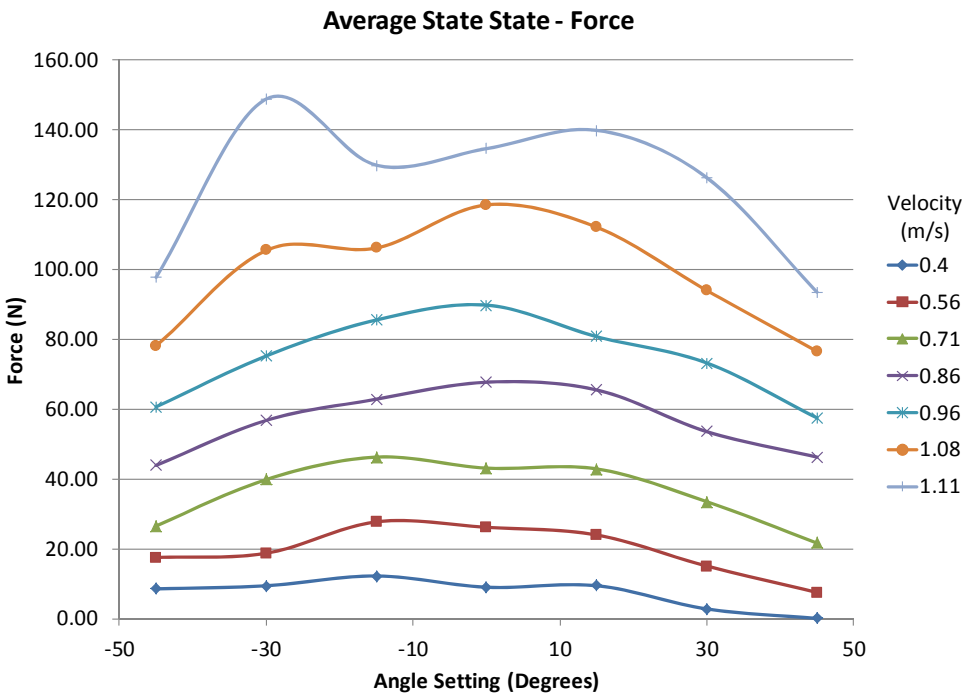

Figure 73 Framed composite average steady state force

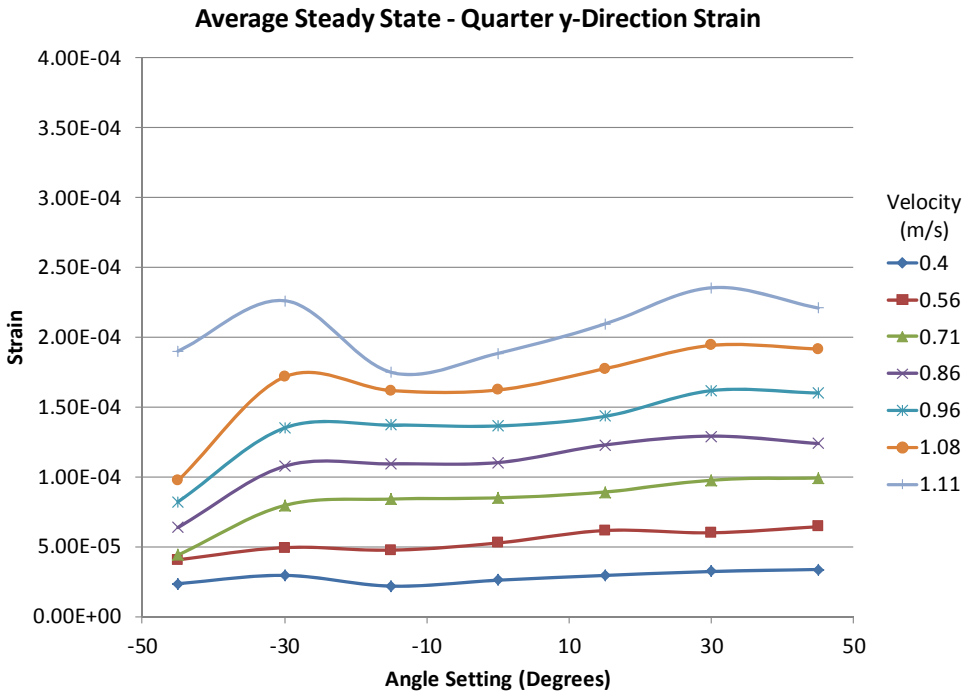

Figure 74 Framed composite average steady state strain at the quarter location in the y-direction

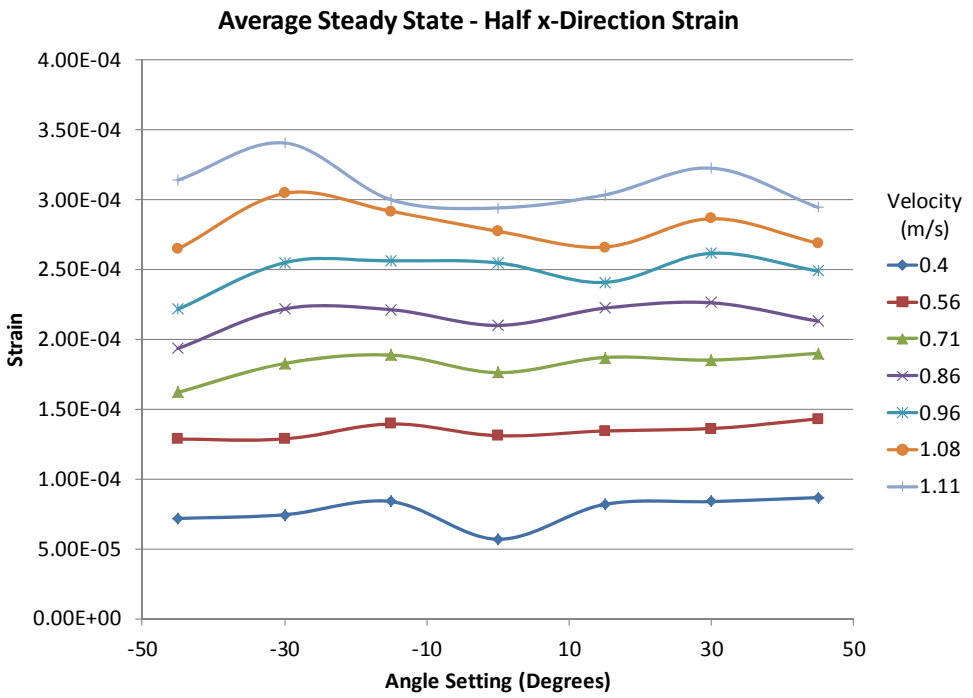

Figure 75 Framed composite average steady state strain in the half location in the x-direction

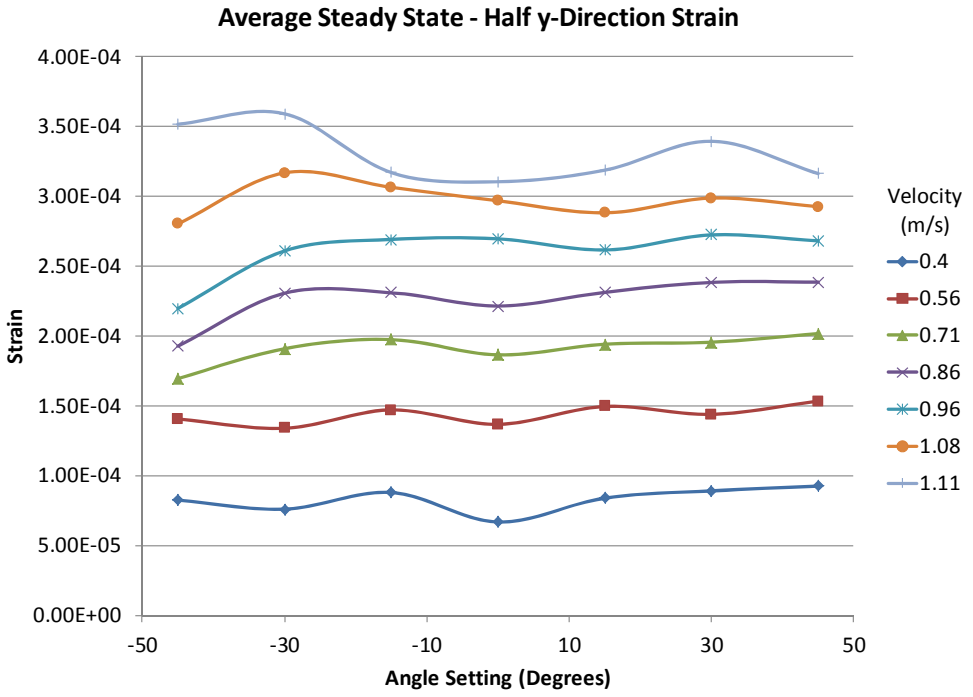

Figure 76 Framed composite average steady state frame at the half location in the y-direction

Steady state force begins to look more like the theoretical response demonstrated. The force shows generally the same shape and trend with angle. As speed is increased the relationship appears to breakdown with varied results at the two highest velocities of 1.08 and 1.11 m/s. This may be due to increased wave action in the tank at these speeds which are reflected off the end of the tank and back onto the sample while testing is still in progress. Ultimately it may be at high speeds that there is no "steady state" region due to the limitation of the testing equipment. For strain in the quarter y-direction measurement, steady state averages demonstrated the lower strain values which were expected compared to the half location strain measurements. The quarter location shows a marked decrease in strain at the extreme negative angle of -45º. Upon investigating the half location, at moderate and higher speeds there is also a noticeable decrease in strain. When considering the quarter location and this sharp decrease in strain only at extreme angles for nearly all speeds it could be demonstrated that close to the boundary condition, the support provided evens out strain regardless of the angle except at the extreme negative angle, where not much strain is experienced. The half locations provide very similar responses regardless of axis orientation showing that at steady state flow the force and response of the composite are much more even. A few cases, specifically the low speed at 0.4 m/s demonstrated a dip in strain at the neutral angle compared to positive and negative degrees. The trend towards lower strain at moderate speeds as previously mentioned can be seen in both axes at 0.71, 0.86, and 0.96 m/s. Velocities of 0.96 and 1.08 m/s in both directions appear to follow a general trend with angle setting. Both show +/- 45º with a lower strain than +/-30º and both show a decrease in local strain at +15º compared to adjacent angle settings. Looking at this closer, speeds above 0.89 m/s seem to show somewhat of a local maximum of strain at +/-30º compared to the adjacent angle settings.

After this data was collected it was thought that maybe more intermediate angles could help determine how the orientation of the composite influences the mechanical response. Increments of 5º were used between the already gathered data and speed settings of 3, 6 and 9 Hz, which corresponds to 0.4, 0.86 and 1.11 m/s. Figure 77, Figure 78, Figure 79 and Figure 80 shows the transient data.

Figure 77 Framed composite maximum transient force for intermediate angles

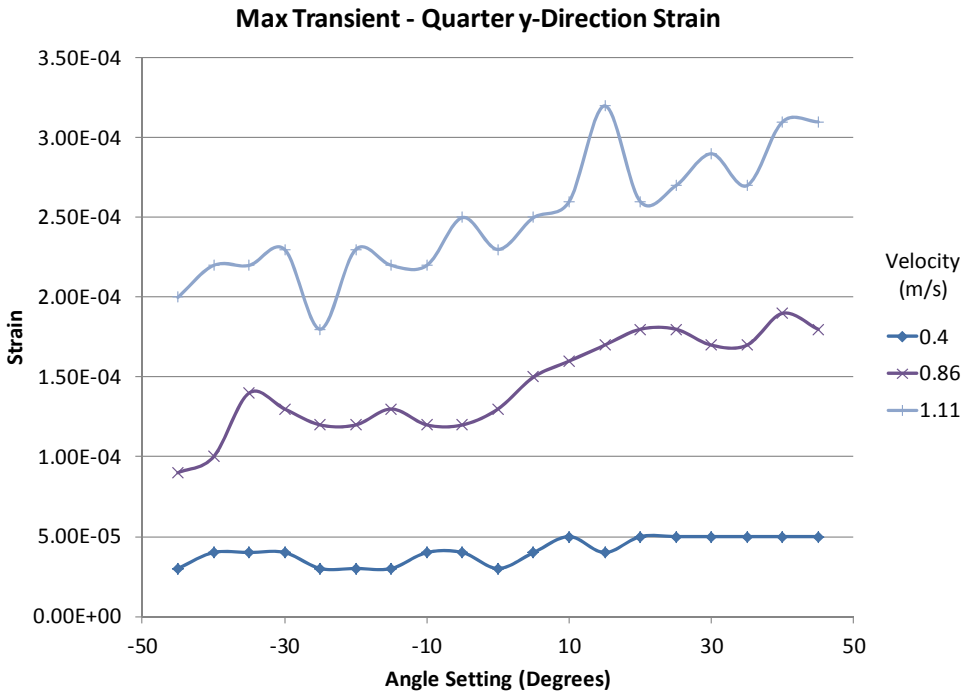

Figure 78 Framed composite maximum transient strain at quarter location in y-direction for intermediate angles

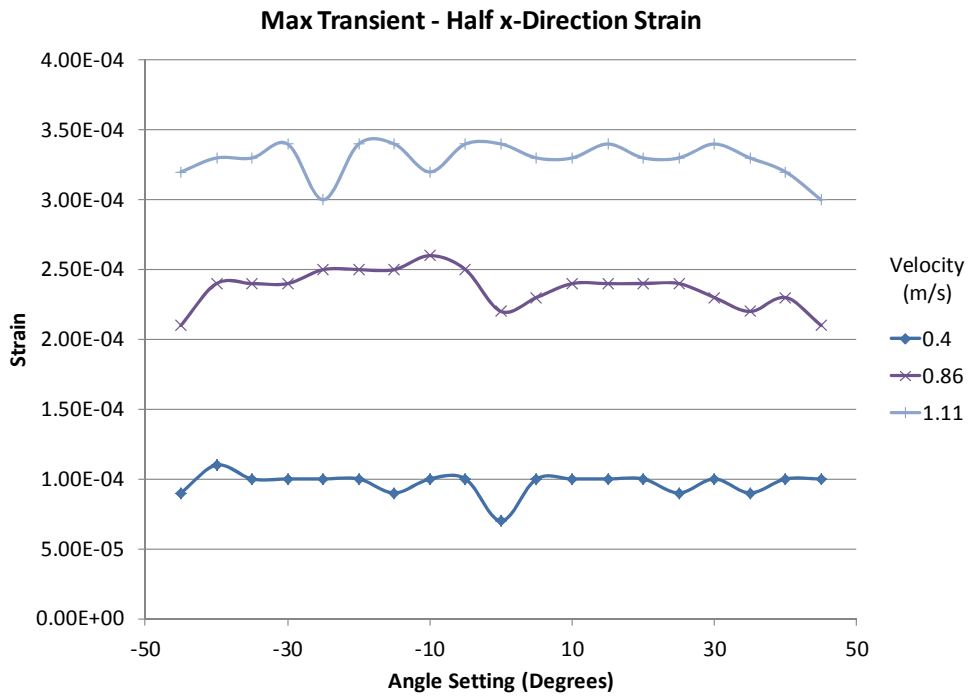

Figure 79 Framed composite maximum transient strain at half location in x-direction for intermediate angles

Figure 80 Framed composite maximum transient strain at half location in y direction for intermediate angles

The maximum transient force shows no relation to angle. The slowest velocity of 0.4 m/s demonstrates consistent force regardless of angle while 0.86 and 1.11 m/s velocities show inconsistent force regardless of angle. The general increasing trend of strain at the quarter location that was noticed in the earlier testing with more speed data but fewer angles is more noticeable at 0.86 and 1.11 velocities while 0.4 m/s shows a minimal increase in strain towards positive angles. This trend does not carry over to the center location which neither the x- nor y-direction provide strong correlation to angle setting. The steady state values were also determined to see if a more obvious correlation could be made, these are provided in Figure 81, Figure 82, Figure 83 and Figure 84.

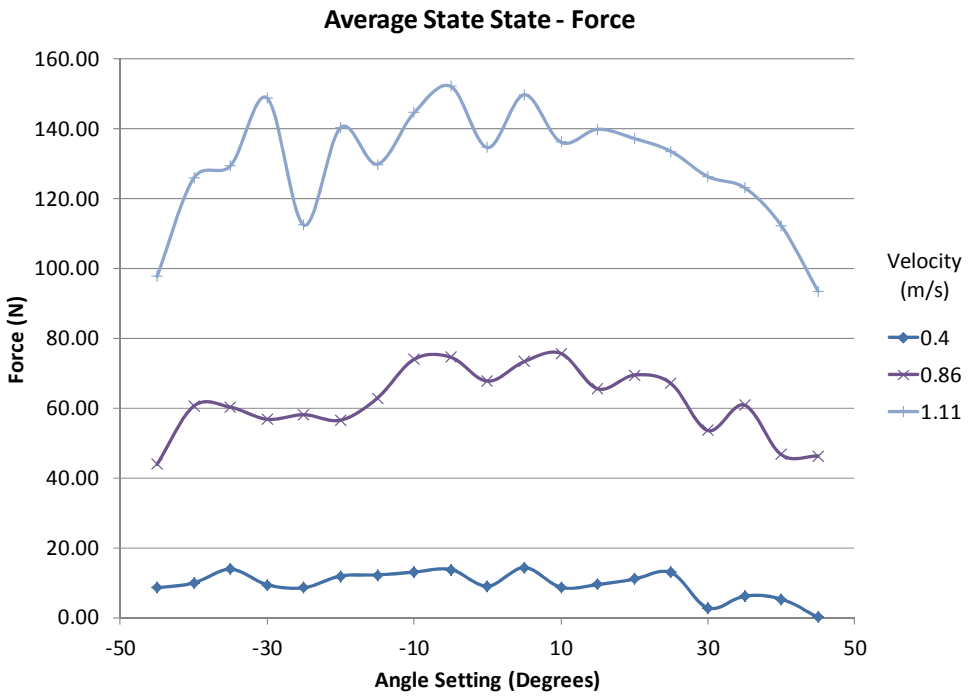

Figure 81 Framed composite average steady state force values for intermediate angles

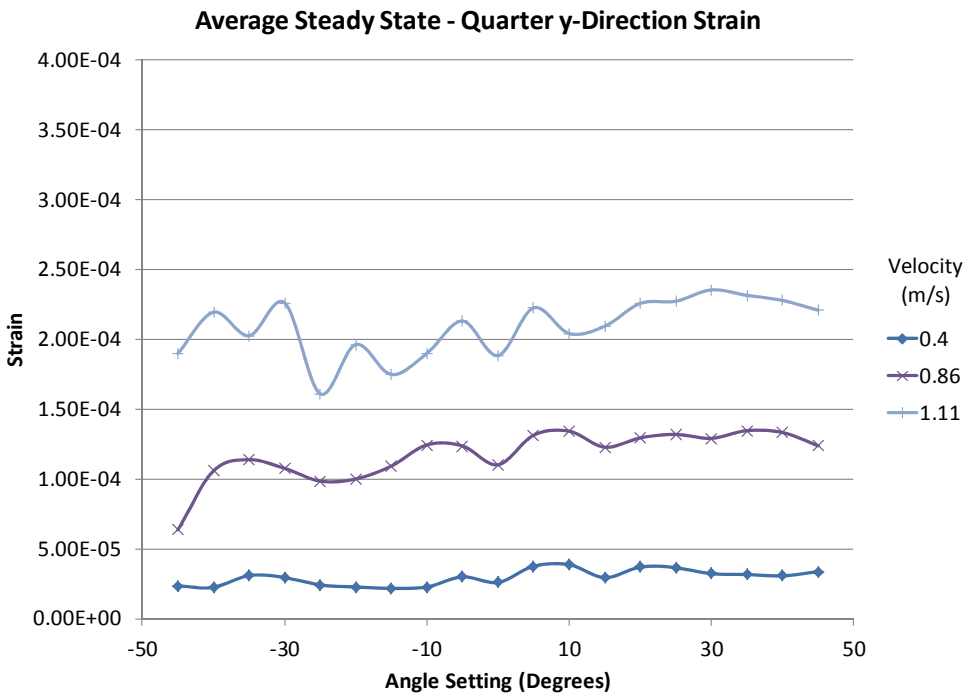

Figure 82 Framed composite average steady state strain at quarter location in y-direction for intermediate angles

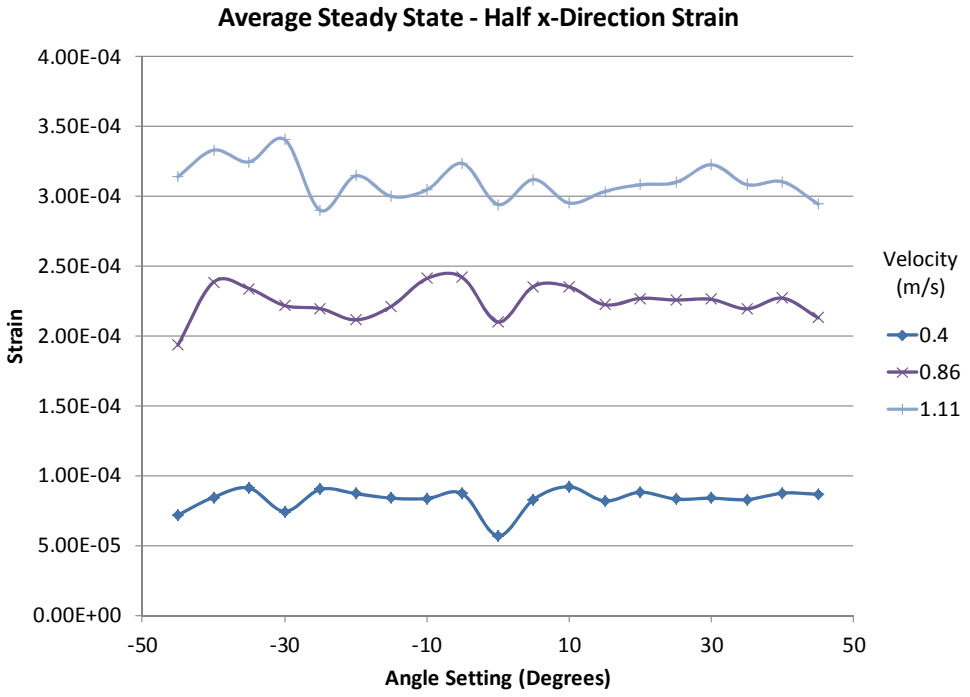

Figure 83 Framed composite average steady state strain at half location in x-direction for intermediate angles

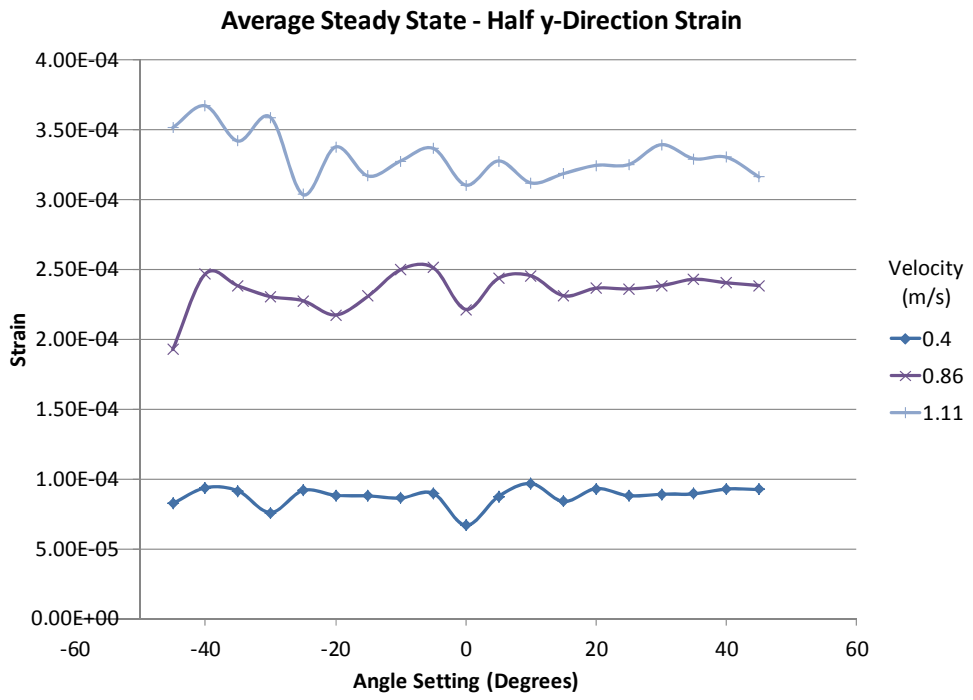

Figure 84 Framed composite average steady state strain at half location in y-direction for intermediate angle

With greater fidelity of angle selection, the steady state force does not look exactly like the theoretical calculations predicted. The overall shape somewhat looks like the theoretical shape but there is far too much variation as speed was increased towards a velocity of 1.11 m/s. There is still a local minimum in strain at the neutral angle with an increase in strain immediately at adjacent angles.

2. Understanding Depth versus Angle

Because of depth of water the piece was tested at was shallow, it is thought that possibly the free surface proximity would have an effect on testing. Because of position angle changes are a fixed radius each positive/negative angle combination is at different depth relative to the surface. Figure 85 shows some key negative position angles with demonstrating the change in relative depth these positions could be in. As mentioned previously, the length of the testing support rig, which serves as the fixed radius, is 0.68 m. Nominal depths of the neutral angle are also shown along with a naming convention for descriptive depths. Table 18 shows what depths the plate will be at relative to the free

surface; note that due to symmetry that positive and negative positions result in the same depth.

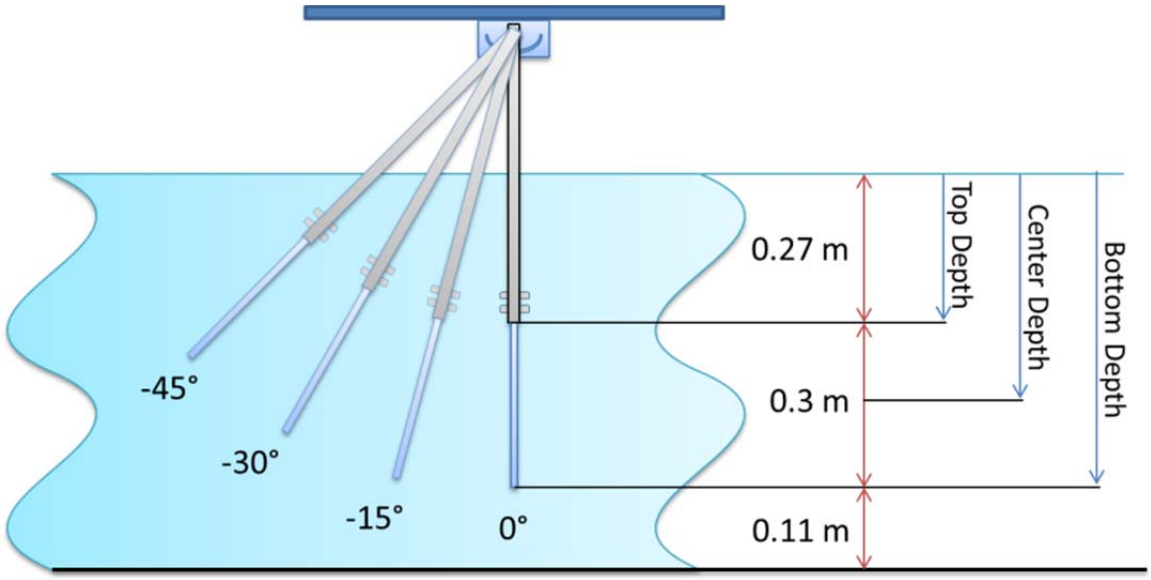

Figure 85 Relative change in depth with angle of framed composite

Table 18 Depth of plate at position angles

Angle	Top Depth (m)	Center Depth (m)	Bottom Depth (m)
0º	0.27	0.42	0.57
+/-5º	0.27	0.42	0.57
+/-10º	0.26	0.41	0.56
+/-15º	0.25	0.39	0.54
+/-20º	0.23	0.37	0.52
+/-25º	0.21	0.35	0.49
+/-30º	0.19	0.32	0.45
+/-35º	0.16	0.28	0.41
+/-40º	0.13	0.24	0.36
+/-45º	0.09	0.20	0.31

3. Visual Analysis

Based on the depth of water, still frames of the video taken by the high speed camera were gathered to analyze how the plate interacted with the free surface at various degrees. At the angles of +/- 45, 30, 15 and 0 degrees speed settings of 3, 6 and 9 Hz,

corresponding to 0.4 0.86, and 1.11 m/s, are compared. In all cases, the starting point (x=0, t=0) was at 10 cm, which is off screen of the still pictures. The position of the sample at the time of freezing the video was chosen at the time which best represents what flow around the sample was in the steady state as shown in Figures 86 through 94

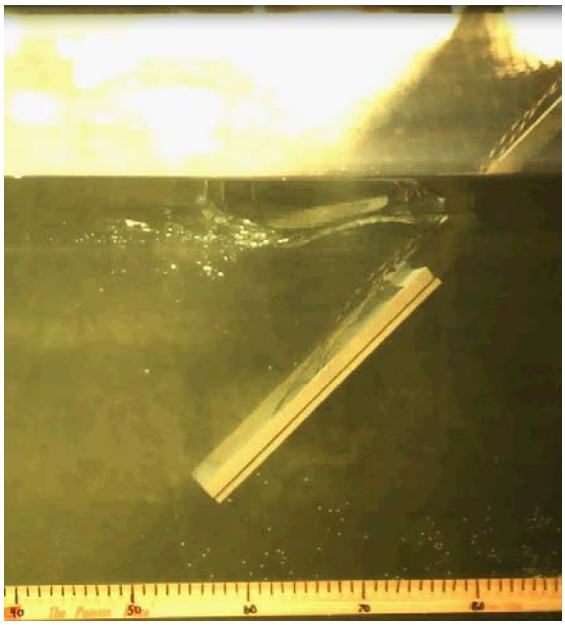

(a)

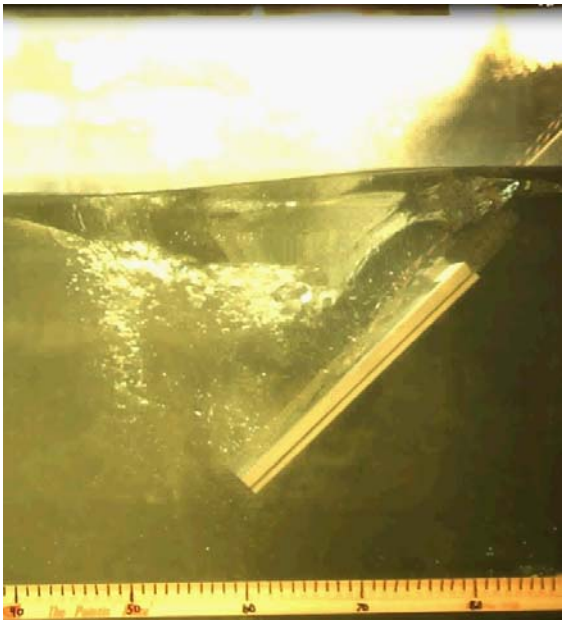

(b)

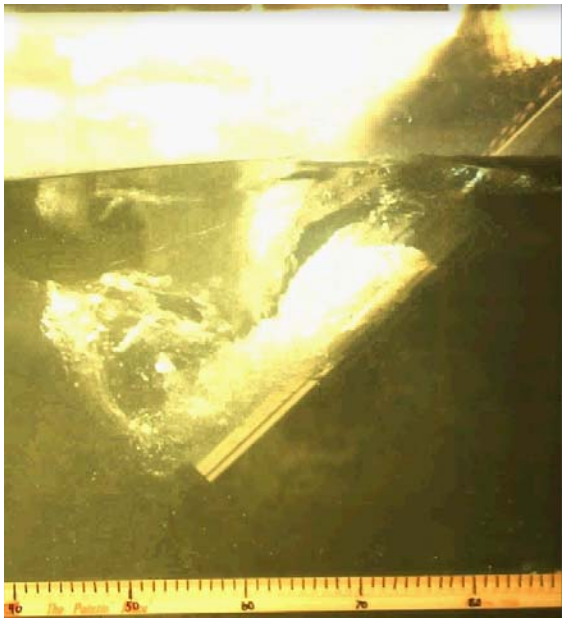

(c)

Figure 86 Video still of -45º position for: (a) 3 Hz, (b) 6 Hz, and (c) 9 Hz

The -45º position shows some of the most profound free surface interaction with the sample. A reduction in depth at the slowest speed begins to appear directly after the sample. At the intermediate speed the void is significantly larger and a rise in the depth begins to appear directly above the sample. At the highest speed not only is the void appearing to interact with the back side of the sample, significant turbulence and possibly some cavitation coming off the top edge of the sample has developed. This interaction of the free surface with the sample could significantly alter the fluid-structure interaction of the sample.

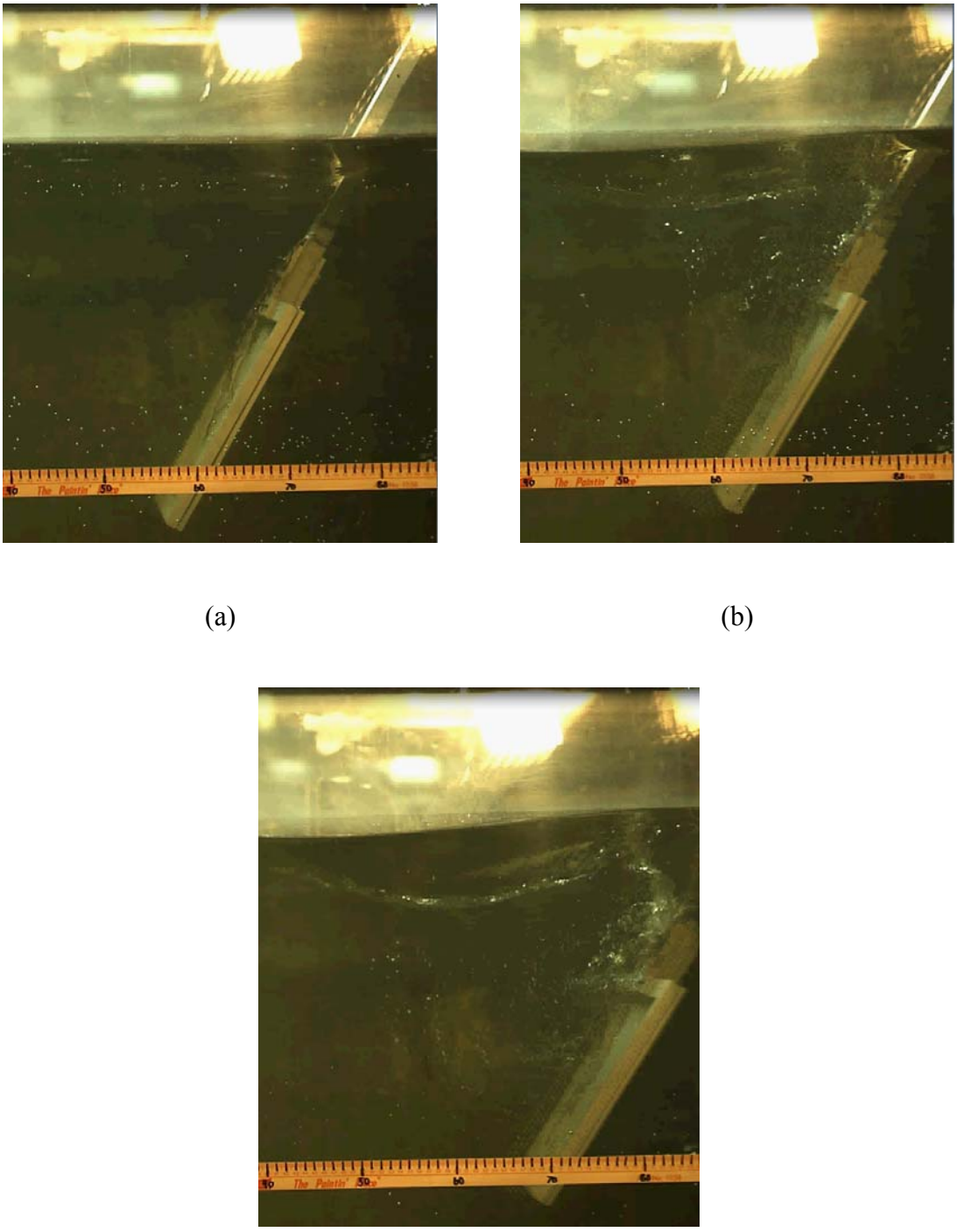

(a) (b)

(c)

Figure 87 Video still of -30º position for: (a) 3 Hz, (b) 6 Hz, and (c) 9 Hz

The -30º position shows very little interaction at the slowest speed, if there is a change in free surface depth at this speed it appears slight. At the moderate speed, the change in free surface depth before and after the sample begins to move becomes observable with a void on the free surface directly above and behind the sample appearing. The fastest speed was difficult to capture at the starting position, what is not visible off to the right should be a rise in the free surface but this was not captured by the camera. Directly behind the sample there is a significant void beginning to appear, and this void is not as pronounced as the -45º case because it does not interact directly with the back side of the sample. The support rig however interacts with the free surface and this interaction appears to translate down the back of the sample with some bubbles.

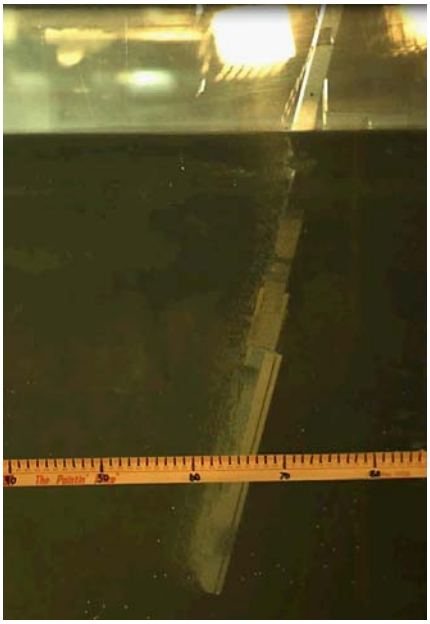

(a)

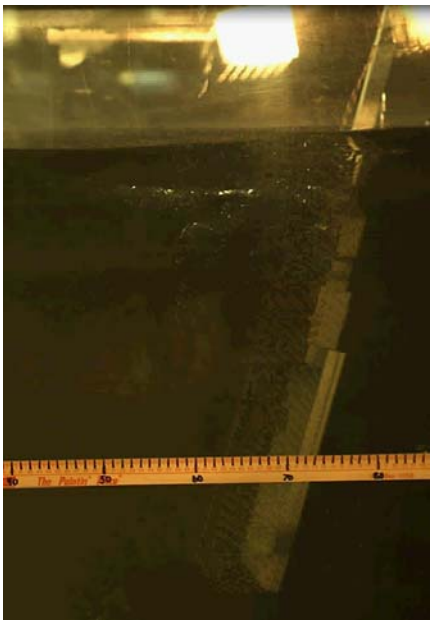

(b)

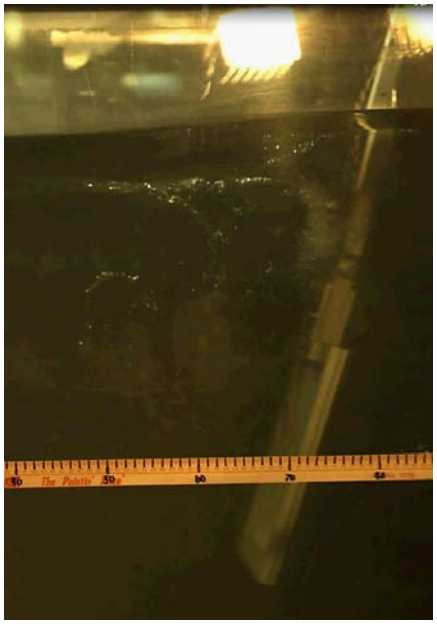

(c)

Figure 88 Video still of -15º position for: (a) 3 Hz, (b) 6 Hz, and (c) 9 Hz

In general, at all speeds at -15º there is no direct interaction of the free surface with the sample. As speed increases, the depth of the free surface begins to change which will influence the fluid structure interaction between the sample and the environment. The support rig has direct interaction with the free surface which leads to a change in the flow beneath the free surface which may interact with the sample, especially at higher speeds.

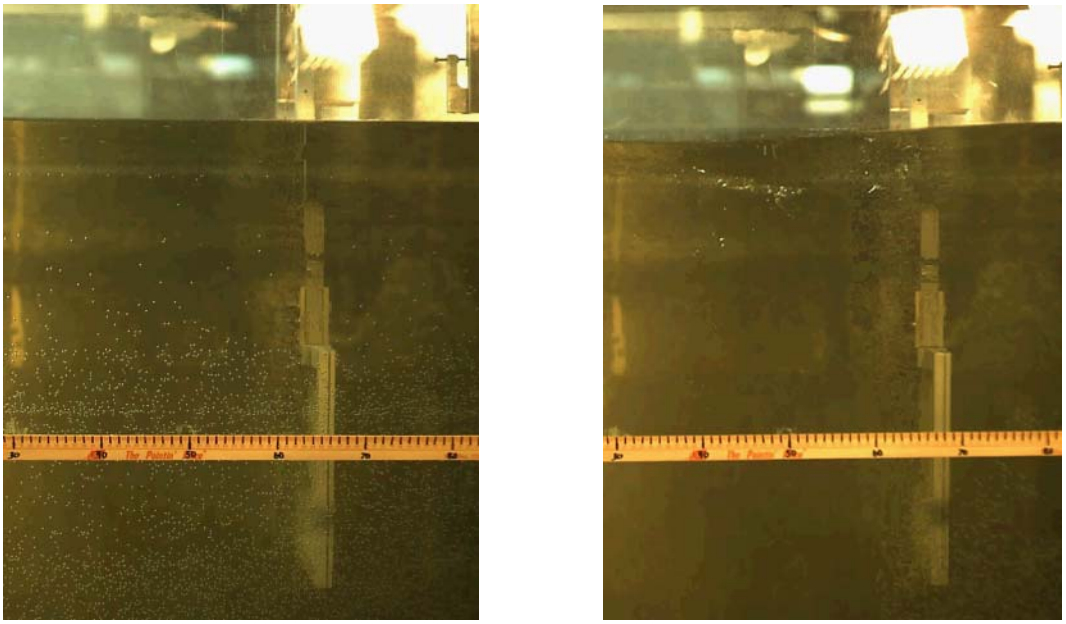

(a) (b)

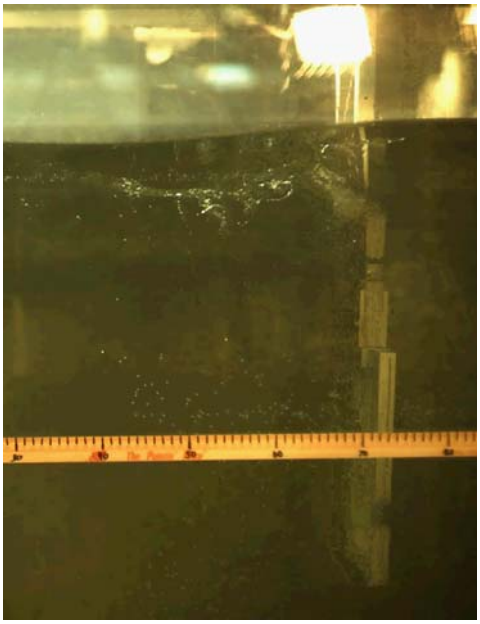

(c)

Figure 89 Video still of 0º position for: (a) 3 Hz, (b) 6 Hz, and (c) 9 Hz

At the neutral angle there appears to be no interaction with the free surface at the lowest speed. As speed increases it appears that most interaction is from the support rig with a minor bow of water beginning to develop in front of the sample. At the highest speed, the support rig has much more interaction with the free surface leading to a change in flow characteristics behind the sample. The bow in front of the sample becomes more pronounced, and in the video at this speed it is possible to see the structural interaction with the fluid as the cantilever nature of the support rig and sample are responding to the force of the water being pushed forward.

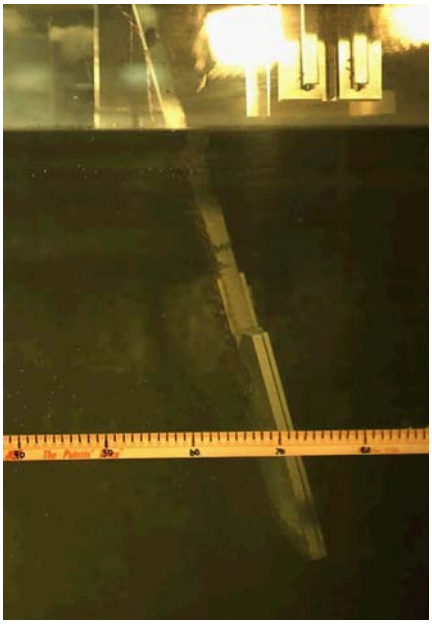

(a)

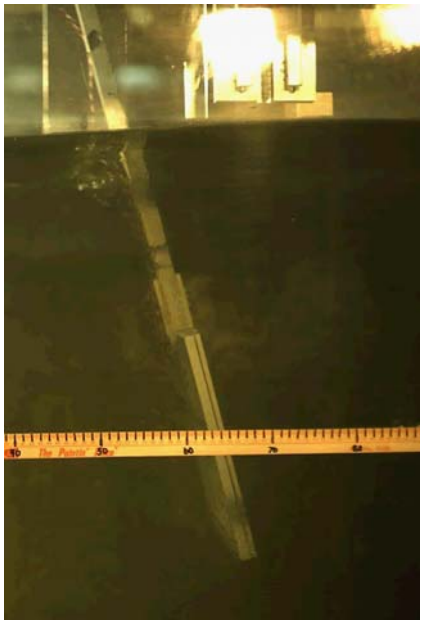

(b)

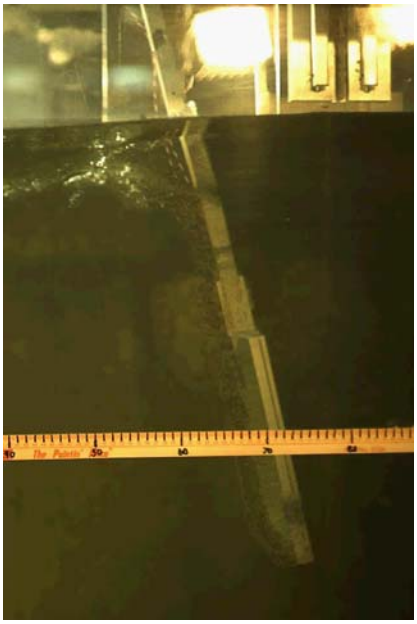

(c)

Figure 90 Video still of +15º position for: (a) 3 Hz, (b) 6 Hz, and (c) 9 Hz

At the +15º position setting the lowest speed demonstrates minimal change in both water depth and interaction with the free surface. The moderate speed begins to show an increase in depth before the plate as a bow is starting to develop. There also appears to be the beginning of interaction of the free surface with the support rig at this speed which was not visible at the lower speed. The highest shows a more pronounced bow with a decrease in depth behind the sample. There is much more interaction of the support rig with the free surface.

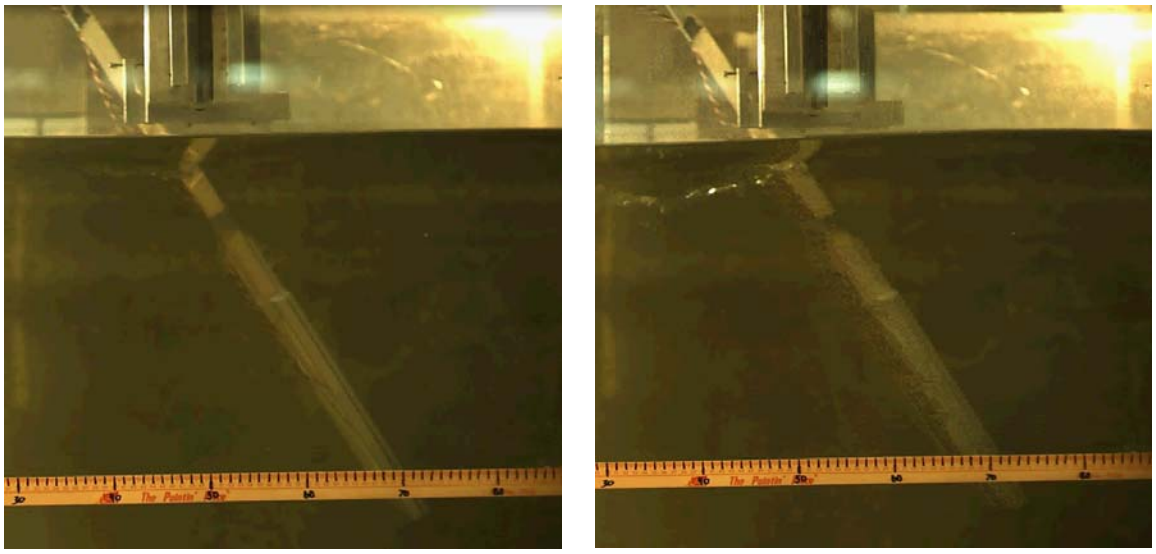

(a) (b)

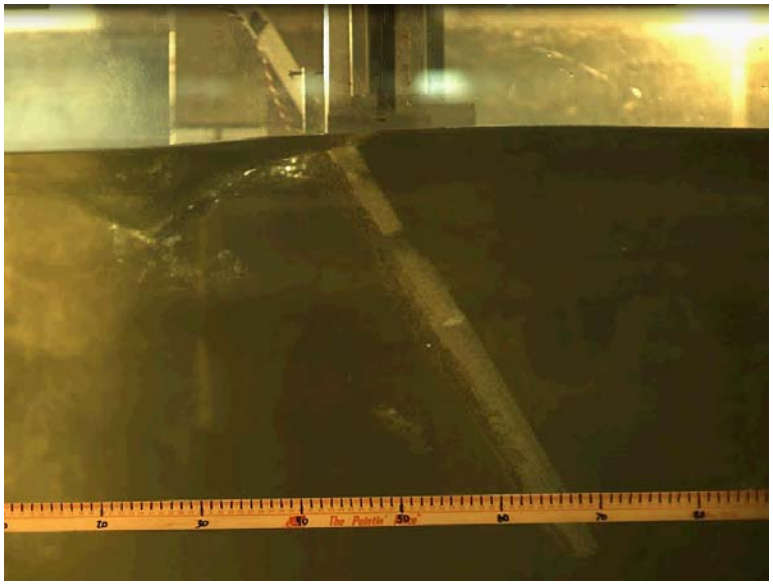

(c)

Figure 91 Video still of +30º position for: (a) 3 Hz, (b) 6 Hz, and (c) 9 Hz

A wider picture frame is required to view position angles above +30º which results in a somewhat smaller printed picture. At this angle setting the 3 and 6 Hz speed

setting seem to create very similar bow wave effects in front of the sample. At the 9 Hz speed the bow wave is not only more pronounced in height but is also wider longitudinally. Furthermore, a larger void is beginning to develop here which was not in previous angle settings that were lower in position than -30º. The most interesting observation at this speed and angle combination is that there appears to be cavitation occurring off of the sample. This is visible in the still shot directly above the 50 cm marking. From the video it is possible to observe bubbles come off the top of the plate and swirls in the wake of the plate before rising to join the void behind the plate at the free surface. Figure 92 and Figure 93 show the development and interaction of joining the free surface for these bubbles.

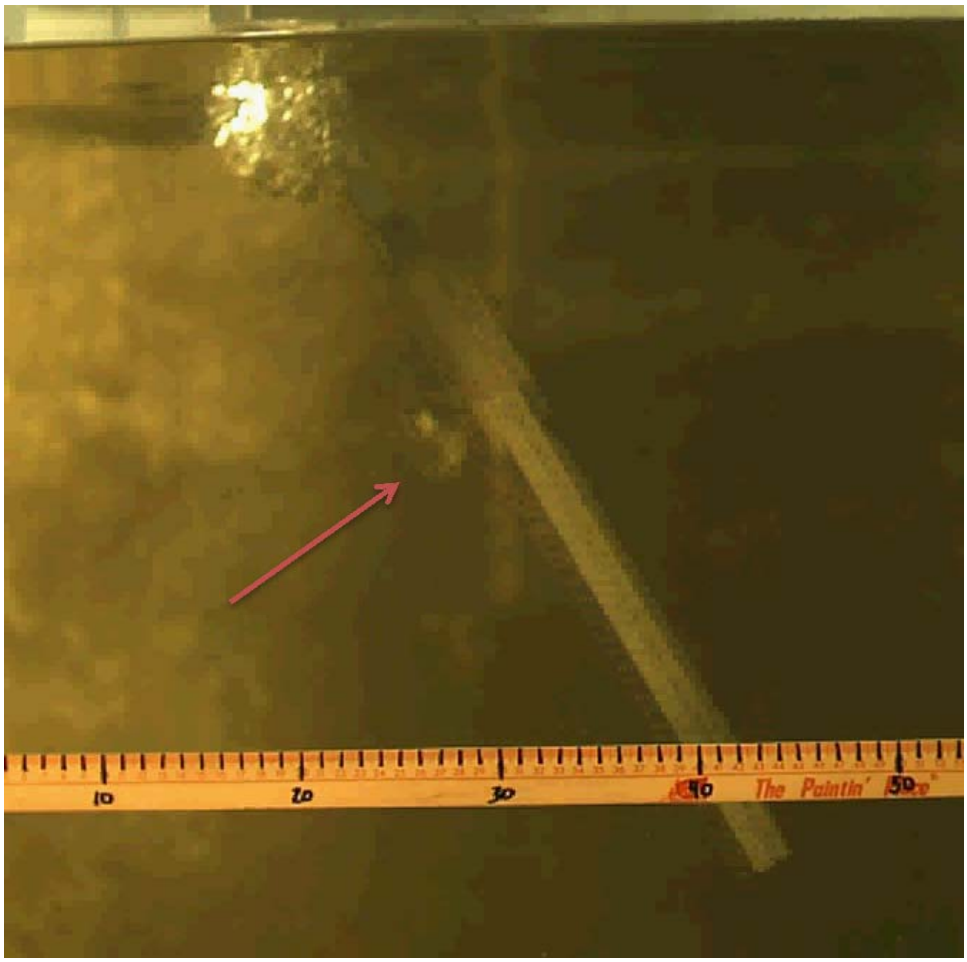

Figure 92 Development of bubbles from top of sample at +30º
(red arrow added)

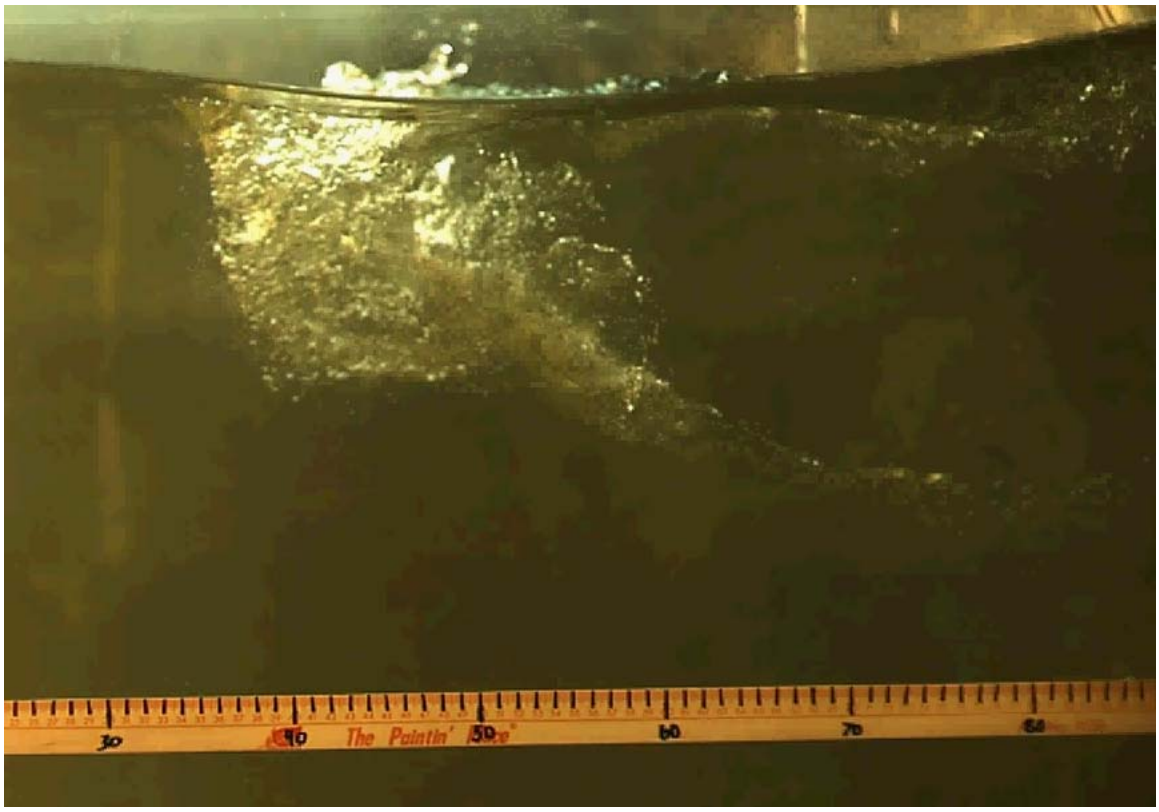

Figure 93 Bubbles from top of plate joining void behind plate for +30º

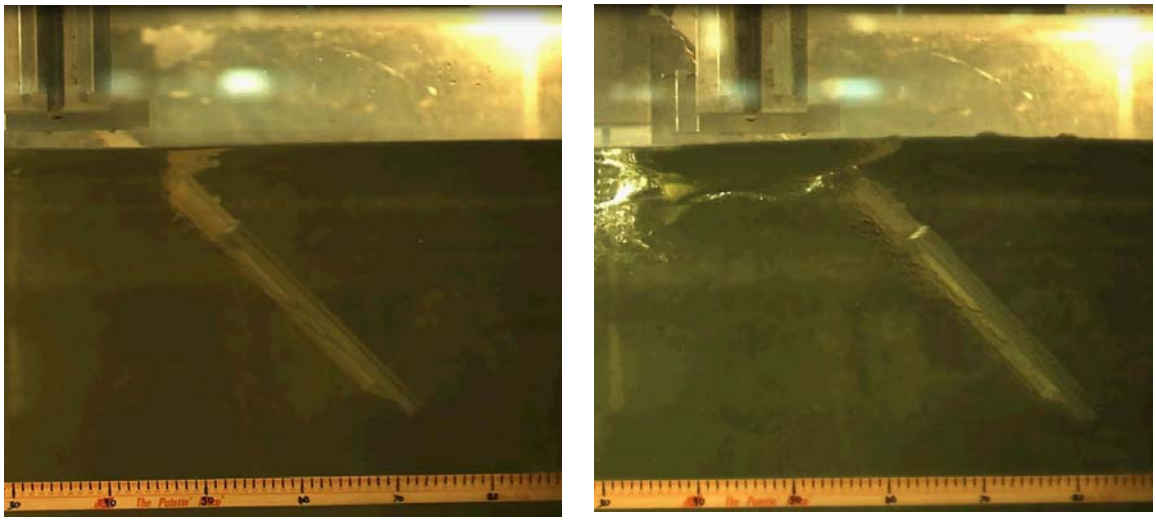

(a) (b)

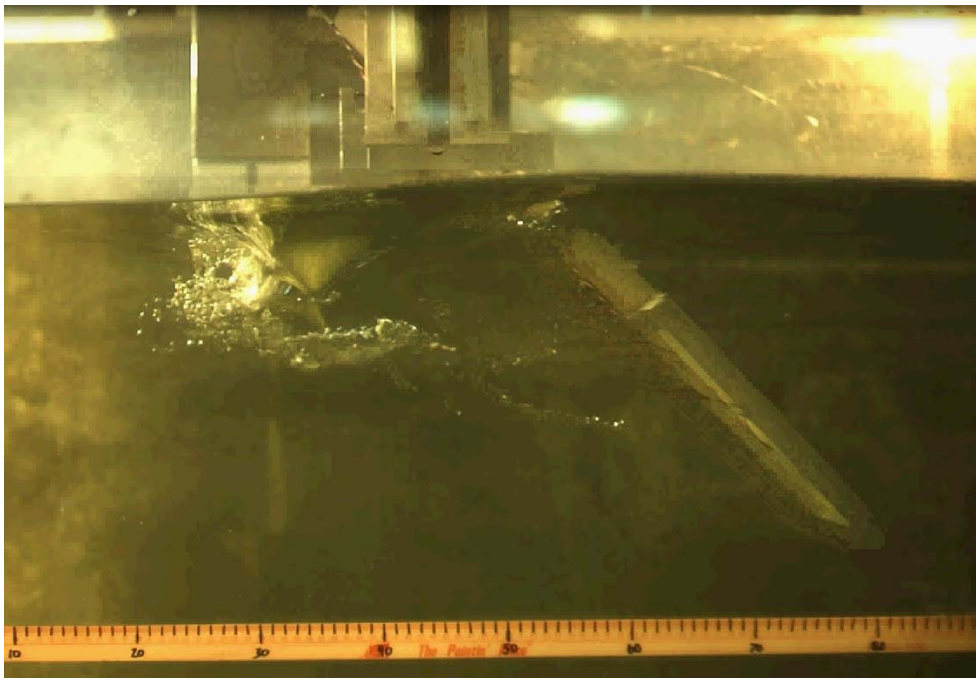

(c)

Figure 94 Video still for -45º position for: (a) 3 Hz, (b) 6 Hz, and (c) 9 Hz

For the -45º position a small bow wave is occurring directly above the plate for the lowest and moderate speeds, which becomes more pronounced at the highest speed. There is little interaction of the free surface at the slowest speed but free surface action is clearly seen at the moderate speed. At the highest speed the plate is interacting with the free surface and the same cavitation that was observed in the previous case is in this case. It is difficult in the video to determine where exactly the cavitation is coming from because bubbles begin forming at the free surface and from the support rig as the time motion begins. Furthermore, the video also shows clear vortices forming off of the top of the sample and interacting with the free surface.

Clearly the proximity to the free surface and position angle the plate affects the fluid structure interaction of the sample. Although there appears to be little interaction of the free surface at 0º at all speeds, at the extreme angles there is more interaction, even at lower speeds. The interaction at negative degree positions is also different than the interaction of positive degree positions. The most important observations appears that at the highest speed and the most extreme negative position angles (-45º and 9 Hz) a void is created behind the sample that is large enough that possibly no water at all is directly behind the plate. This effect can explain why the strain readings show a marked decrease from -30º to -45º in nearly all measurements and why this was pronounced at higher speeds and not as noticeable at lower speeds. Another important observation is that nearly at all angles there is an increased bow wave that occurs in front of the sample which in most cases is also a function of the speed the plate is at. This effect results in a mass change that is going on that directly will affect the force response of the sample.

F. SOURCES OF ERROR

1. Slippage of Pulley System

It was noticed that higher motor RPM does not translate to higher speeds of a sample through the water. This is noticeable when comparing Figure 16 showing motor RPM to Figure 37 containing the velocity of the plate in water in the steady state region. Motor RPM shows a near perfect linear increase while the velocity of the plate in the water does not linearly increase through higher speeds. This could be related to the drive

mechanism of the tow tank. The motor turns a pulley system, one of which drives the carriage via a braided steel cable. Although the pulley connection between the motor and the drive axle may slip this system contains a tensioner device. More likely, the braided steel cable is slipping against the drive pulley which has a quarter-inch groove for the cable but is otherwise smooth. Figure 95 is RPM vs linear velocity of the frame through water for each speed setting possible. If there was perfect transmission of the motor RPM to linear motion, there would be a proportional increase between the two.

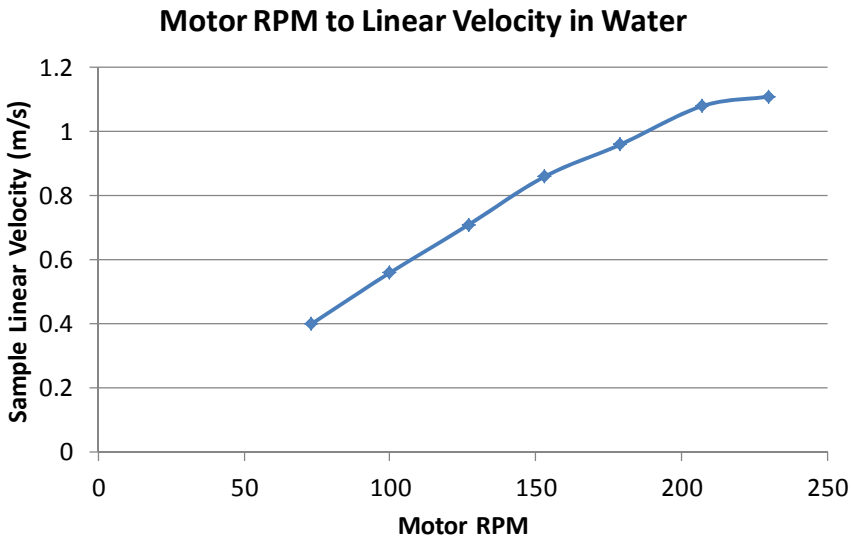

Figure 95 Comparison of motor speed to linear speed in water per speed setting

2. Short Tow Tank

The testing environment could have introduced error into the test due to the size and limitations of the tow tank. It was noticed at higher speeds that there was no true steady state zone with great fluctuation of data. With a short tow tank, very little time is able to be tested at high speeds. Furthermore, the short tank with blunt ends results in significant wave reflection. As waves are reflected back during testing, new forces are introduced that would otherwise not be there in open water.

3. Manual Determination of Transient Zone and Steady State Zone

With no computer algorithm or program to analyze the output, all data analyzed was manually processed and left up to the author's best judgment when force was no longer transient but had entered the steady state period. Although an attempt was made to use mathematical analysis of the velocity data for this determination, without longer velocity data this process was ultimately still left up to the judgment of the author. Finally, even though a mathematically approach was attempted on the velocity data, the velocity data and data acquisition system providing the force and strain data are in no way linked and therefore the force data is void of knowledge of velocity at that time.

4. Camera Accuracy for Velocity

Even with a camera that recorded at high speeds, high frame rates of 600 frames per second were about the highest that were able to be used with testing still visible. The camera is able to record up to 1000 frames per second but at this high frame rate the amount of light needed was far greater than able to be provided even with camera aperture opened the entire way. When trying to line up the sample in video analysis with marking of 0.01 meters the sample does not always perfectly fall in line with the position marking due to frame rate.

5. Manual Acquisition of Position and Time

Because the position versus time data was all obtained manually, frame by frame from video recording, the chance of error being introduced into this data is possible. This is worth noting because such error would not be introduced into the force and strain data obtained via a computer data system.

6. Change in Strain Gauge Accuracy with Time

The electronics technician pointed out that the adhesive and water-proofing on the strain gauges can break down with time. To minimize the contact with water the sample was stored at the most extreme angle of -80º whenever testing was not occurring which placed the sample above the water level. However, it was still of concern that there could be degradation. The static strain was compared for each test in the order the test was

completed; Figure 96 shows the x-direction information. The static strain appears stable across the test order so it does not appear that for the testing performed that any degradation of the strain gauges occurred.

Figure 96 Static strain in order of test performed

IV. CONCLUSIONS AND RECOMMENDATIONS

A. APPLICABILITY TO THE LARGER SCALE

Truly understanding mechanical reaction in a fluid system is a complex problem. Applying theory can only do so much; investigation through experimentation is required to move forward with broad application and design implications. This experiment proved troublesome as the testing equipment used may not provide an ideal testing environment, especially considering that at higher speeds a few secondary problems such reduction of power transferred from the motor to the sample piece and reflected wave forces could be encountered. This results in high speed data being very unreliable to draw major conclusions from. However, a stiff aluminum plate sample appears to respond as expected compared to theoretical data. This does not transfer over to the expectations of the composite plate, clearly there are factors making the composite material interact differently that have not been accounted for. Furthermore, when investigating a clamped boundary condition of the composite plate, there is universally a reduction in strain when near the clamped boundary and at a steep negative angle. This could be analogous to the difference in hull design between a DDG-51 Arleigh-Burke Class destroyer and DDG-1000 Zumwalt Class's tumblehome hull. Figure 97 shows how these hulls have different angles at the waterline which should factor into the design of a composite hulled ship.

Figure 97 Comparison of DDG-51 to DDG-1000 waterline hull angles, from [20] and [21]

This study will also go to further the idea of fluid structure interaction with composite material. Taking the results of this study and comparing them to CFD and FSI models will help to validate the models ability to accurately predict force response. This will improve the ability to apply composite materials to construction where no testing or experimentation is possible. When a large warship is built, there is no prototype and therefore little room for error. Having a robust computer solution to a large problem will not only reduce cost but even more importantly when considering large naval ships, save lives.

B. RECOMMENDATIONS

Further research is needed to expand this study. The data produced by this investigation proved very difficult to analyze and a more exhaustive research effort could help refine this. Further tests at the same speeds and angles with the same equipment could be conducted to begin to understand the statistical variability of the data. If many tests were done and the average values presented with error analysis between the tests, it could help refine how unpredictable the material's mechanical response is compared to how much influence the testing equipment has on erroneous readings.

Obtaining speed data of the plate from position and time measurements using a camera and ruler could be improved on. Not only is this process manpower intensive to collect, there is a degree of error involved between the equipment and manual collection of data. Furthermore this data is limited in the length of testing available. If an optical position encoder were installed on the tank, velocity of the carriage could be measured for the entire length of the tank which would correspond directly to the velocity of the test piece in the tank. Furthermore, by adding a computer data acquisition system to obtain time and position information, this can be tied directly in with the data acquisition system already in place allowing direct comparison between time, position, velocity, acceleration, force and strain at any given moment while testing.

Another recommendation would be to improve the mechanical connection between the carriage and the drive motor, the current configuration does not allow for complete transfer of motive force to the carriage due to slippage of the braided tow cable.

As mentioned this has introduced uncertainty into the fidelity of the higher speed test data.

Strain information for the unclamped rectangular sections would provide more information about how these plates deform during testing which could help understand the area reduction and therefore further refine the theoretical force response of the plate.

C. CONCLUSION

Understanding the velocity profile and acceleration of a composite structure is important for use in computer based FSI models. By developing a robust velocity profile for various conditions, this informant can be used as a variable in computer models to understand how the result compares to experimental data. In Knutton's thesis, separate acceleration situations of monotonically increasing, linearly increasing and monotonically decreasing along with step increases were considered for computer modeling [10]. However in practice, combinations of these situations may be occurring and it may be that for the same object lower speed acceleration may be a different profile compared to higher speed acceleration. This was observed not just for the aluminum rigid body scenario but also for the composite pieces which demonstrated not only a combination of acceleration situations but also at lower speeds the situation involved monotonically increasing whereas higher speeds were monotonically decreasing.

Because of the small relative difference in density between composites and water, the fluid structure interaction between the two becomes complex. The lower density and lower stiffness of the composite plate compared to the aluminum plate influences significantly the pressure forces applied to the composite plate as the speed of the plate increases. The density and elastic modulus of the composite plate are about 55% and 30% of those of aluminum, respectively.

The position angle of the sample can change the way the composite sample interacts with the free surface. By changing the combination of the speed and position angle, the degree of free surface interaction with the sample changes which influences the fluid structure interaction. Not only do extreme angles (and therefore closest proximity to the free surface) and high speeds produce the more pronounced effects, but the

variations of positive to negative angles also produce different effects. At an extreme negative position angle, water cannot be replaced behind the plate fast enough exposing the sample to air. And an extreme positive position, the change in pressure across the top of the plate can cause cavitation and vortices. These free surface effects can explain why strain decreases at the most extreme negative angles and does so sharply and higher speeds.

This study helped to expand the body of knowledge about composite materials and their mechanical response to loads encountered in a marine environment. By furthering this research will allow the greatest use of composite materials for shipboard application.

APPENDIX A. FRAME SCHEMATIC

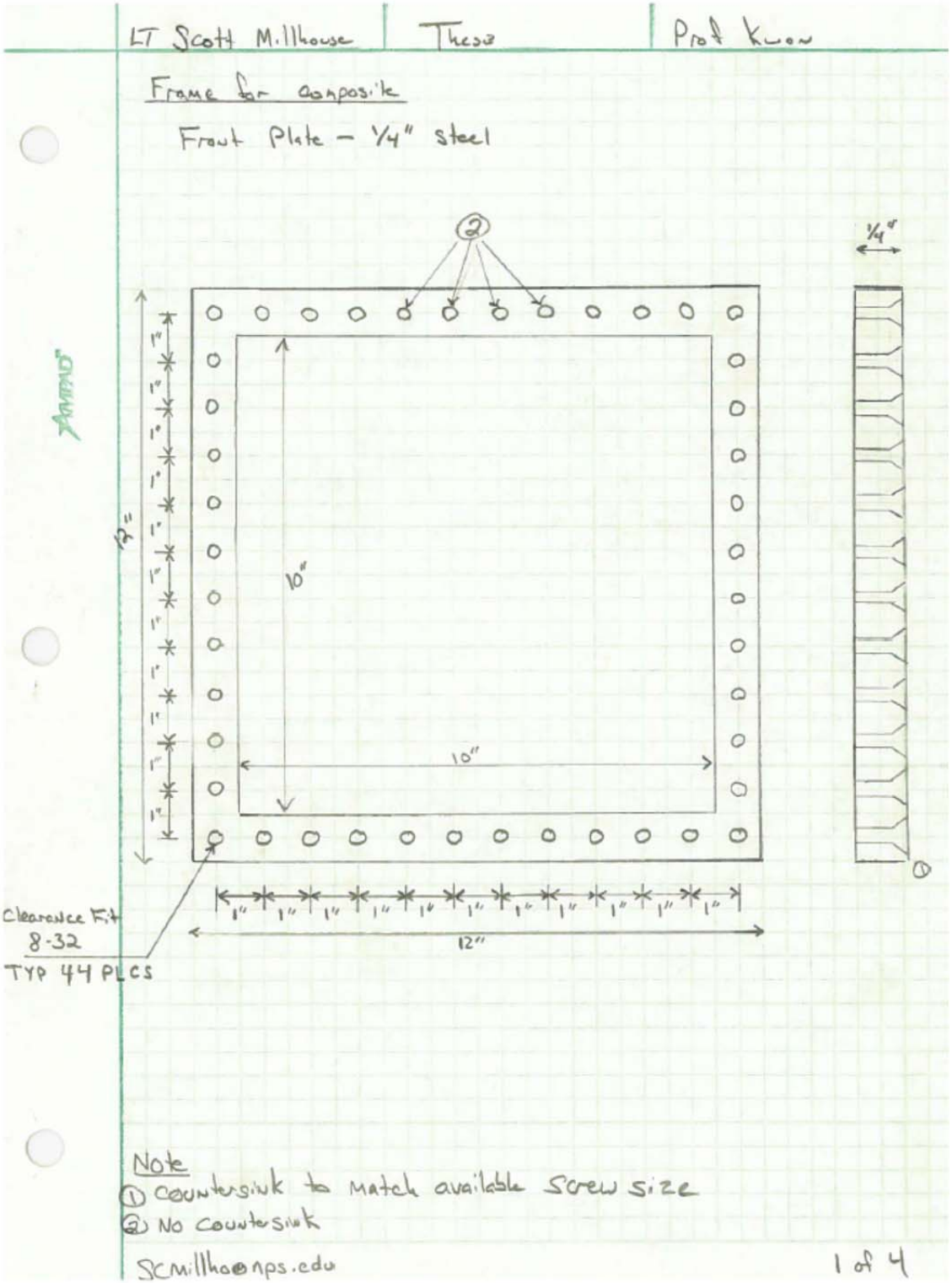

LT Scott Millhouse | Thesis | Prof Kwon

Frame For Composite

Back Plate – ½" steel

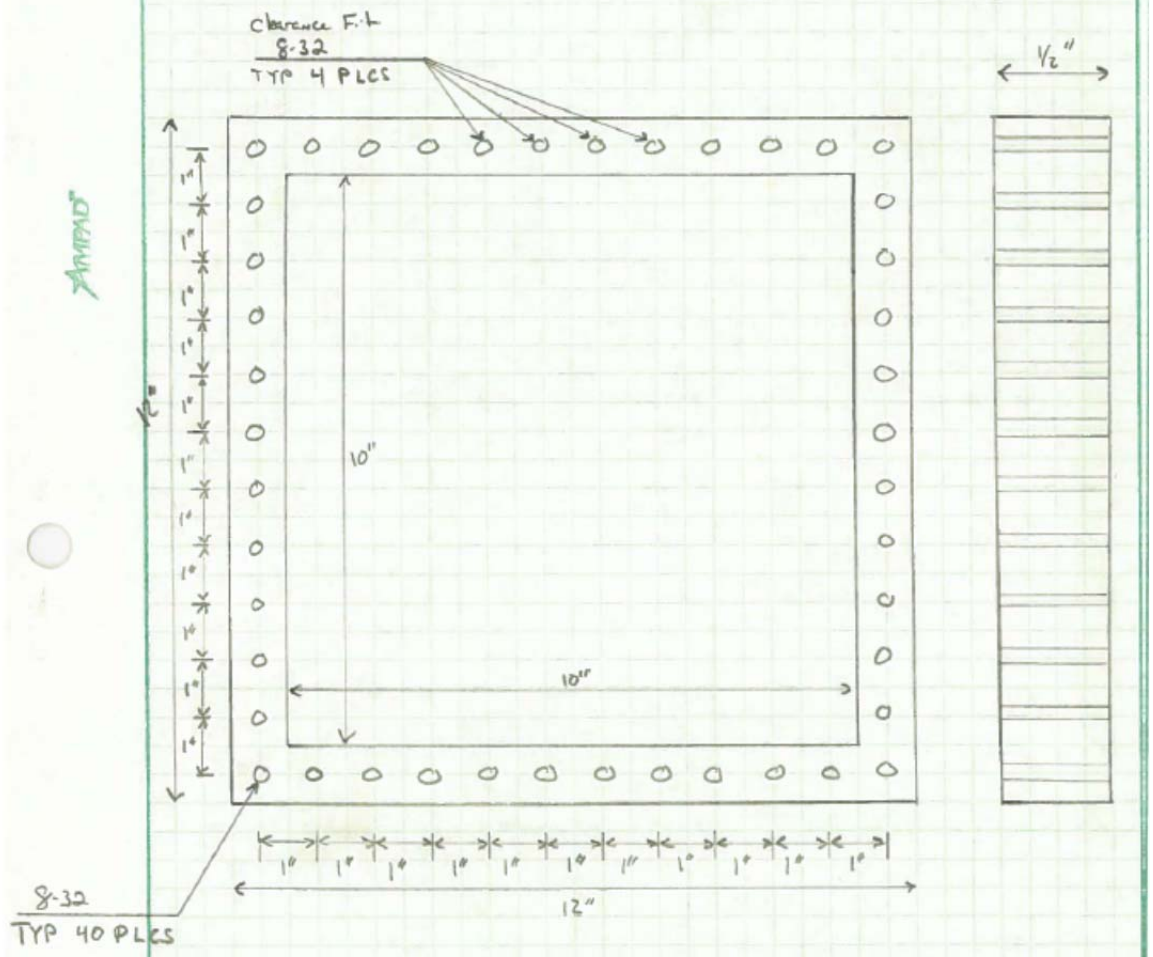

SCMillho@aps.edu

2 of 4

LT Scott Millhouse | Thesis | Prof Kwon

Frame For Composite

Front support T - 1/4" Steel

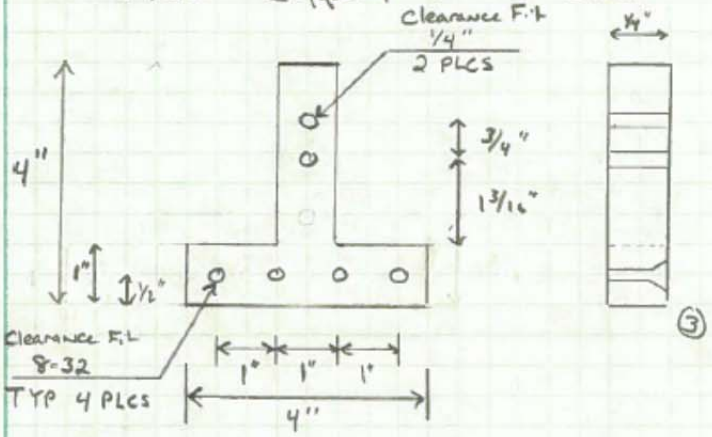

Note
③ Countersink to available screw size

Back support T - 1/4" Steel

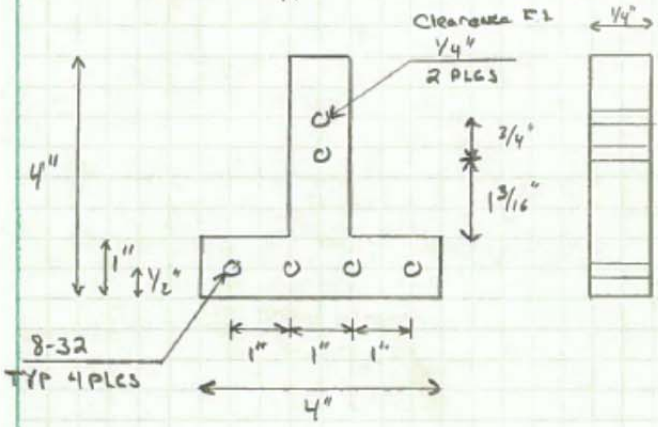

Spacers X3 - 1/16" Steel

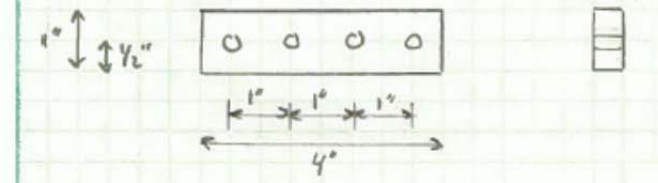

SCMillho@nps.edu

3 of 4

assembly at connection with arm

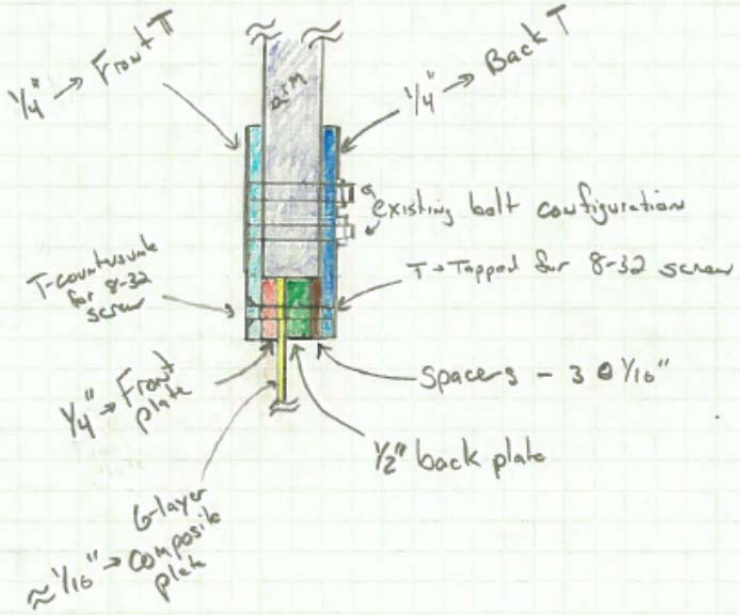

SCMillho@nps.edu

APPENDIX B. ANGLE SELECTOR SCHEMATIC

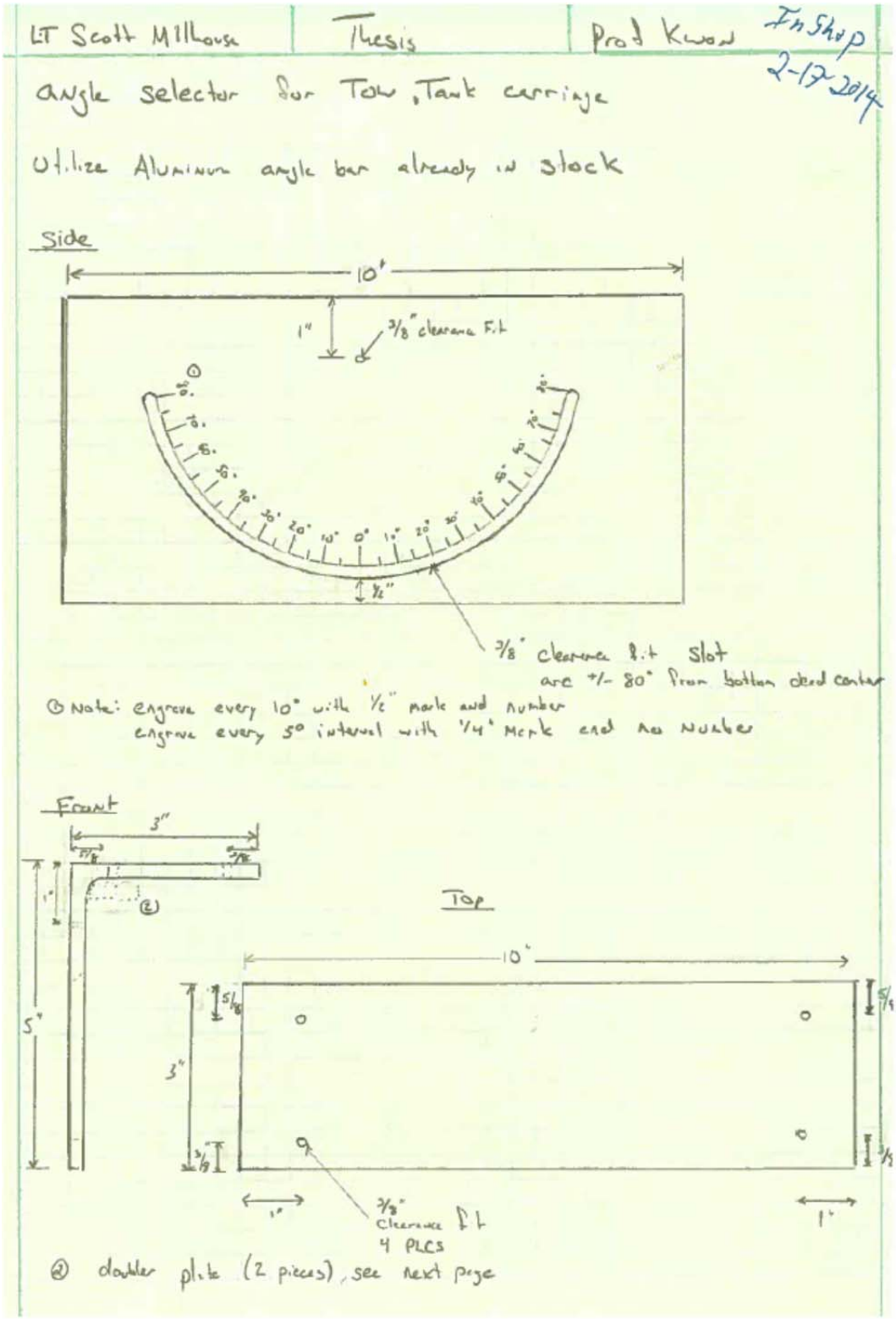

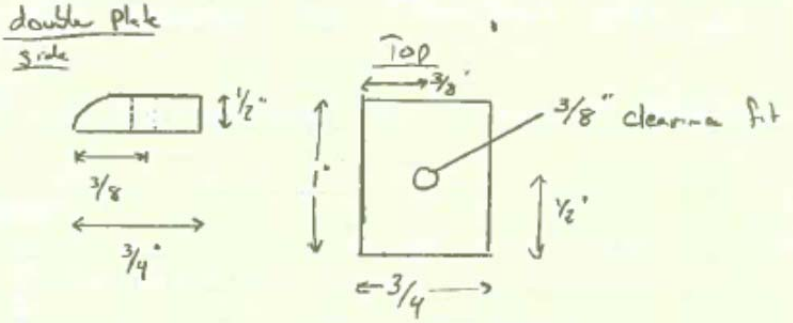
double plate
side
1/2"
3/8
3/4"
Top
3/8"
1"
3/8" clearance fit
1/2"
3/4

APPENDIX C. TOW TANK STANDARD OPERATING PROCEDURE

1. Tow Tank Location

The tow tank is located in Halligan Hall in the Hydrodynamics Laboratory, Room 101C. Figure 98 is provided of the Naval Postgraduate School Public Works floor plan to show location on the first floor and provide orientation of North and South.

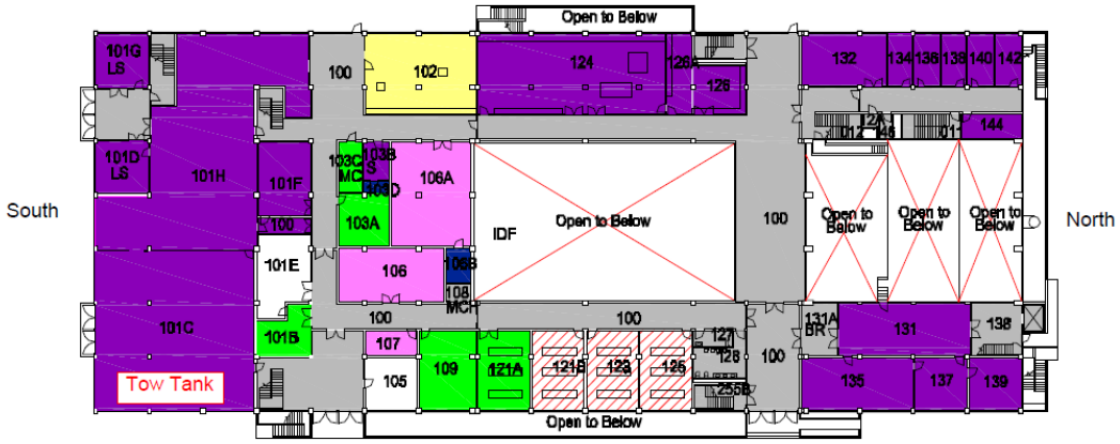

Figure 98 Tow tank location in Halligan Hall

2. Filling and Draining

The fill and drain locations are located at opposite ends of the tank. Both fill and drain connections have ball valves which require a 90° turn between full open and full close. The fill connection is located at the north end of the tank and is shown in Figure 99. The drain connection is under the tank as show in Figure 100 at the south end and provides drainage to a dedicated open floor drain in the trough system that runs throughout Halligan Hall. Care should be taken not to drain water directly into the trough system away from the dedicated drain as not all drains in the system are open and stagnant water will remain in the trough system.

Figure 99 Tow tank fill valve at north end of the tank

Figure 100 Tow tank draining location located at south end under tank

3. Tank Control

To turn the tank motor on, two power switches must be in the on position; these are located on the south end of Halligan Hall across from the drain connection. The location of the switches is specified in Figure 101.

Figure 101 Motor power switch location

The motor is controlled by a control panel shown in Figure 102 which has 100 feet of cable allowing control of the tank remotely from any location in the tank vicinity. The direction forward for the tow tank moves the carriage towards the north end of the tank and the reverse direction moves the carriage to the south end. The panel performs the following functions

- ENTER: press once to change speed setting in Hz, use up and down to toggle speeds, press ENTER again to set speed.
- LOCAL/REMOTE: press such that “Local” is in the upper right corner of the screen for operation from the control panel.
- JOG: press such that JOG is illuminated, then press and hold FWD or REV for motion at 3 Hz; motion only while direction is held, as soon as released motion stops. Only moves carriage at 3 Hz.
- FWD or REV: instantly moves carriage in direction at the set speed. Carriage motion continues until STOP is pressed.

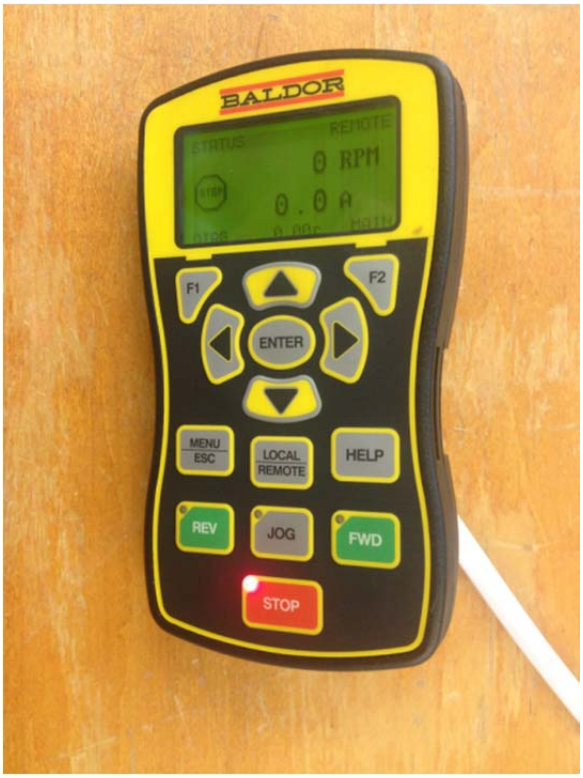

Figure 102 Motor control panel

THIS PAGE INTENTIONALLY LEFT BLANK

APPENDIX D. VELOCITY DATA

1. Aluminum Plate in Air

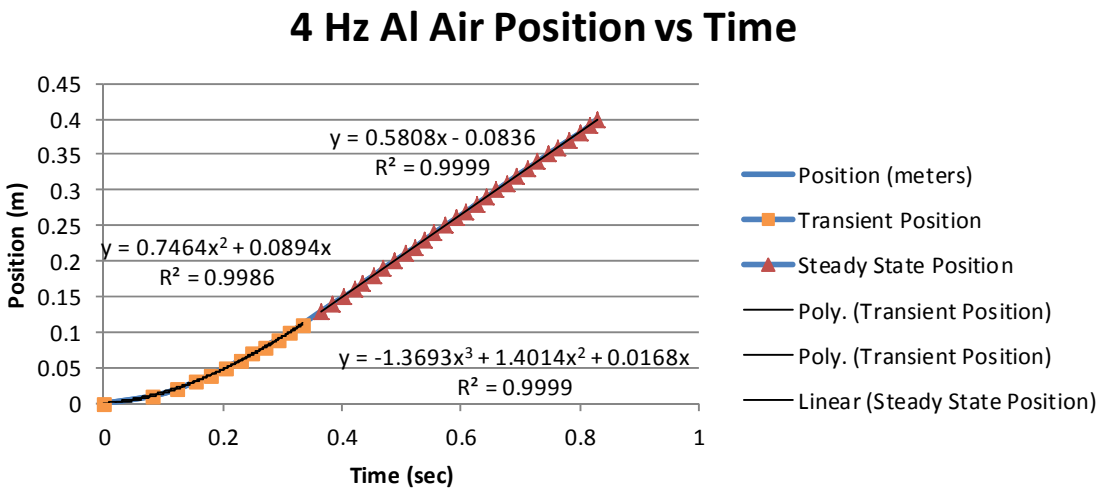

Figure 103 Aluminum sample position vs time at 4 Hz speed setting

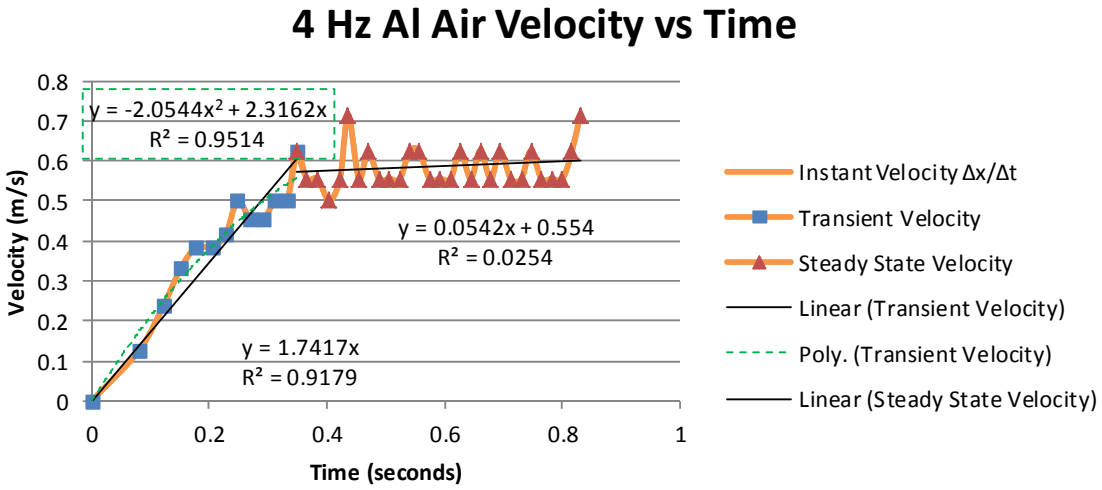

Figure 104 Aluminum sample velocity vs time at 4 Hz speed setting

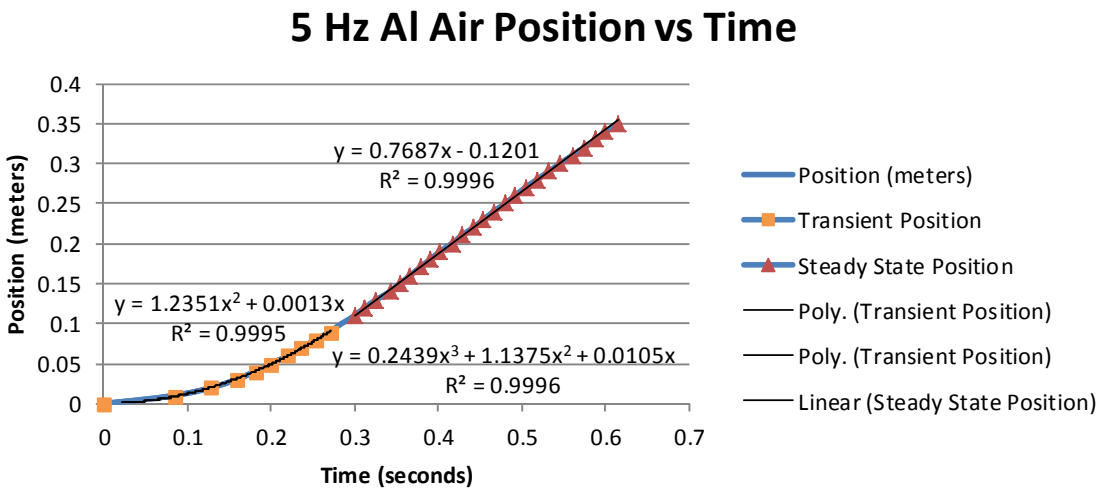

Figure 105 Aluminum sample position vs time at 5 Hz speed setting

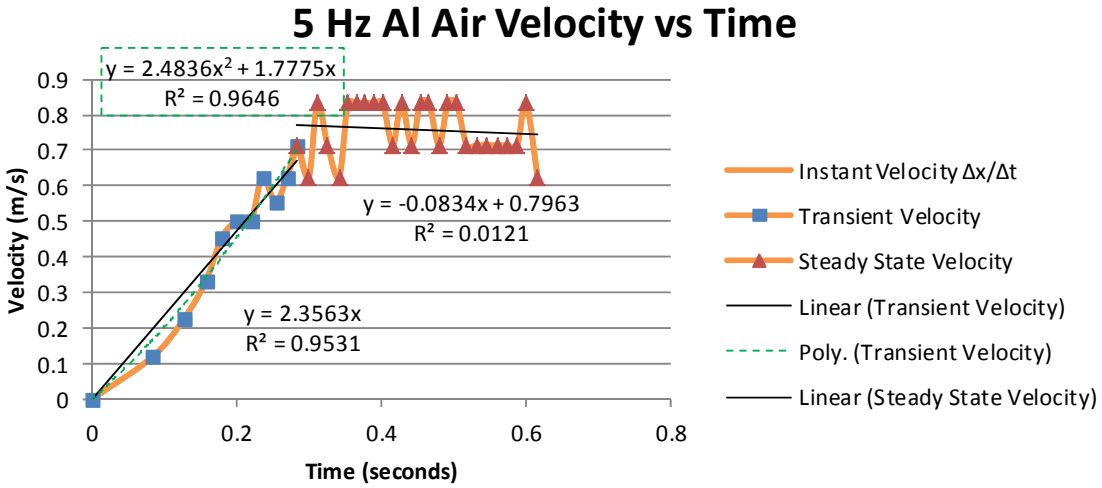

Figure 106 Aluminum sample velocity vs time at 5 Hz speed setting

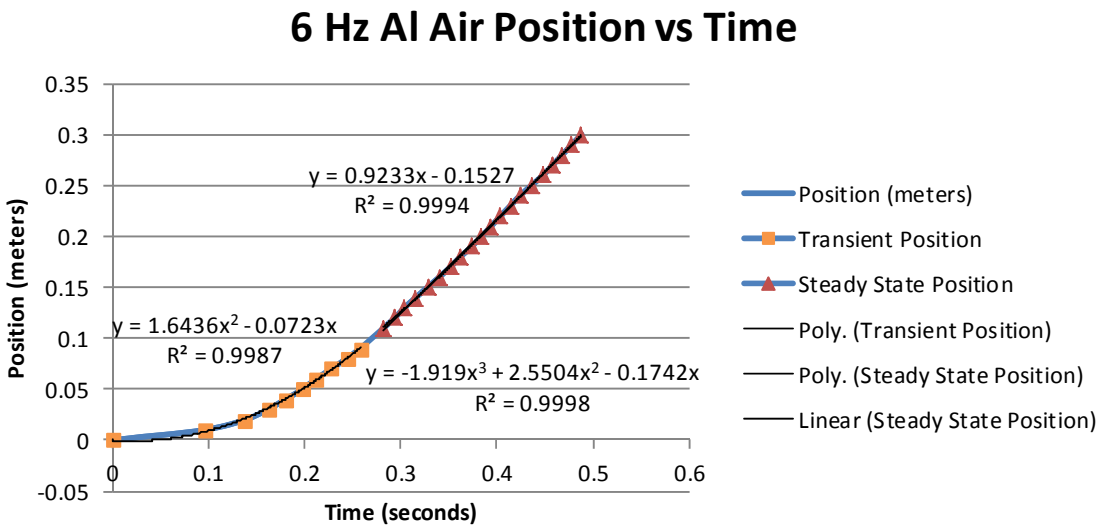

Figure 107 Aluminum sample position vs time at 6 Hz speed setting

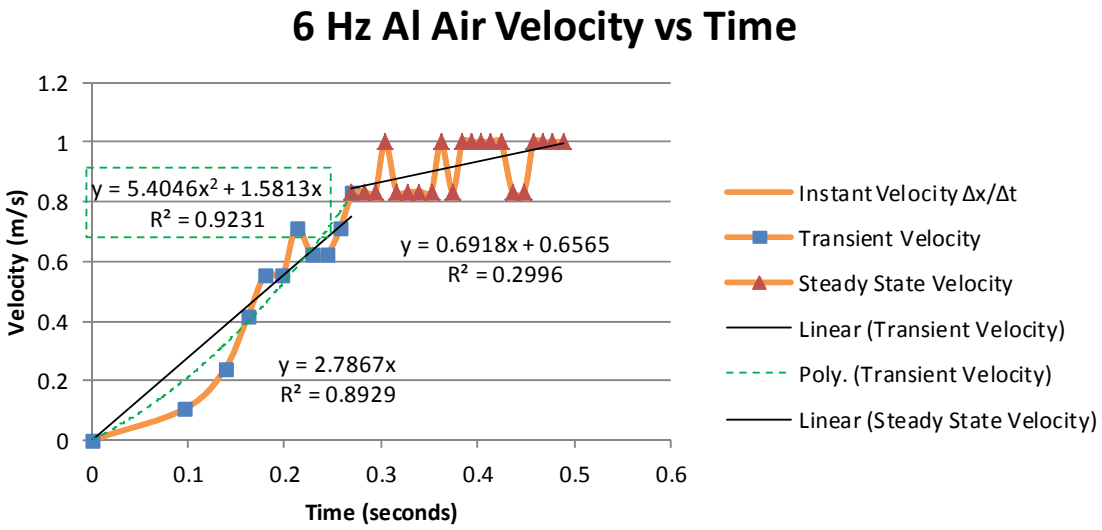

Figure 108 Aluminum sample velocity vs time at 6 Hz speed setting

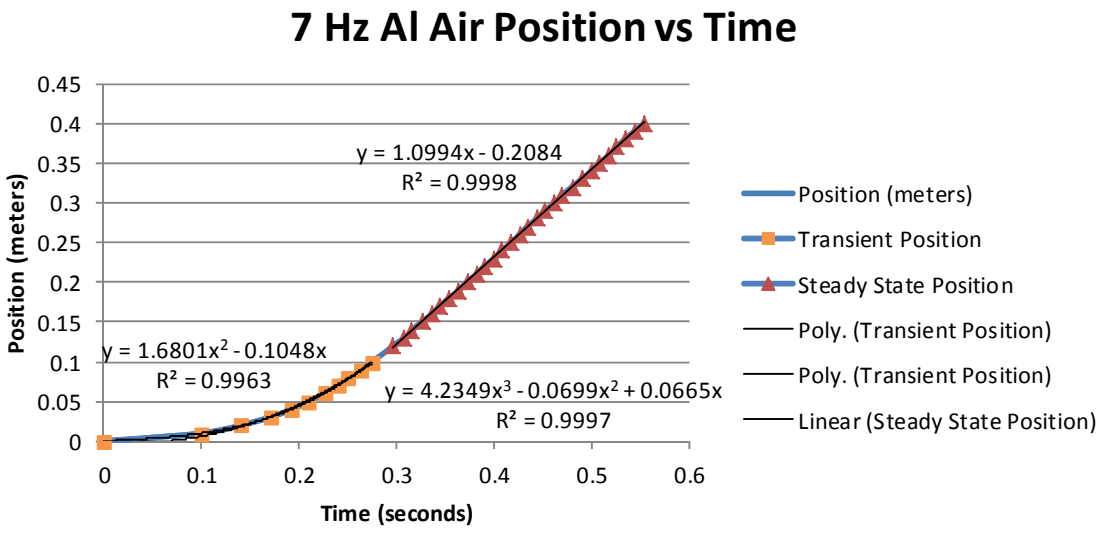

Figure 109 Aluminum sample position vs time at 7 Hz speed setting

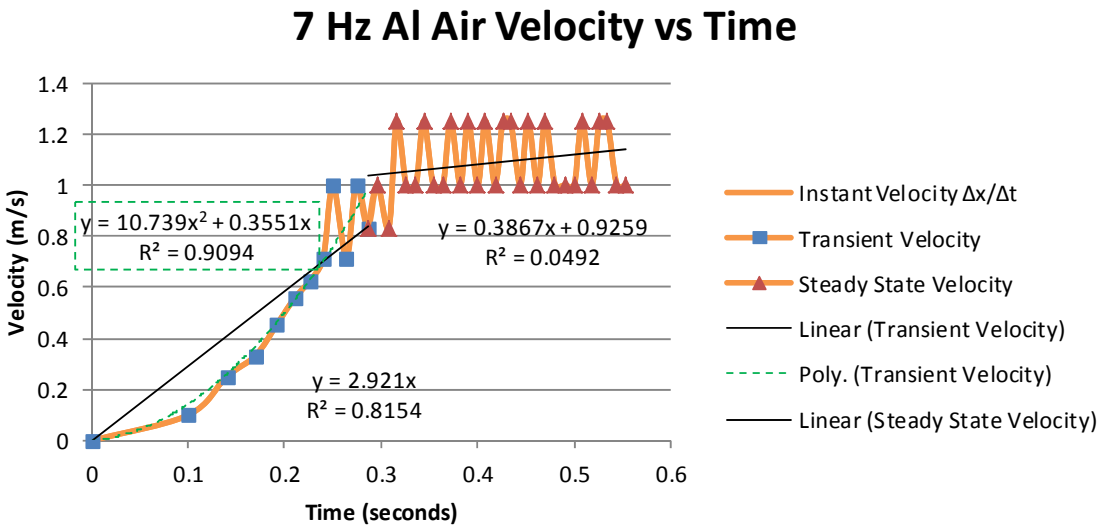

Figure 110 Aluminum sample velocity vs time at 7 Hz speed setting

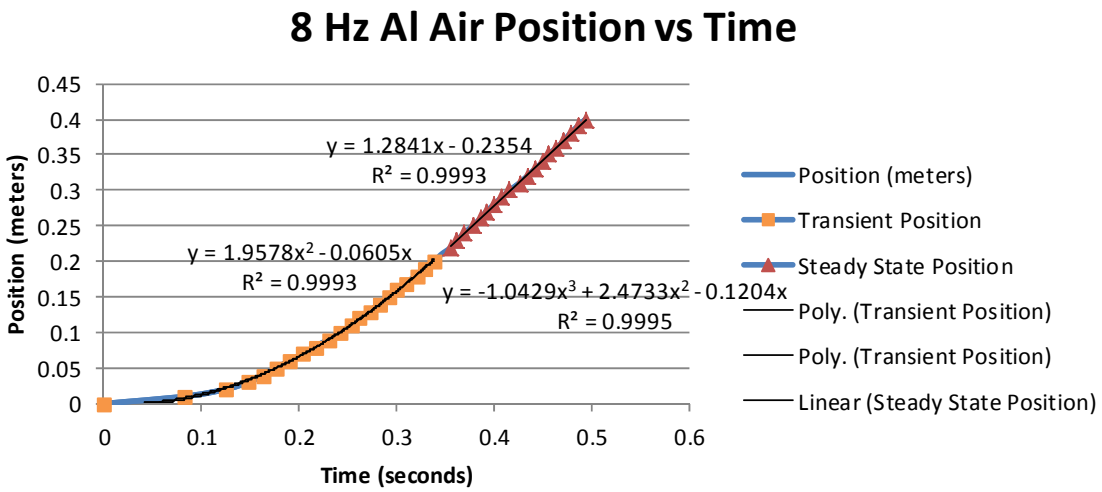

Figure 111 Aluminum sample position vs time at 8 Hz speed setting

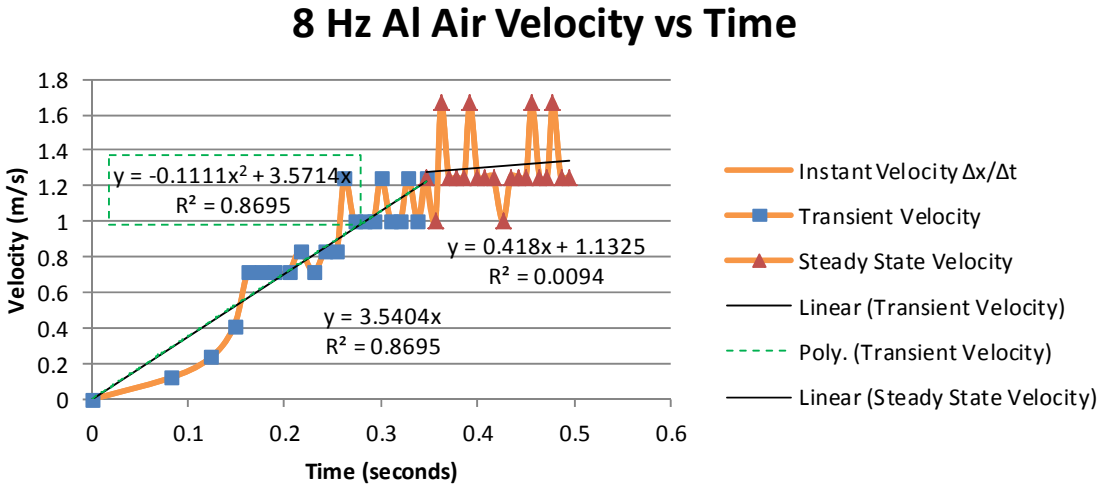

Figure 112 Aluminum sample velocity vs time at 8 Hz speed setting

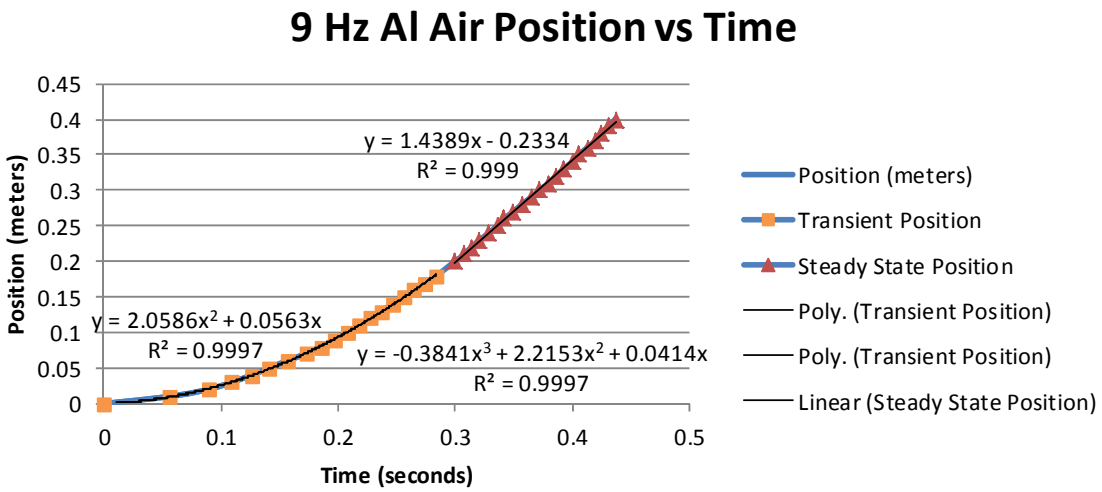

Figure 113 Aluminum sample position vs time at 9 Hz speed setting

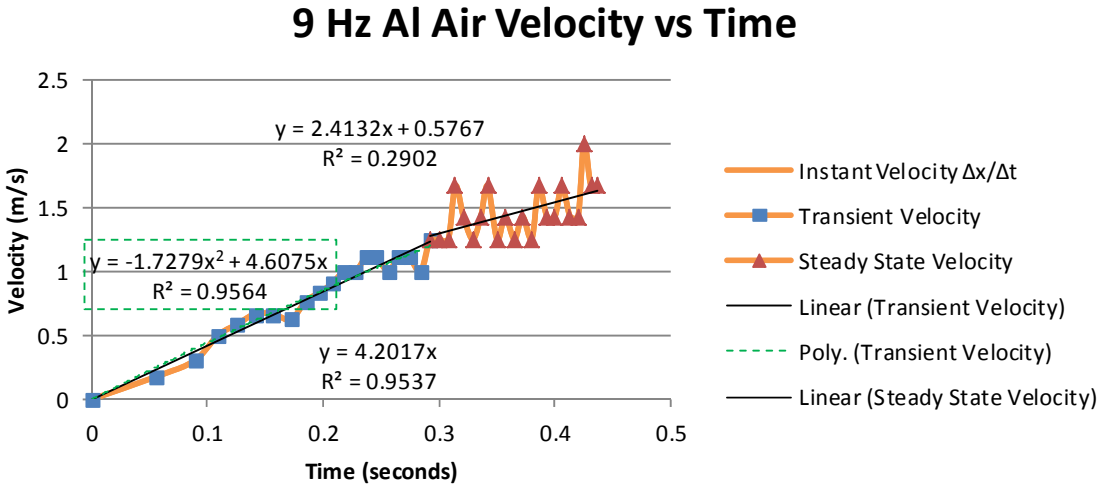

Figure 114 Aluminum sample velocity vs time at 9 Hz speed setting

2. Six-Layer Composite with Frame in Air

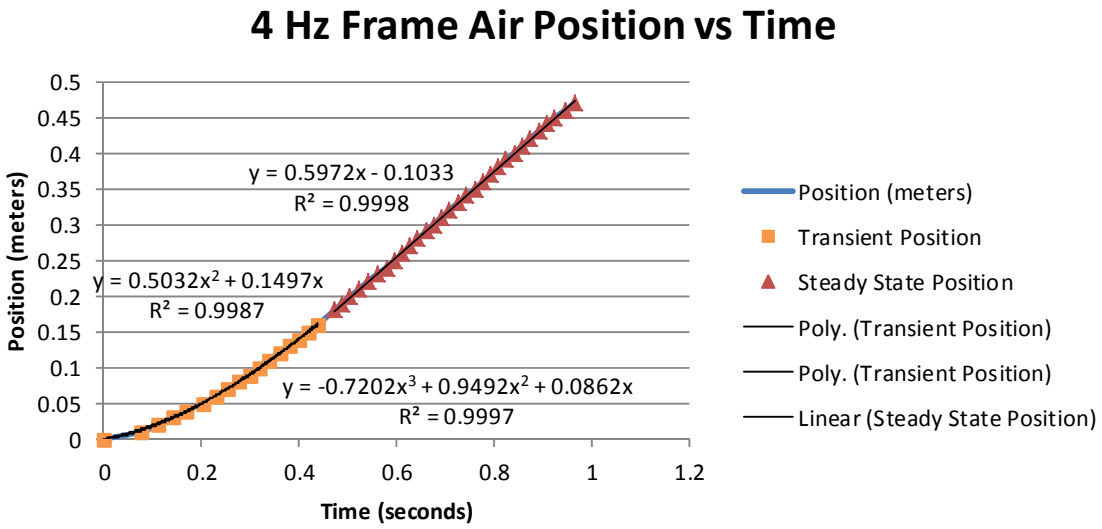

Figure 115 Frame position vs time at 4 Hz speed setting

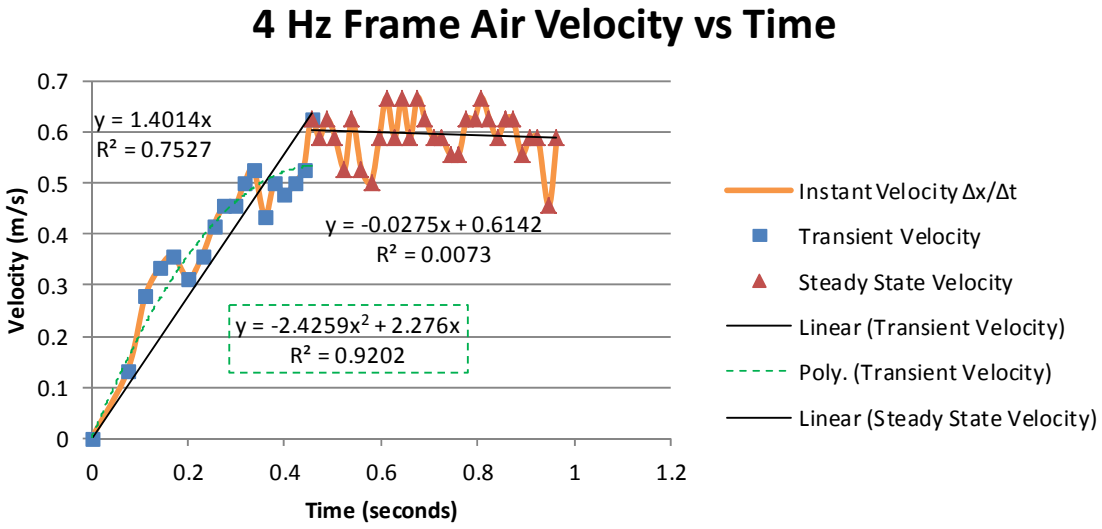

Figure 116 Frame velocity vs time at 4 Hz speed setting

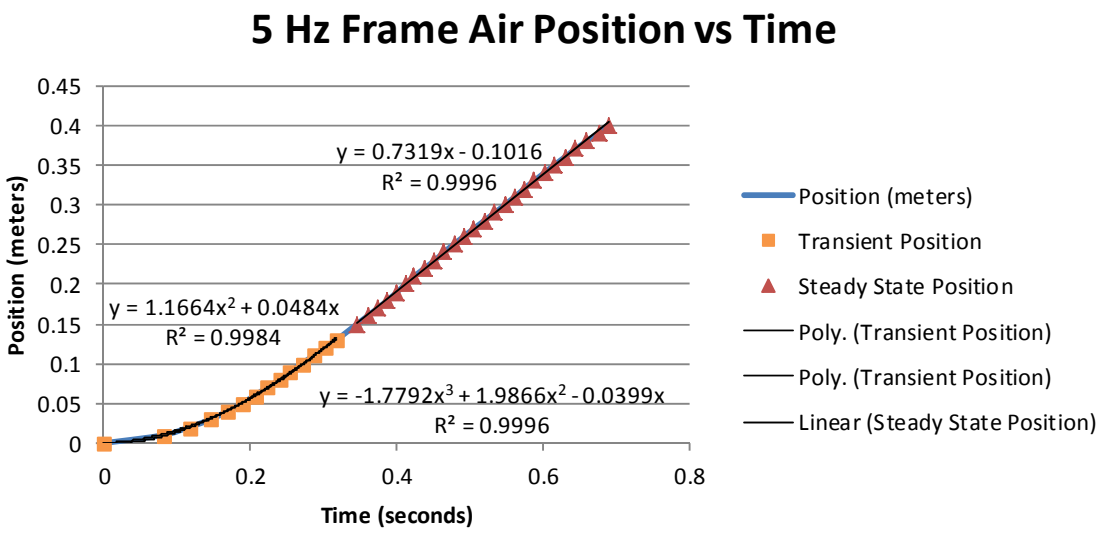

Figure 117 Frame position vs time at 5 Hz speed setting

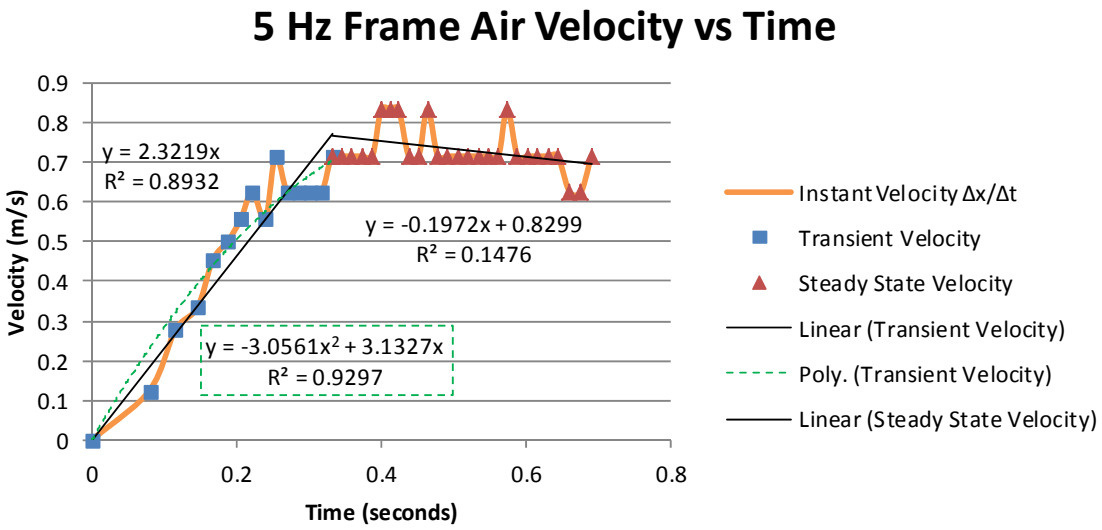

Figure 118 Frame velocity vs time at 5 Hz speed setting

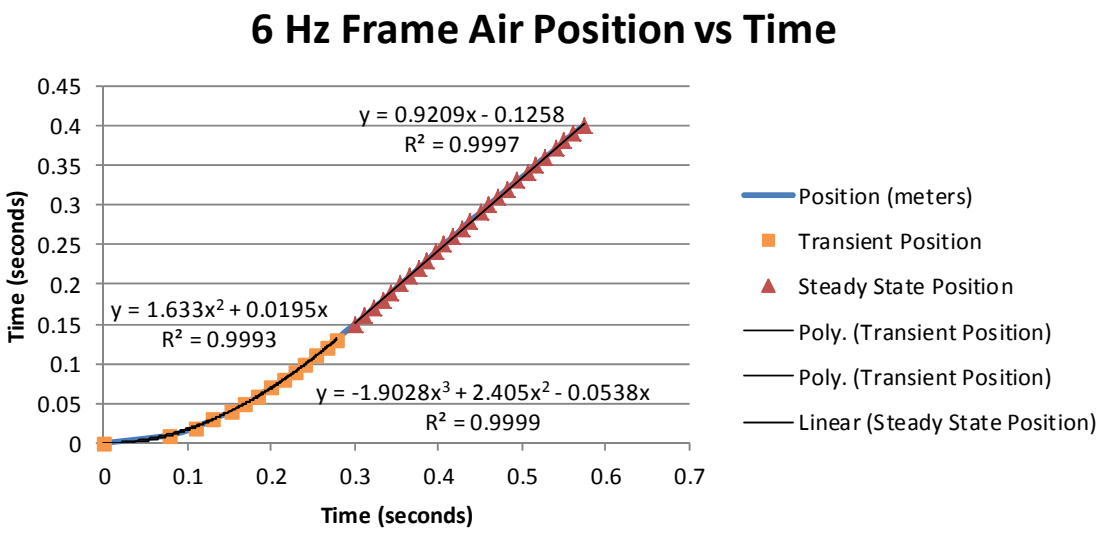

Figure 119 Frame position vs time at 6 Hz speed setting

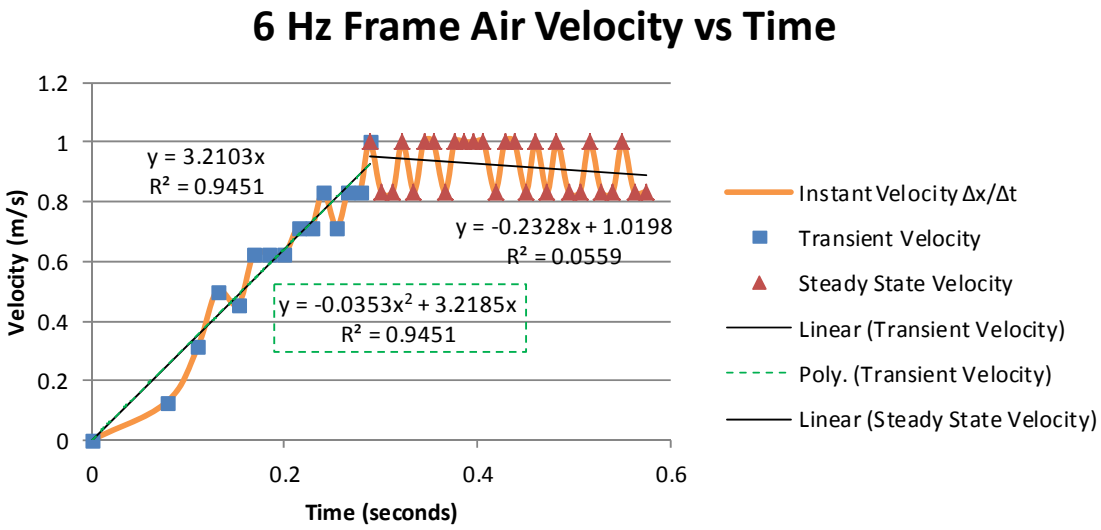

Figure 120 Frame velocity vs time at 6 Hz speed setting

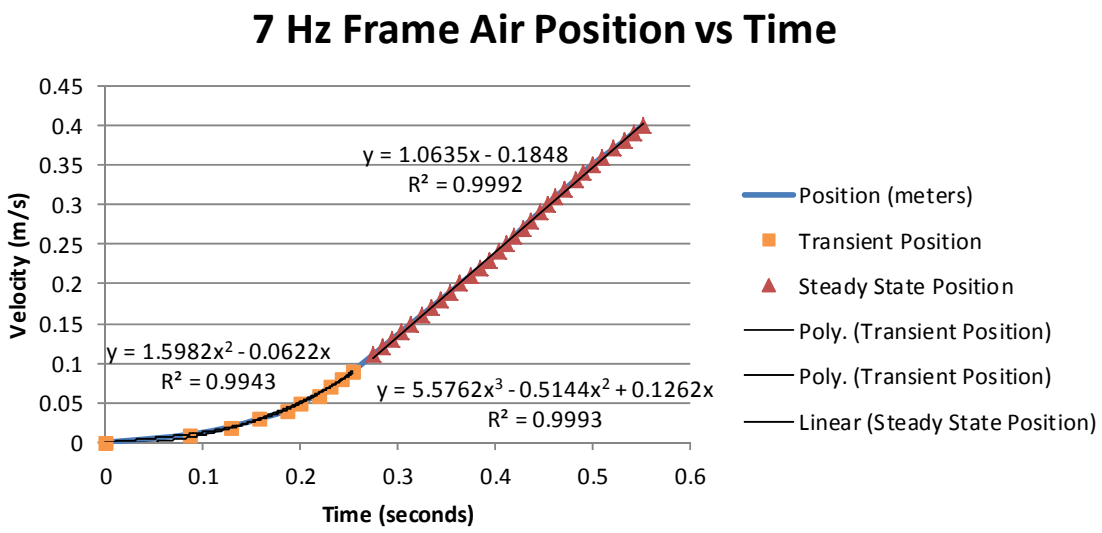

Figure 121 Frame position vs time at 7 Hz speed setting

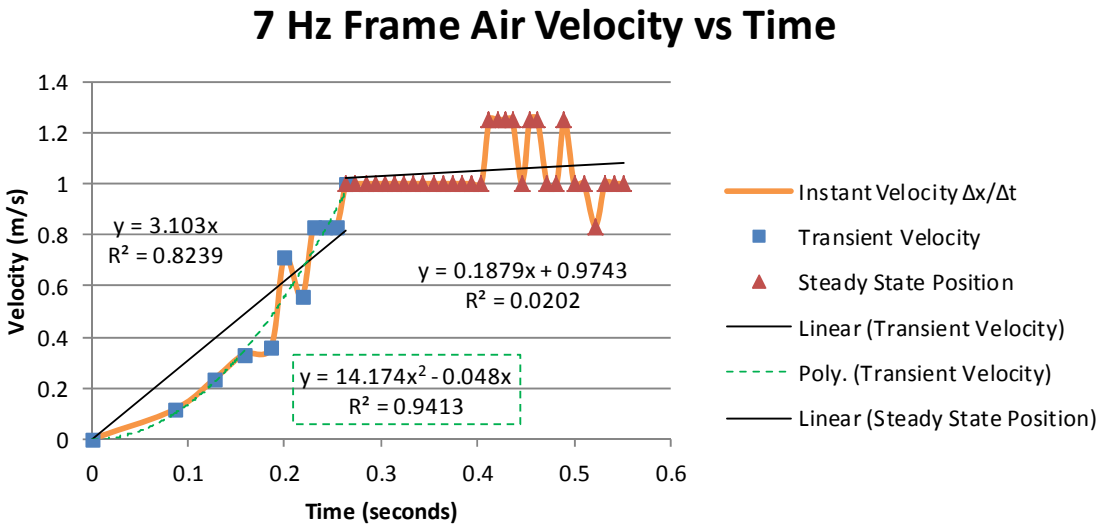

Figure 122 Frame velocity vs time at 7 Hz speed setting

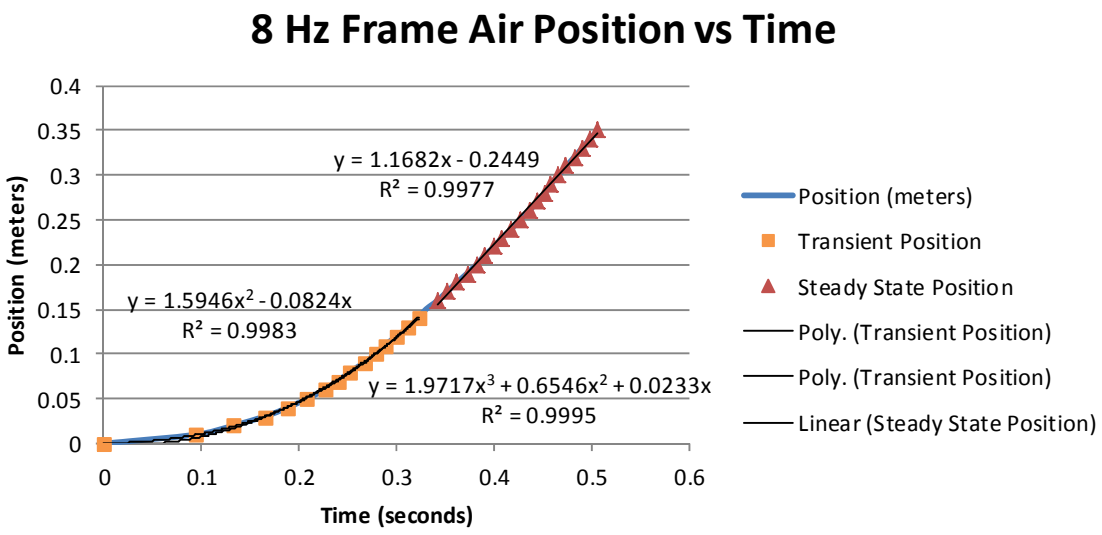

Figure 123 Frame position vs time at 8 Hz speed setting

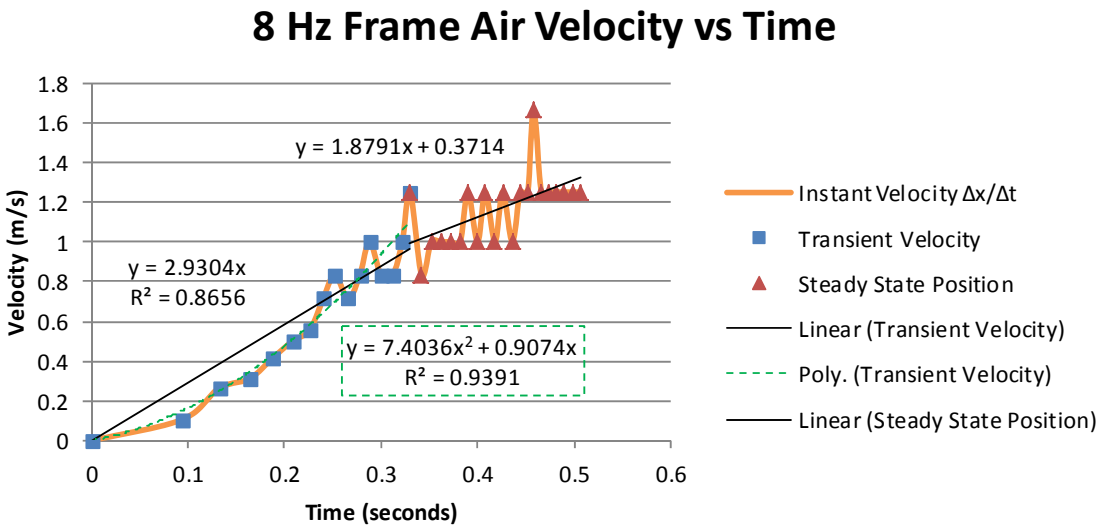

Figure 124 Frame velocity vs time at 8 Hz speed setting

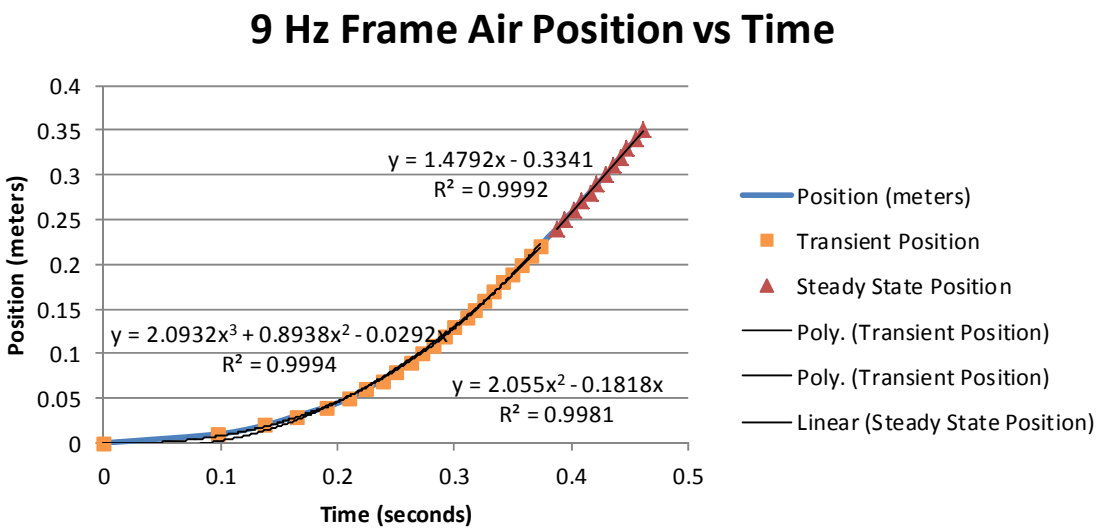

Figure 125 Frame position vs time at 9 Hz speed setting

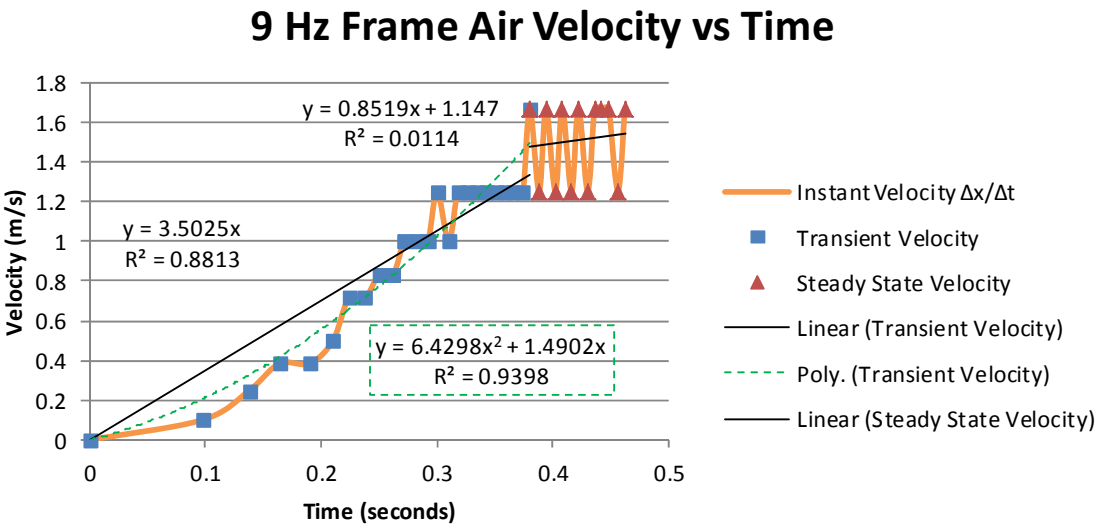

Figure 126 Frame velocity vs time at 9 Hz speed setting

3. Six-Layer Composite Frame in Water

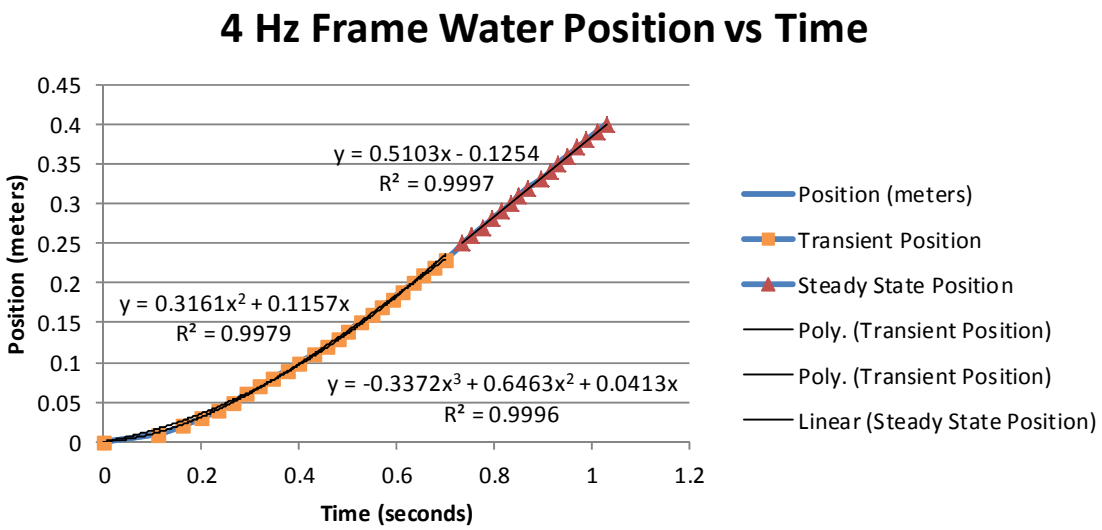

Figure 127 Frame position vs time at 4 Hz speed setting

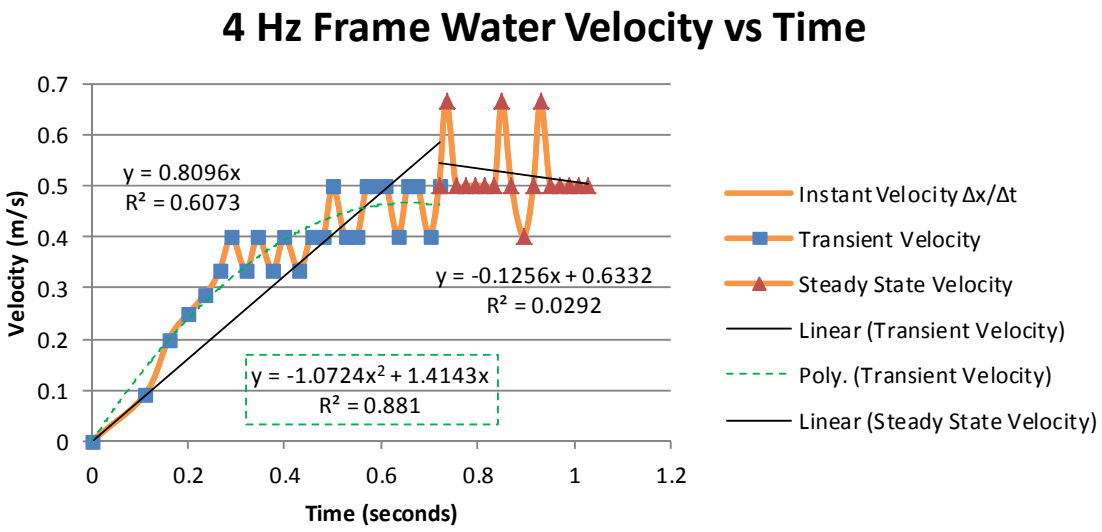

Figure 128 Frame velocity vs time at 4 Hz speed setting

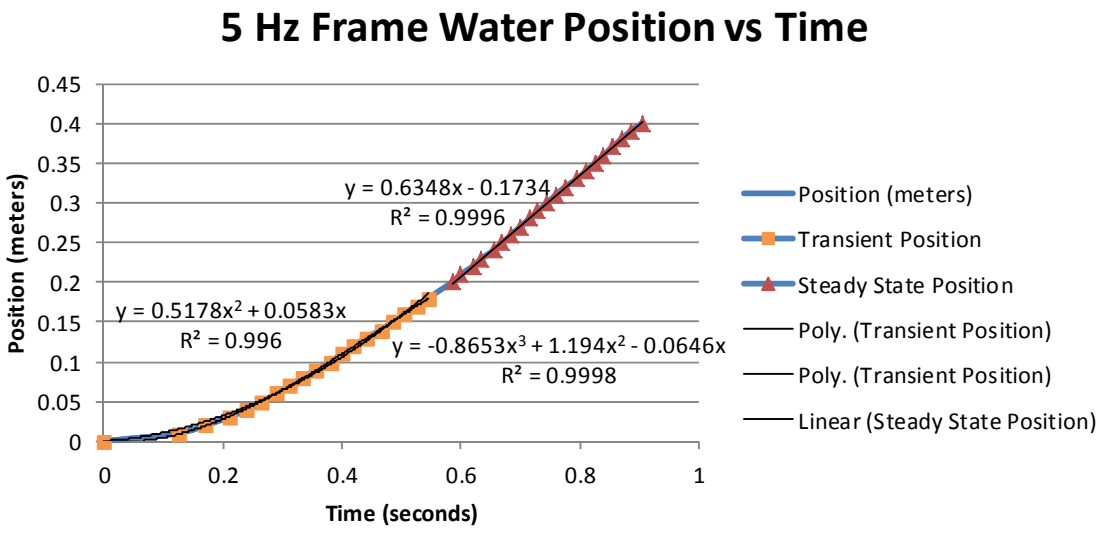

Figure 129 Frame position vs time at 5 Hz speed setting

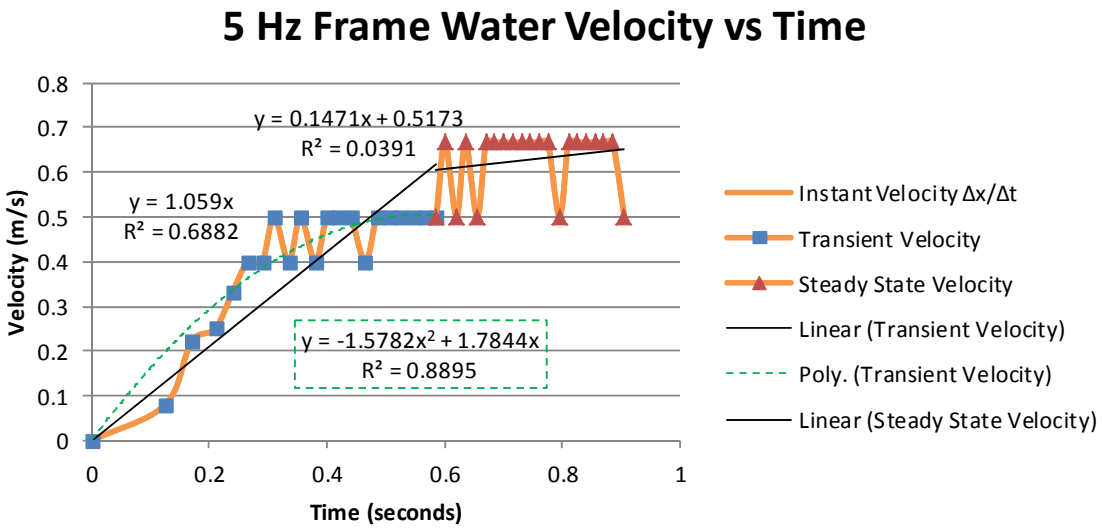

Figure 130 Frame velocity vs time at 5 Hz speed setting

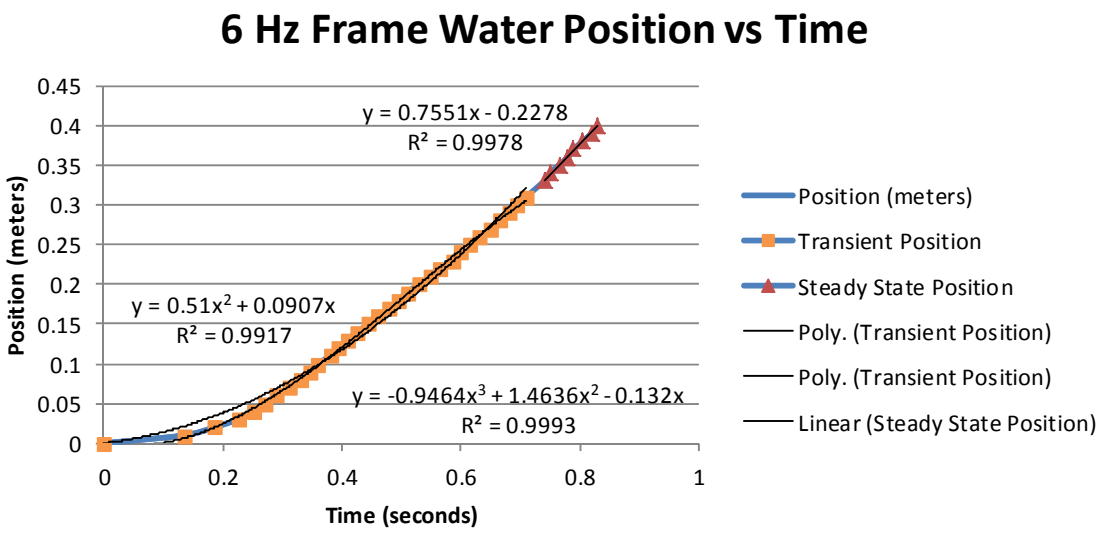

Figure 131 Frame position vs time at 6 Hz speed setting

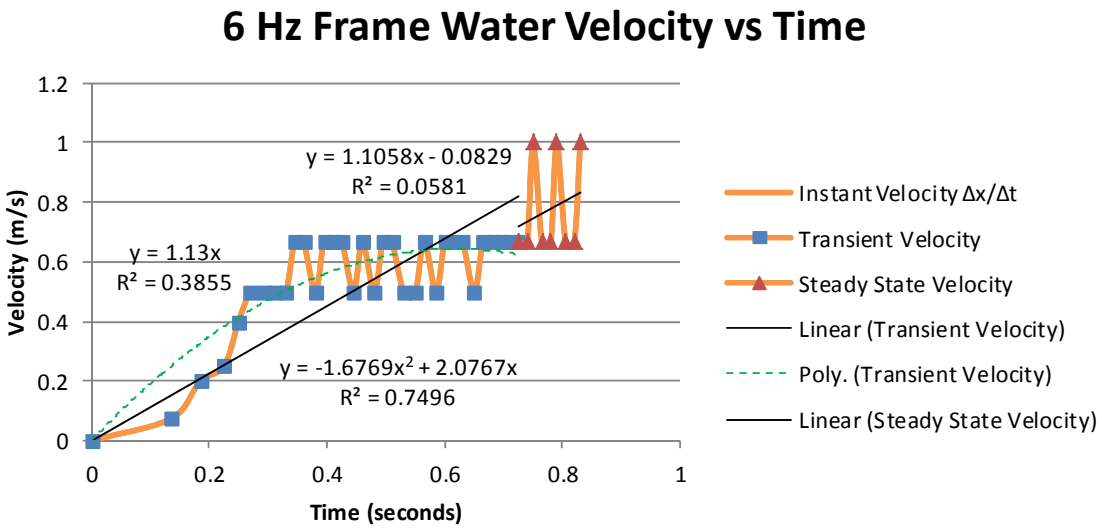

Figure 132 Frame velocity vs time at 6 Hz speed setting

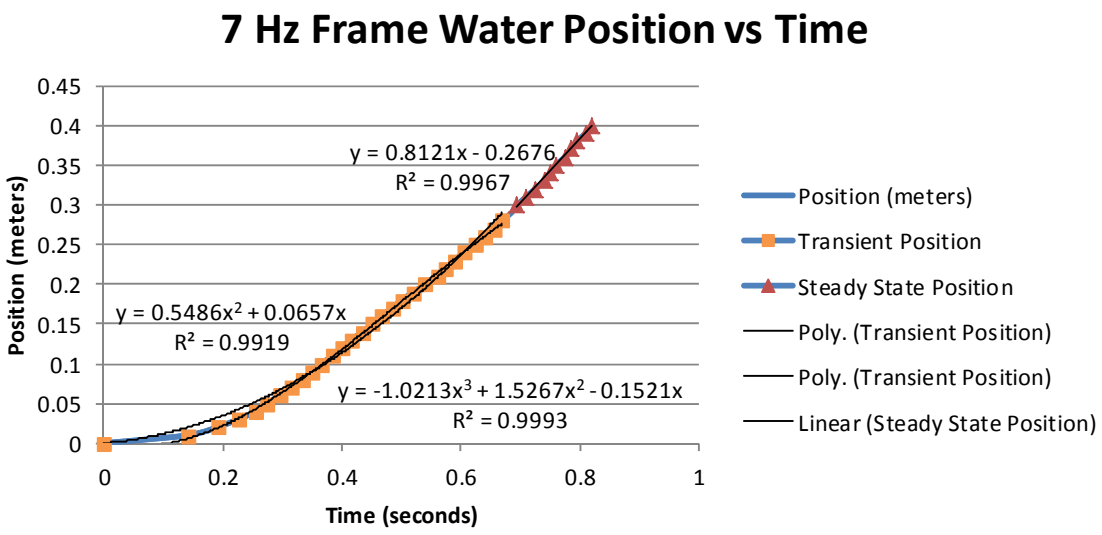

Figure 133 Frame position vs time at 7 Hz speed setting

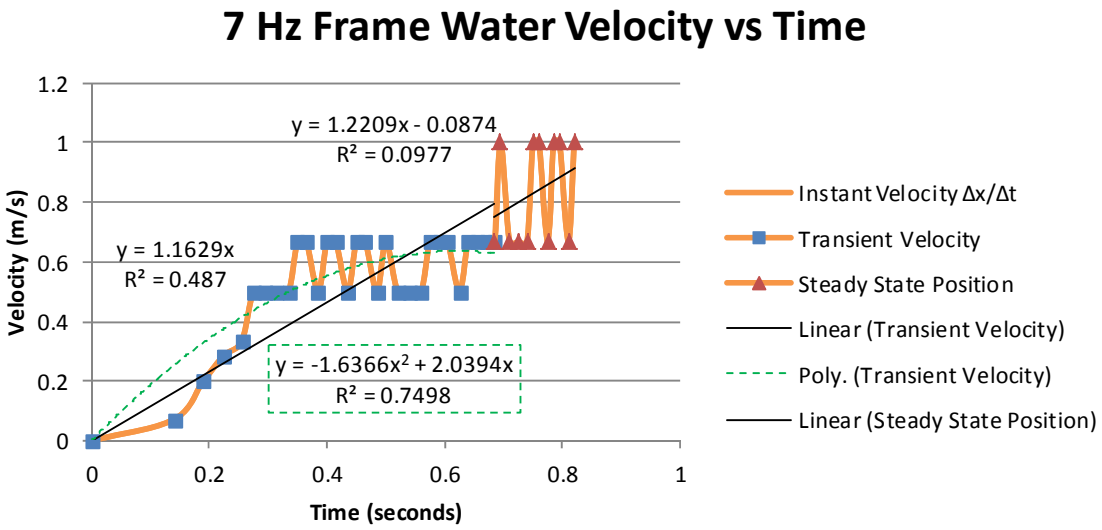

Figure 134 Frame velocity vs time at 7 Hz speed setting

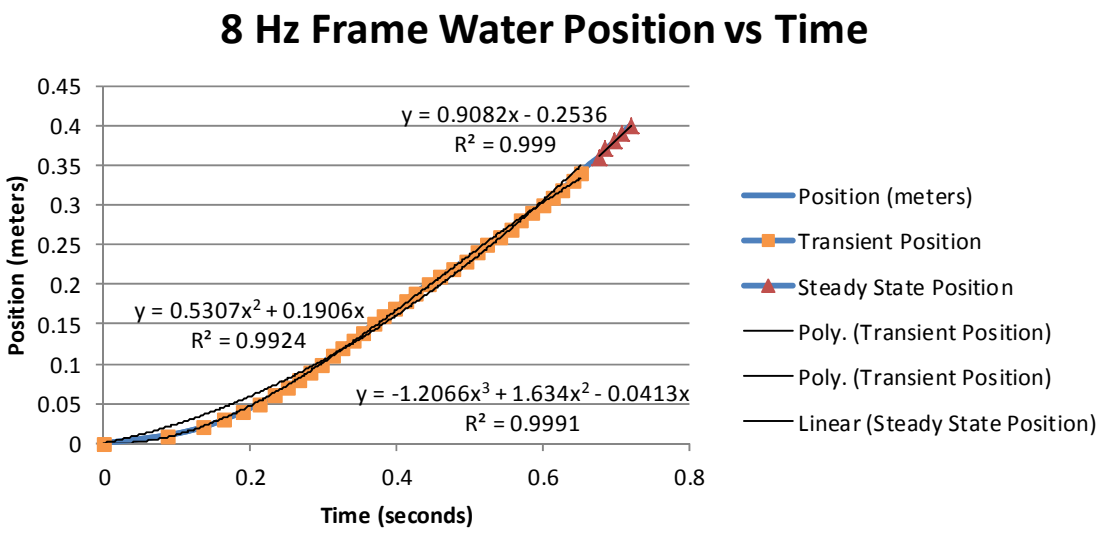

Figure 135 Frame position vs time at 8 Hz speed setting

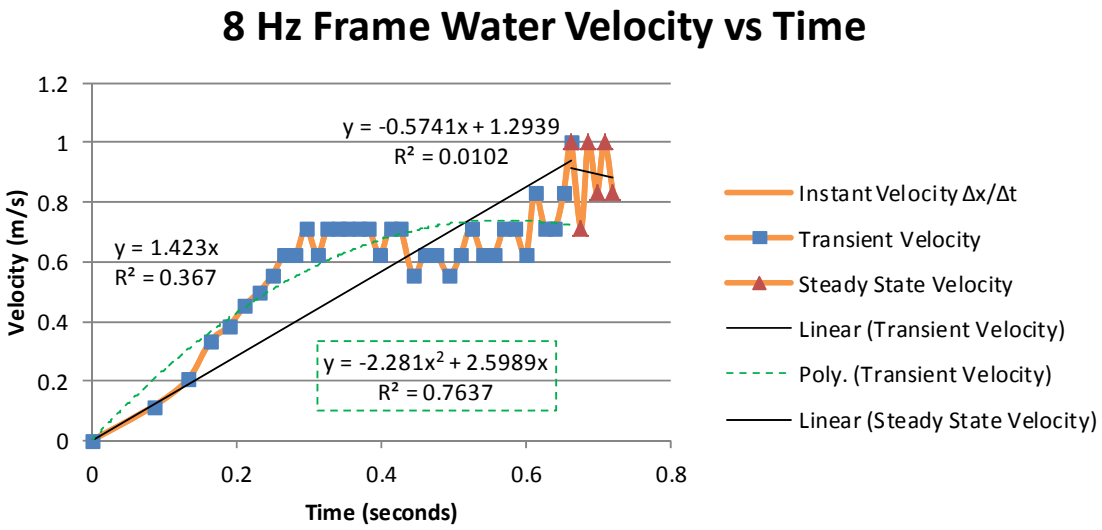

Figure 136 Frame velocity vs time at 8 Hz speed setting

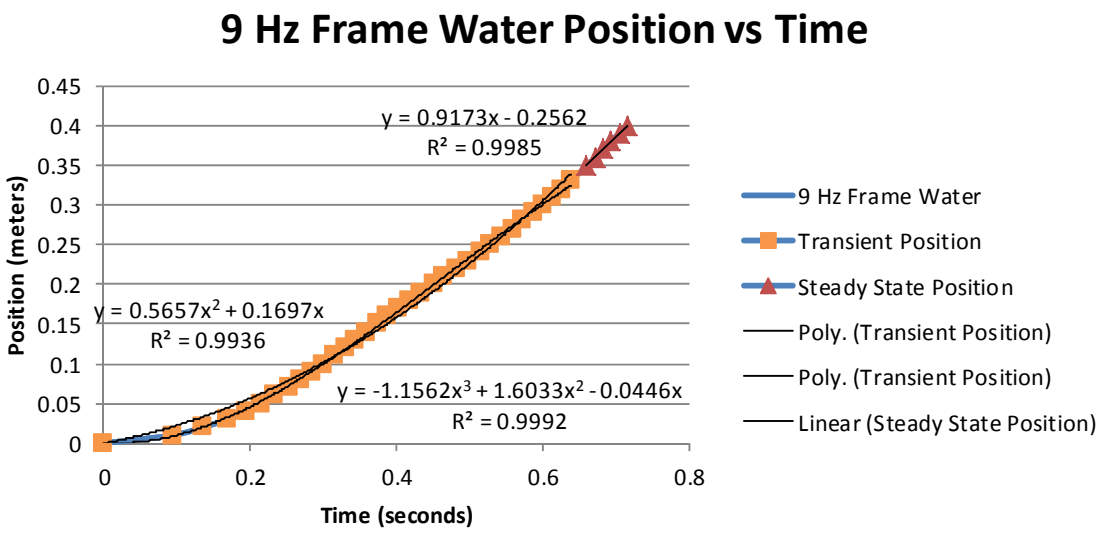

Figure 137 Frame position vs time at 9 Hz speed setting

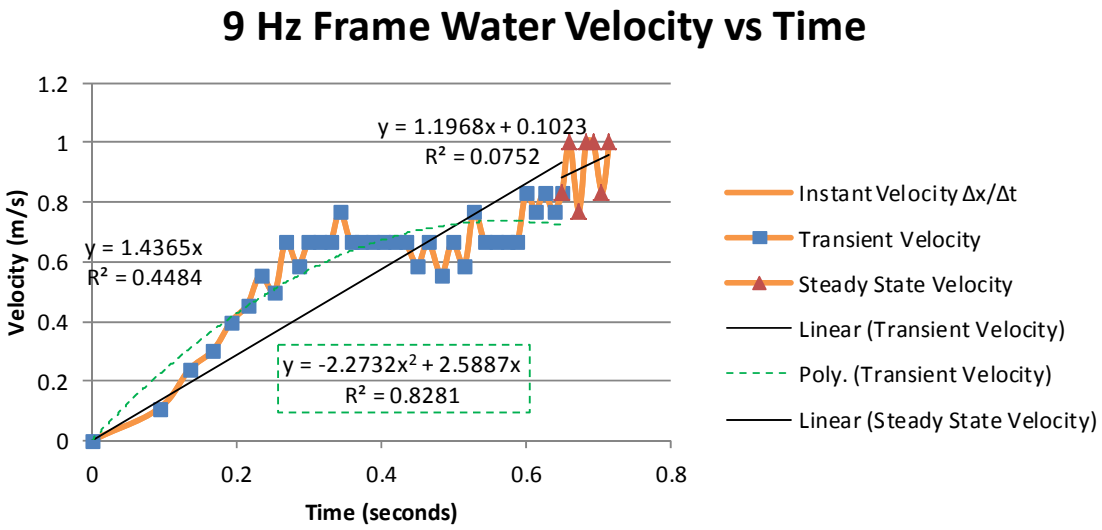

Figure 138 Frame velocity vs time for 9 Hz speed setting

APPENDIX E. FRAMED COMPOSITE TEST DATA

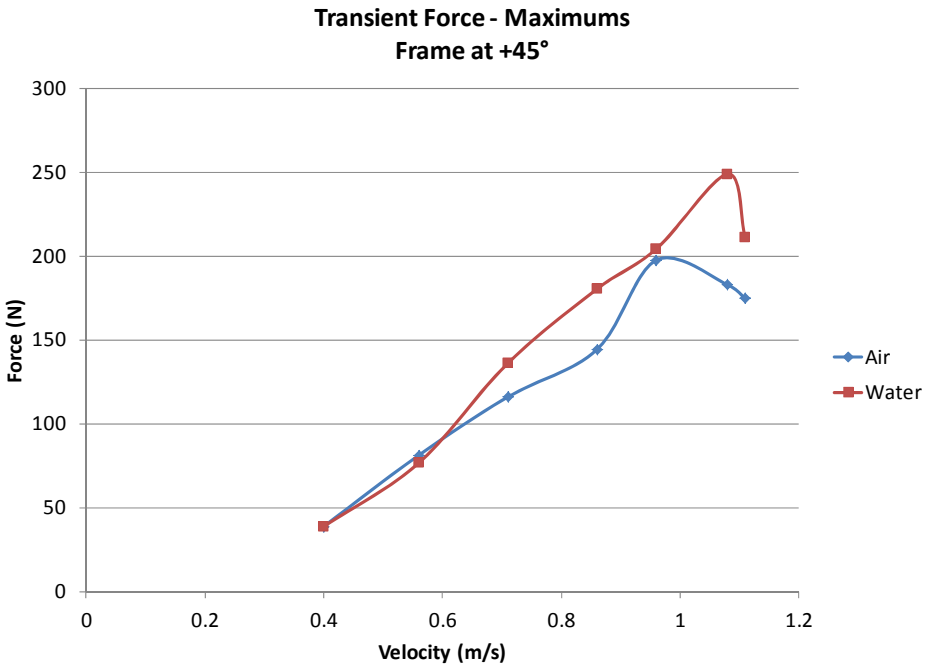

Figure 139 Transient max peak force for framed composite at +45º

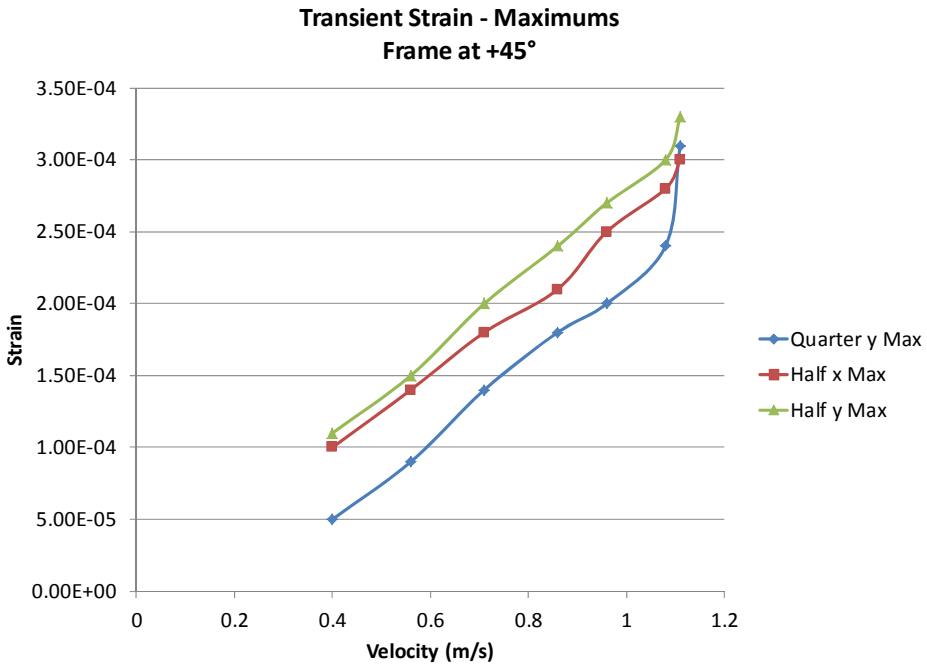

Figure 140 Transient maximum peak strain for framed composite at +45º

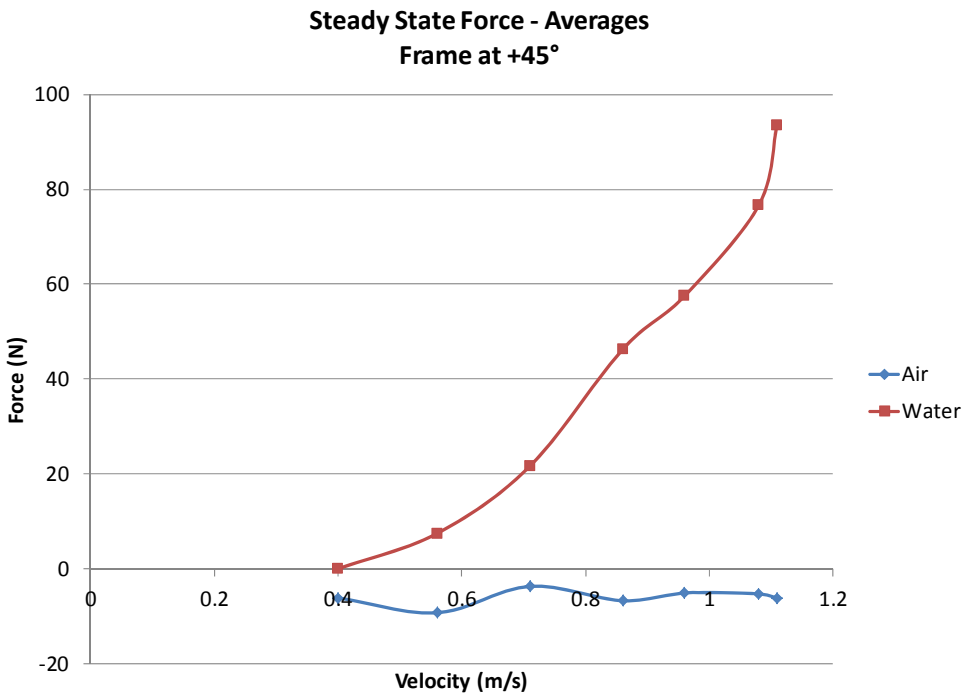

Figure 141 Steady state average force on framed composite at +45º

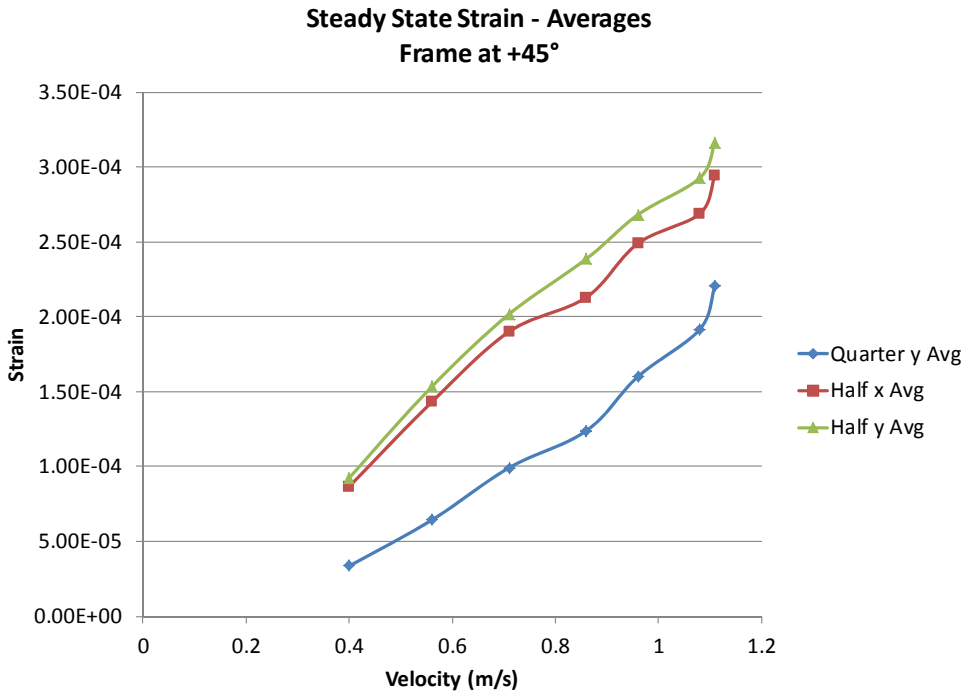

Figure 142 Steady state average strain for framed composite at +45º

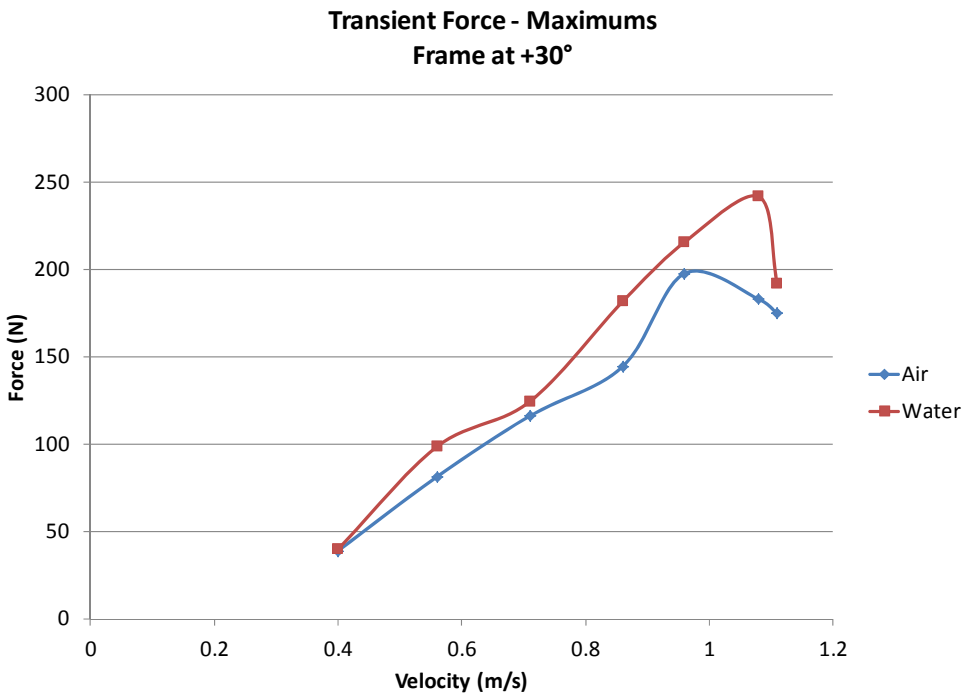

Figure 143 Transient max peak force for framed composite at +30º

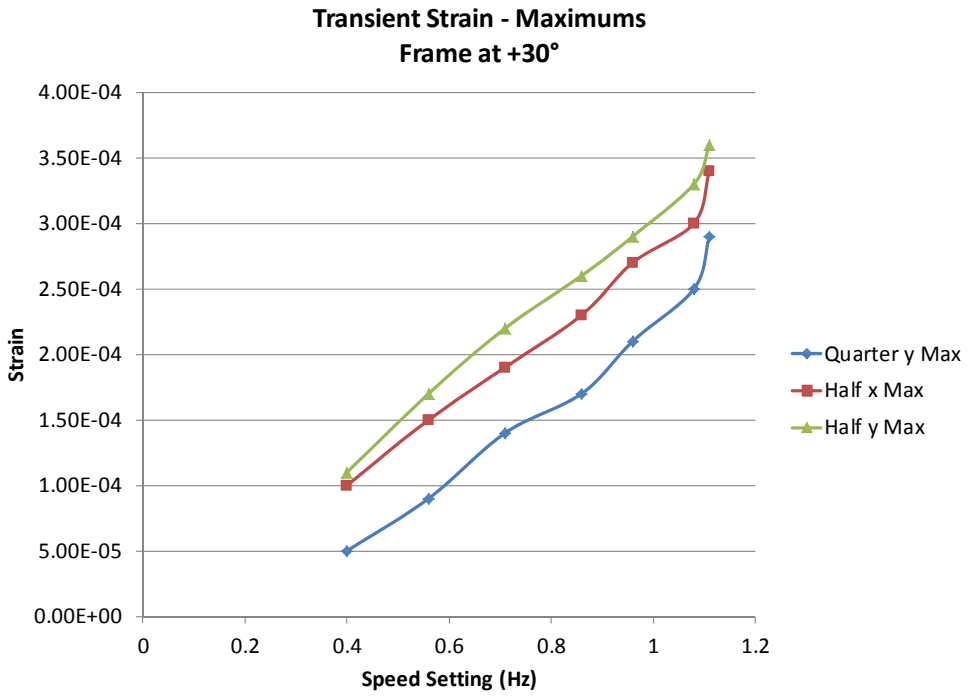

Figure 144 Transient maximum peak strain for framed composite at +30º

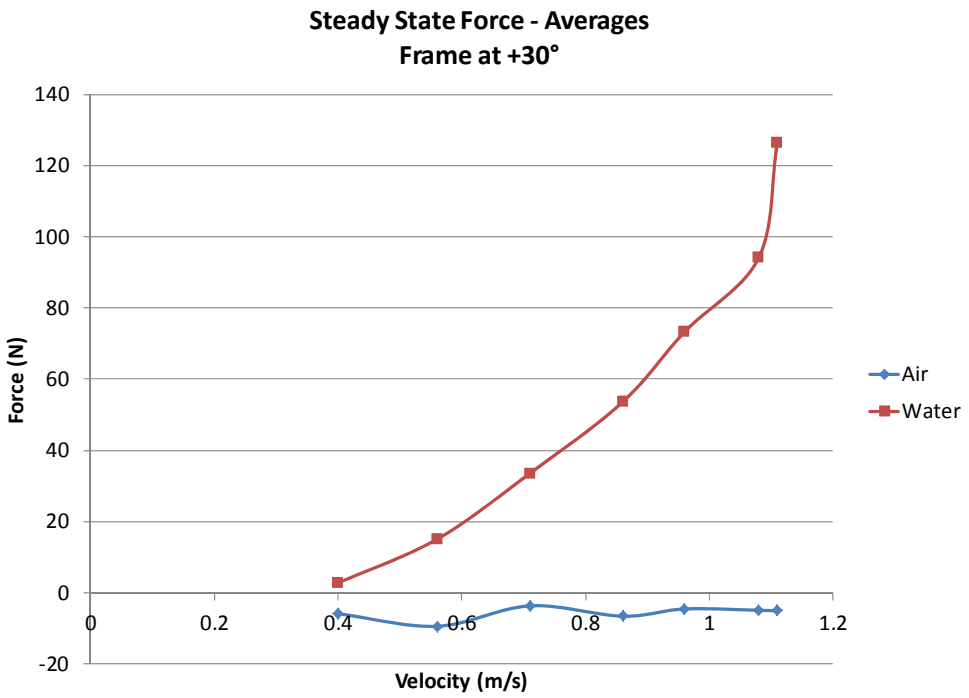

Figure 145 Steady state average force on framed composite at +30º

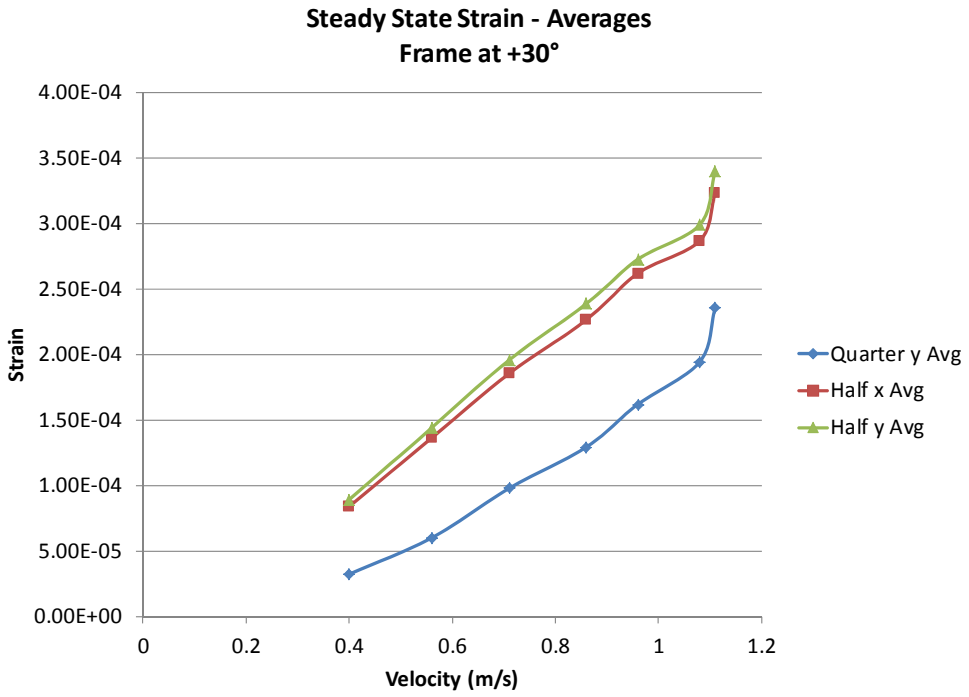

Figure 146 Steady state average strain for framed composite at +30º

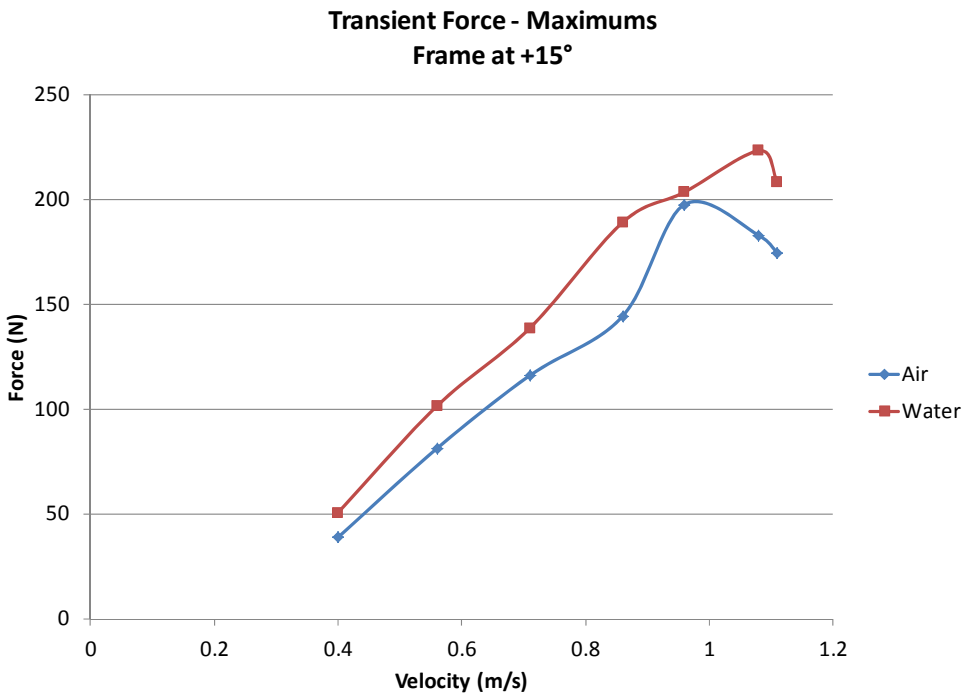

Figure 147 Transient max peak force for framed composite at +15º

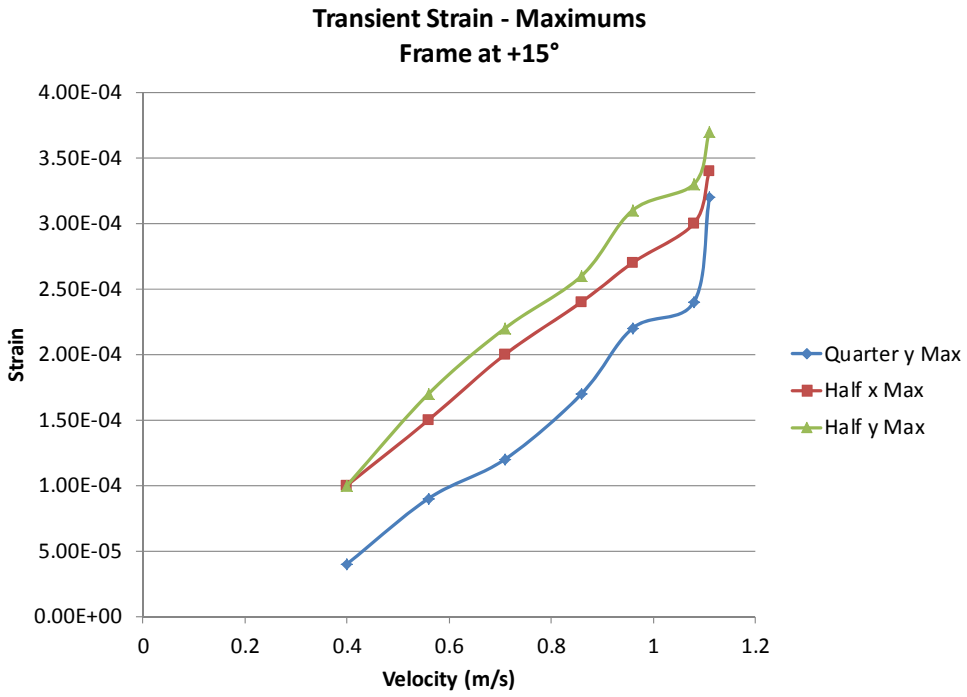

Figure 148 Transient maximum peak strain for framed composite at +15º

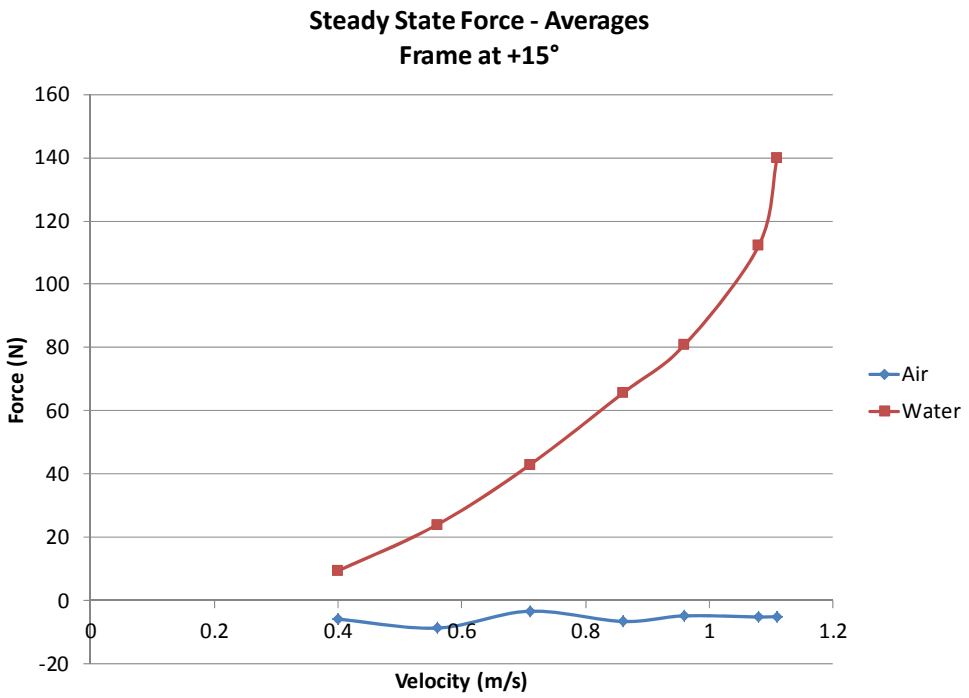

Figure 149 Steady state average force on framed composite at 15º

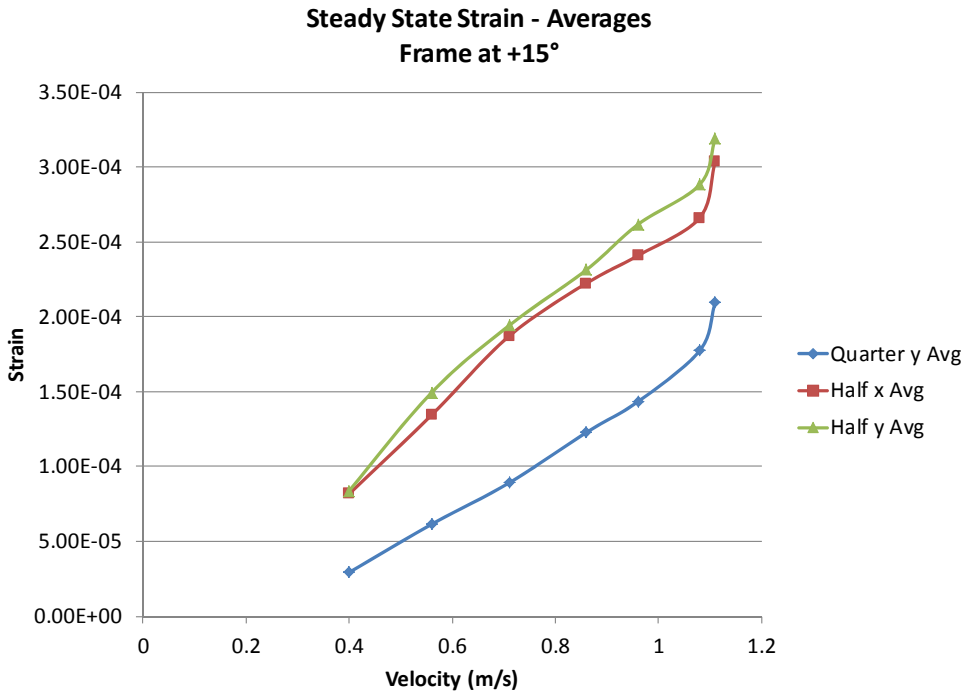

Figure 150 Steady state average strain for framed composite at +15º

Figure 151 Transient max peak force for framed composite at 0º

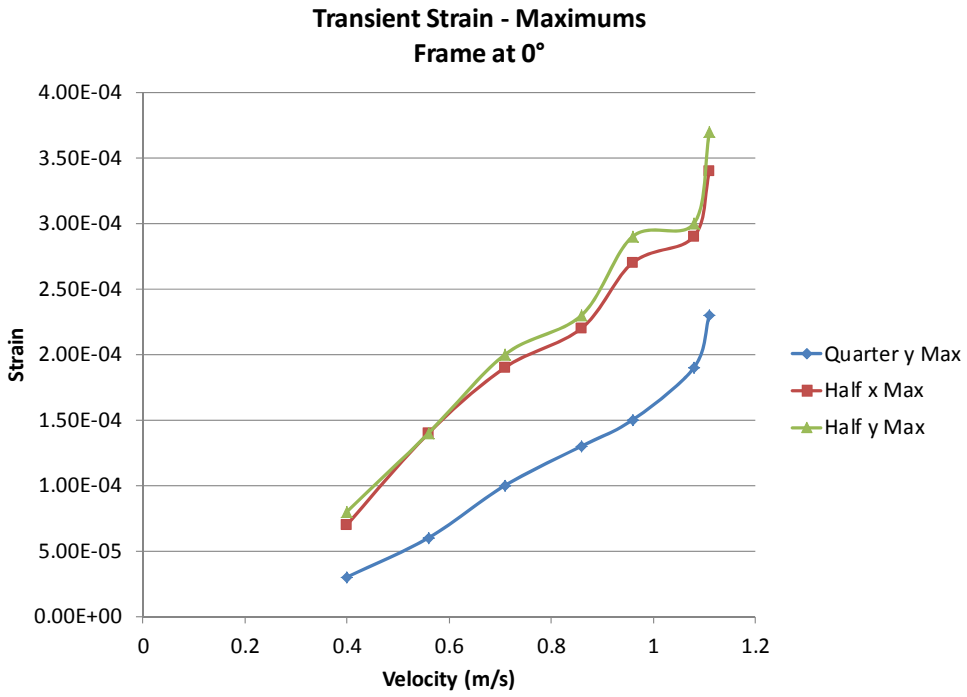

Figure 152 Transient maximum peak strain for framed composite at 0º

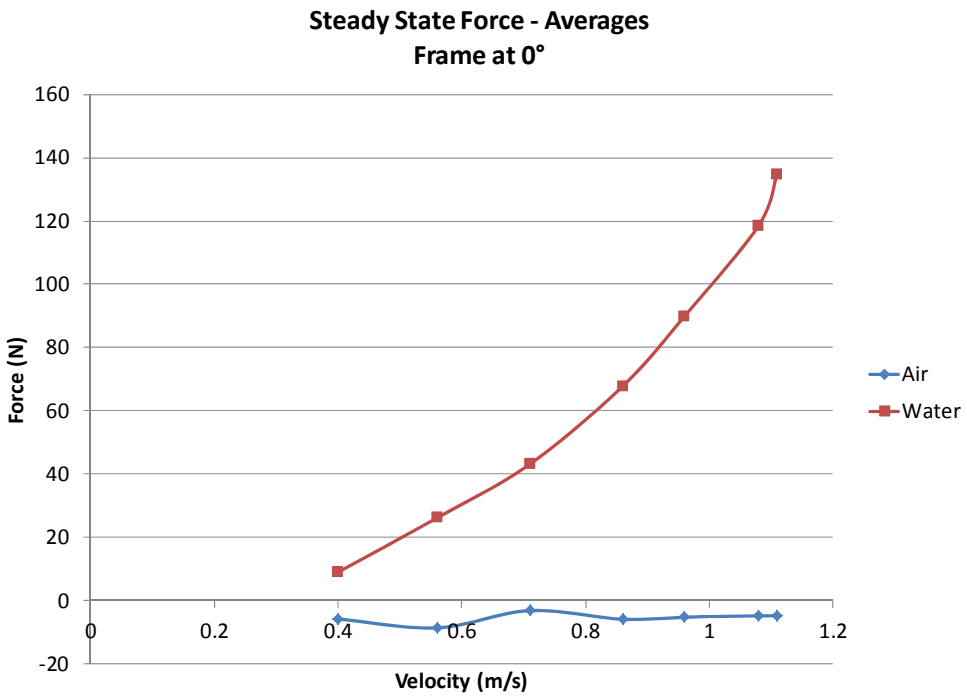

Figure 153 Steady state average force for framed composite at 0º

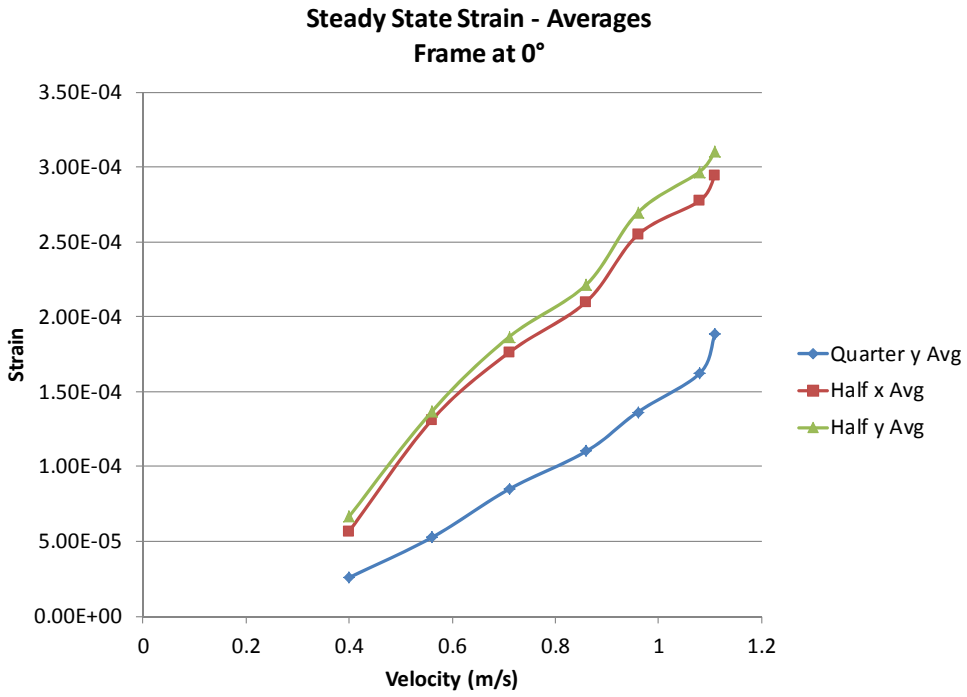

Figure 154 Steady state average strain for framed composite at 0º

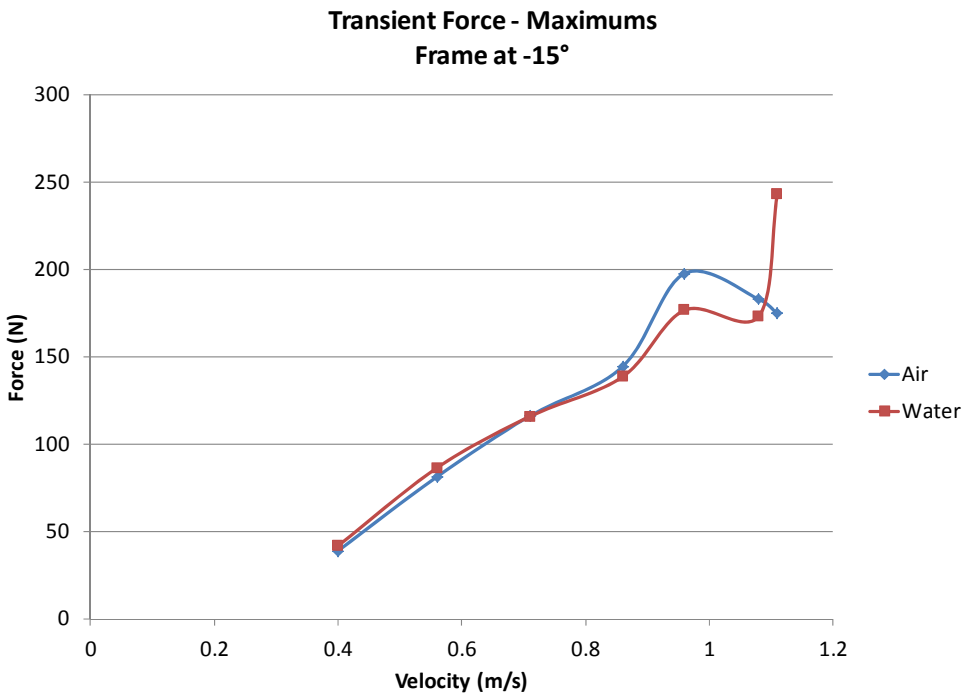

Figure 155 Transient max peak force for framed composite at -15º

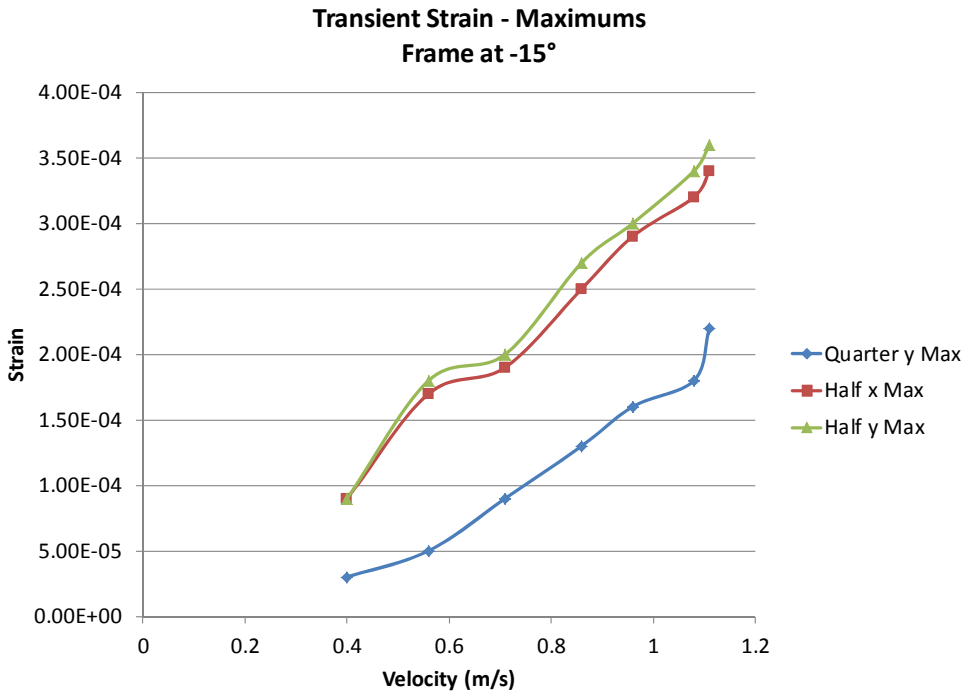

Figure 156 Transient maximum peak strain for framed composite at -15º

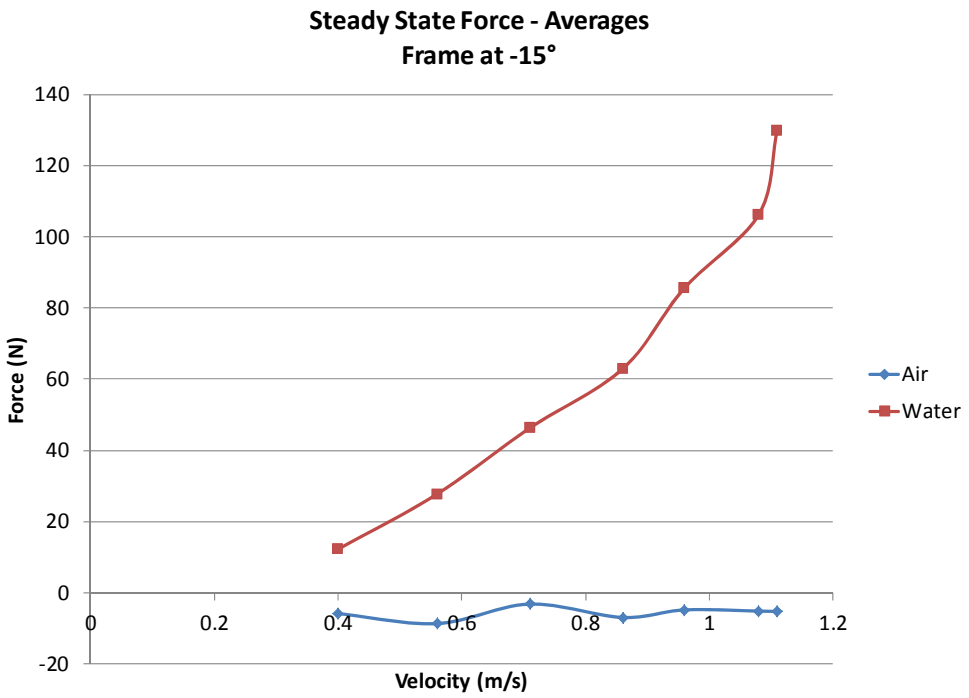

Figure 157 Steady state average force for framed composite at -15º

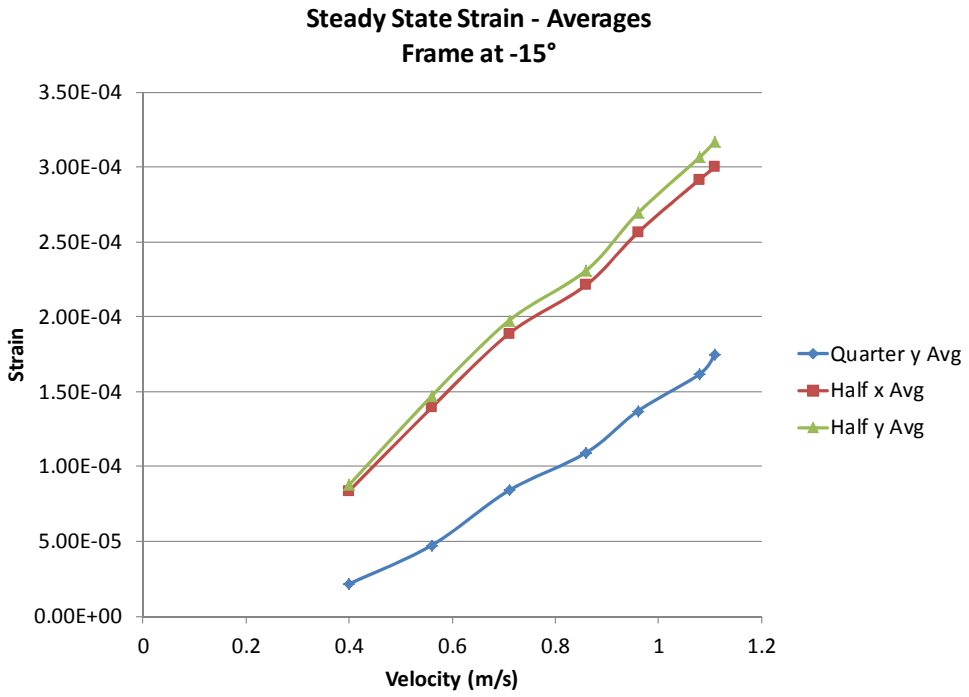

Figure 158 Steady state average strain for framed composite at -15º

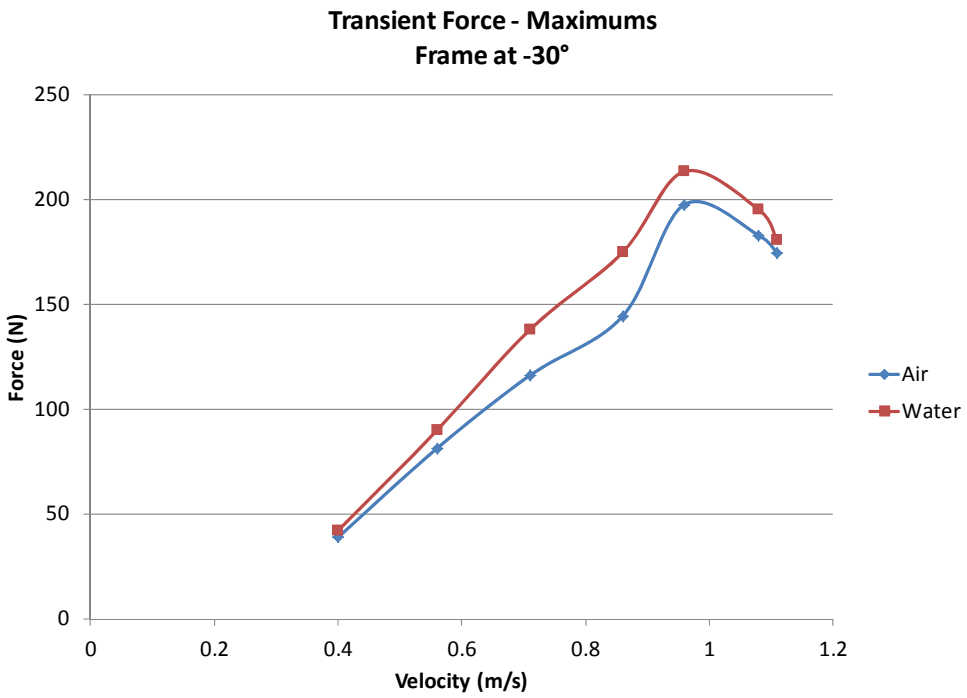

Figure 159 Transient max peak force for framed composite at -30º

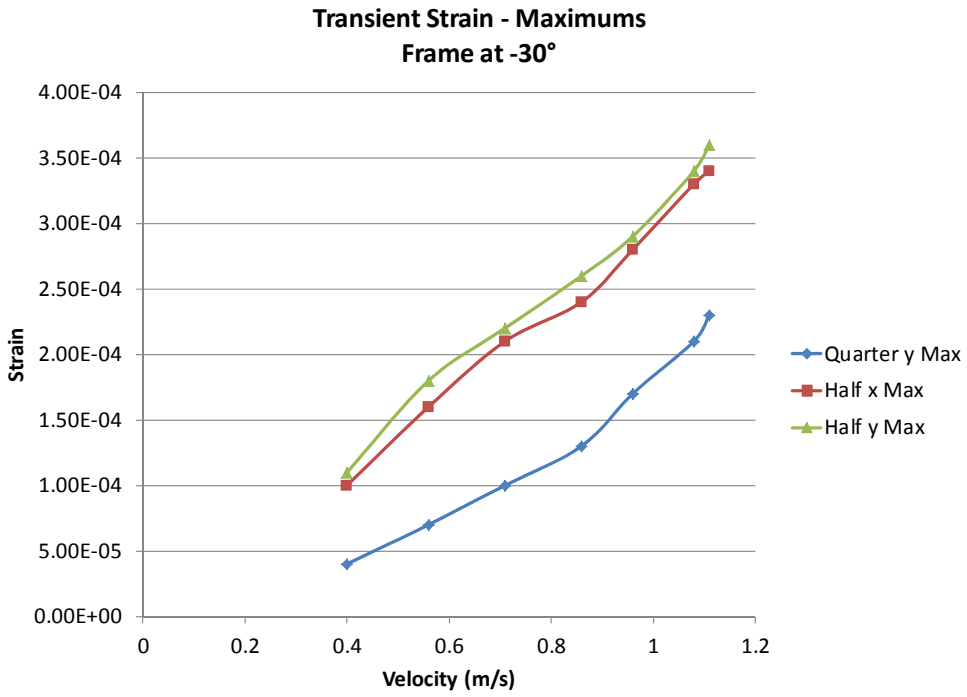

Figure 160 Transient maximum peak strain for framed composite at -30º

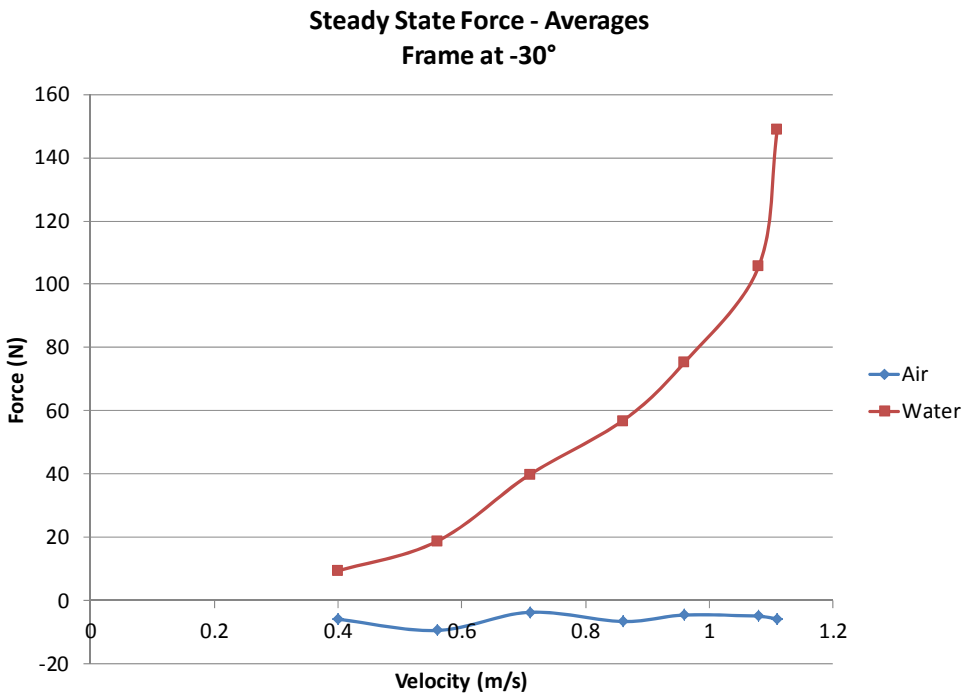

Figure 161 Steady state average force for framed composite at -30º

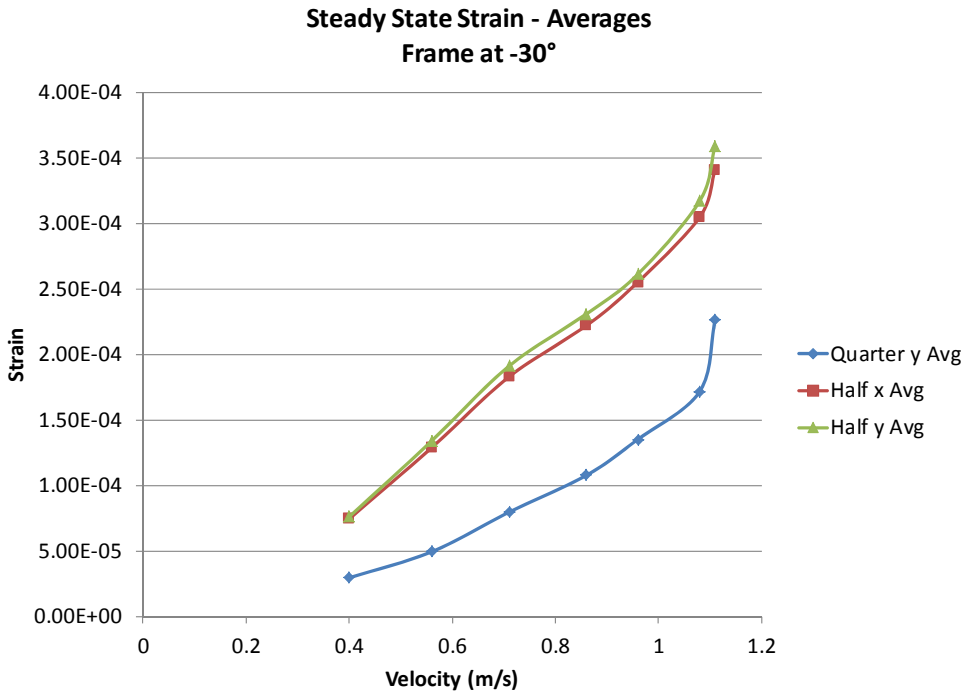

Figure 162 Steady state average strain for framed composite at -30º

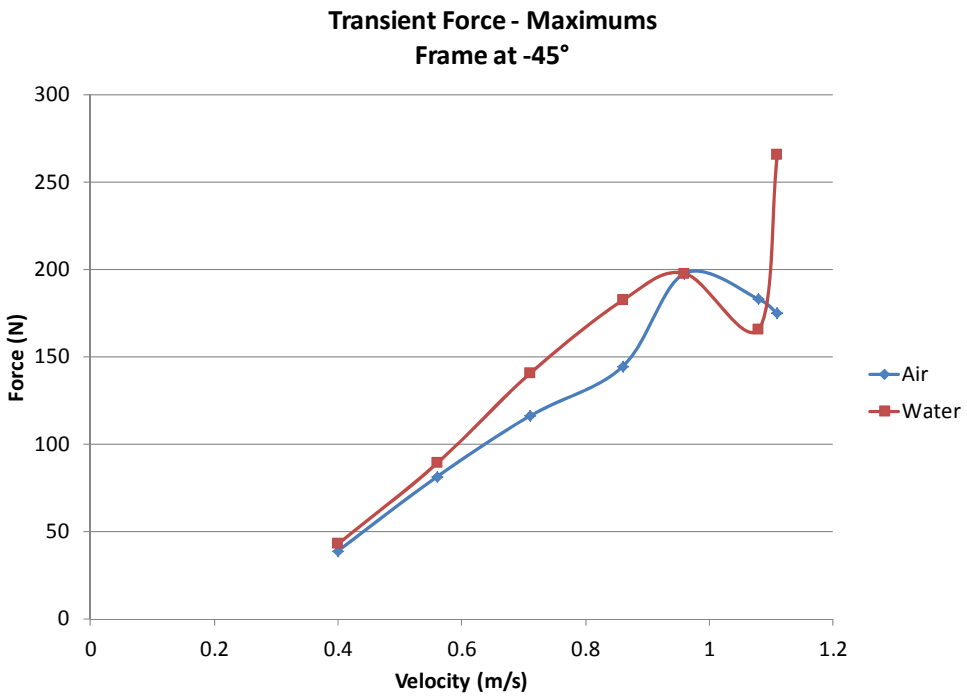

Figure 163 Transient max peak force for framed composite at -45º

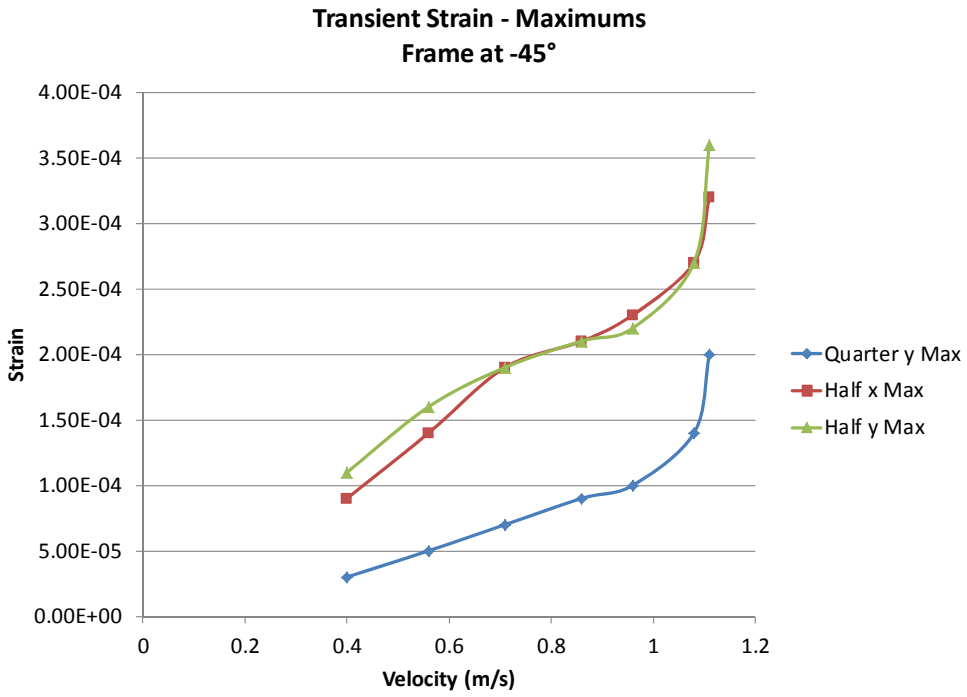

Figure 164 Transient maximum peak strain for framed composite at -45º

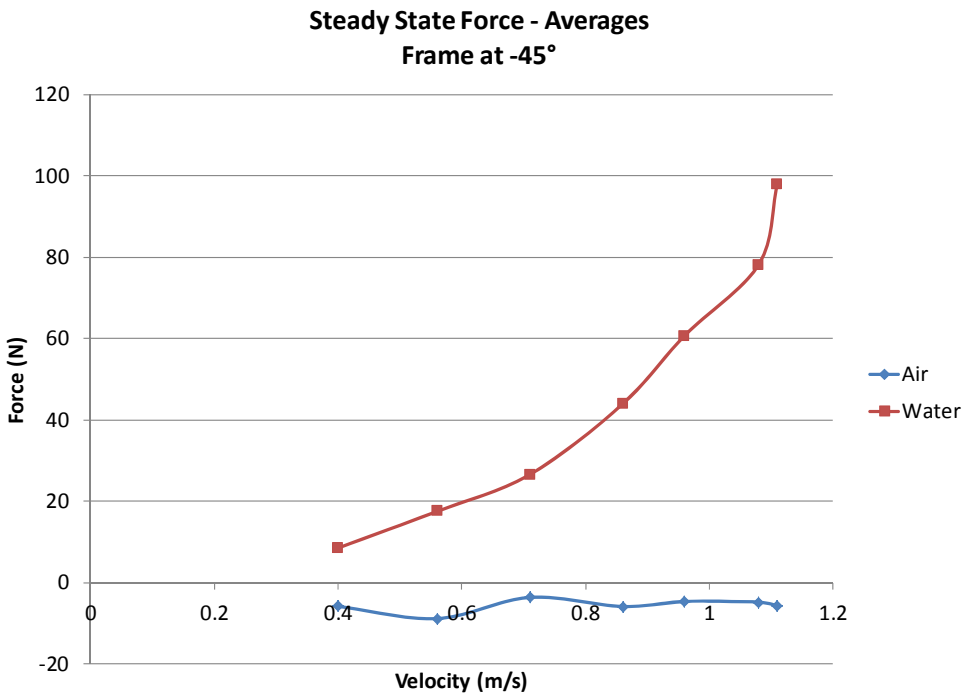

Figure 165 Steady state average force for framed composite at -45º

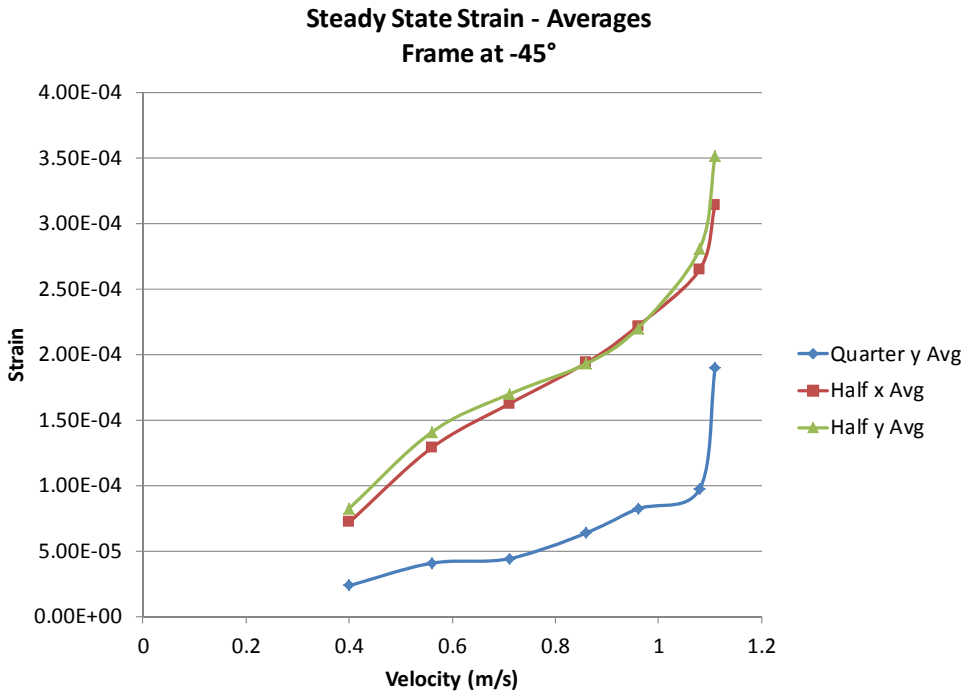

Figure 166 Steady state average strain for framed composite at -45º

LIST OF REFERENCES

[1] G. H. Staab, "Introduction to composite materials," in *Laminar Composites*, Woburn, MA: Butterworth-Heinemann, 1999, pp 1–15

[2] United States Navy, "Mine countermeasure ships," 15 November 2013. [Online]. Available: http://www.navy.mil

[3] S. Bartlett and B. Jones, "NSWC Carderock presentation for ASNE Day 2013: Composite ship structures, 2013. [Online]. Available: https://www .navlengineers.org/ProceedingsDocs/ASNEDay2013/Jones_pres.pdf

[4] M. M. Matthews, *U.S. Navy supervisor of salvage and diving—NAVSEA 00C,* Monterey, CA. Presentation at NPS on 2 May 2013, 2013.

[5] W. Palmer, "Composite primary hull: increasing payload and range of Navy ships with lightweight, affordable composite hulls," *SeaFrame,* vol. 4, no. 2, pp. 13–14, 2008.

[6] K. Galanis, "Hull construction with domposite materials for hips over 100 m in length," M.S. thesis, Dept of Ocean Eng., MIT, Boston, 2002.

[7] H.-J. Bungartz and M. Schafer, "Preface" in *Fluid-Structure Interaction: Modeling, Simulation, Optimization*, Berlin: Springer, 2016, p. v.

[8] P. K. Kendall, "Numerical study of effects of fluid-structure interaction on dynamic responses of composite plates," M.S. thesis, Dept. Mech. Eng., Naval Postgraduate School, Monterey, CA, 2009.

[9] S. Ma and H. Mahfuz, "Finite element simulation of composite ship structures with fluid structure interaction," *Ocean Engineering,* vol. 52, pp. 52–59, 2012.

[10] S. C. Knutton, "Computational analysis of effect of transient force on composite structures," M.S. thesis, Dept. Mech. Eng., Naval Postgraduate School, Monterey, CA, 2013.

[11] F. M. White, "Flow past immersed bodies" in *Fluid Mechanics*, New York: McGraw-Hill, 2011, pp. 457-492.

[12] A. C. Ugural and S. K. Fenster, "Plates and shells," in *Advanced Strength and Applied Elasticity*, 4th ed., Upper Saddle River, NJ: Prentice Hall, 2003, pp. 472–478.

[13] S. Timoshenko and S. Woinowsky-Krieger, *Theory of Plates and Shells*, New York, NY: McGraw-Hill, 1959, pp. 197–2020.

[14] D. W. Callister, "Composites," in *Materials Science and Engineering: An Introduction*, 5th ed., New York, NY: John Wiley & Sons, 2000, pp. 520–534.

[15] Y. W. Kwon and A. Altekin, "Multilevel, micro/macro-approach for analysis of woven-fabric composite plates," *Journal of Composite Materials,* vol. 36, no. 8, pp. 1005–1022, 2002.

[16] U.S. Composites, "Fiberglass cloth," 2011. [Online]. Available: http://www.uscomposites.com/cloth.html

[17] J. E. Russell, "Dynamic response of composite structures underwater," M.S. thesis, Dept. Mech. Eng., Naval Postgraduate School, Monterey, CA, 2013.

[18] G. T. Bryan, "Experimental and Computational Fluid Dynamic Analysis of Axial-Flow Hydrodynamic Power Turbine," M.S. thesis, Dept. Mech. Eng., Naval Postgraduate School, Monterey, CA, 2013.

[19] T. Christian, "Tow tank software integration and programming for NPS Tow tank," Naval Postgraduate School, Monterey, 2012.

[20] U.S. Navy, "Navy.mil, 1 August 2009. [Online]. Available: http://www.navy.mil /view_image.asp?id=74693

[21] U.S. Navy, "Navy.mil," 28 October 2013. [Online]. Available: http://www.navy .mil/view_image.asp?id=164137

[22] R. C. Hibbeler, "Strain," in *Mechanics of Materials*, Boston: Prentice Hall, 2011, pp. 65–66.

INITIAL DISTRIBUTION LIST

1. Defense Technical Information Center
   Ft. Belvoir, Virginia

2. Dudley Knox Library
   Naval Postgraduate School
   Monterey, California